Investigations of the role of disorder in heavy fermion compounds

Von der Gemeinsamen Naturwissenschaftlichen Fakultät
der Technischen Universität Carolo-Wilhelmina
zu Braunschweig
zur Erlangung des Grades eines
Doktors der Naturwissenschaften
(Dr.rer.nat.)
genehmigte

D i s s e r t a t i o n

von Igor Maksimov
aus Ust-Kamenogorsk

1. Referent:	Prof.Dr. F.J. Litterst
2. Referent:	Prof.Dr. A. Eichler
eingereicht am:	13. 01. 2003
mündliche Prüfung (Disputation) am:	21. 03. 2003

2003
(Druckjahr)

Vorabveröffentlichungen

Teilergebnisse aus dieser Arbeit wurden mit Genehmigung der Naturwissenschaftlichen Fakultät in folgenden Beiträgen vorab veröffentlicht:

Publikationen:

- I. Maksimov, D. Baabe, H.H. Klauss, F.J. Litterst, R. Feyerherm, D.M. Többens, A. Matsushita and S. Süllow, *Structure and Magnetic Order in* $Fe_{2+x}V_{1-x}Al$, J. Phys.: Condens. Matter **13** (2001) 5487.
- I. Maksimov, F.J. Litterst, S. Süllow and J.A. Mydosh, *Composition dependence of the electronic properties of* $UPd_{2-x}Sn$, Physica B **312-313** (2002) 283.
- I. Maksimov, F.J. Litterst, D. Menzel, J. Schoenes, A.A. Menovsky, J.A. Mydosh and S. Süllow, *Irreversibility lines of the heavy fermion spin glass* URh_2Ge_2, Physica B **312-313** (2002) 289.
- A.U.B. Wolter, A. Bosse, D. Baabe, I. Maksimov, D. Mienert, H.H. Klauss, F.J. Litterst, D. Niemeier, R. Michalak, C. Geibel, R. Feyerherm, R. Hendrikx, J.A. Mydosh and S. Süllow, *Structure and magnetic order of the Heusler compound* Co_2NbSn, Phys. Rev. B **66** (2002) 174428.
- I. Maksimov, F.J. Litterst, R. Feyerherm, J.A. Mydosh and S. Süllow, *Structural and magnetic ordering in* $UPd_{1.85}Sn$, Acta Physica Polonica, in print (2003).
- S. Süllow, I. Maksimov, F.J. Litterst and J.A. Mydosh, *Decoupling of magnetic ground state and electronic transport properties in* URh_2Ge_2, Acta Physica Polonica, in print (2003).
- D. Baabe, I. Maksimov, J. Kreitlow, H.H. Klauss, F.J. Litterst, A. Matsushita and S. Süllow, *Mössbauer spectroscopy on ferromagnetic* Fe_2VAl, Hyperfine Interact., in print (2003).
- I. Maksimov, F.J. Litterst, H. Rechenberg, M.A.C. de Melo, R. Feyerherm, R.W.A. Henrikx, T.J. Gortenmulder, J.A. Mydosh and S. Süllow, *The effect of disorder on the magnetic and transport properties of* $UPd_{2-x}Sn$, Phys. Rev. B, accepted (2003).

Tagungsbeiträge:

- I. Maksimov, D. Baabe, S. Süllow, H.H. Klauss, F.J. Litterst, R. Feyerherm, D. Többens, A. Matsushita, *Interdependence of structural and ground state properties in* Fe_2VAl, XII Workshop on Strongly Correlated Electron Systems, Trieste, Italy (2000).
- I. Maksimov, F.J. Litterst, S. Süllow and J.A. Mydosh, *Composition dependence of the magnetic and electronic properties of* $UPd_{2-x}Sn$, Frühjahrstagung der DPG, Hamburg (2001).
- I. Maksimov, F.J. Litterst, R. Feyerherm, J.A. Mydosh and S. Süllow, *Magnetic order in* $UPd_{2-x}Sn$, Frühjahrstagung der DPG, Regensburg (2002).
- I. Maksimov, F.J. Litterst, R. Feyerherm, J.A. Mydosh and S. Süllow, *Magnetic structure of disordered* $UPd_{2-x}Sn$, SCES, Krakow, Poland (2002).

Contents

1 Preface

In this thesis, we present a study on the role of disorder and frustration on the physical properties of strongly correlated electron systems. For this, a number of heavy fermion materials and related compounds with very unusual physical properties, like magnetic ground state instabilities or anomalous electronic transport, have been thoroughly investigated in view of the crystallographic disorder aspect.

The thesis is organized as follows: In chapter 2 we will introduce the basic physical concepts relevant to our subject. We will review the main properties of archetypical heavy fermion compounds and address those aspects of the behavior of spin glasses that play a role for the materials studied in this thesis. Further, as a major topic of this thesis will be the electronic transport behavior of disordered heavy fermions, we will discuss the important models in this field. Finally, we will briefly address the present situation concerning studies on disordered heavy fermion systems.

In chapter 3 we present the case of Fe_2VAl, where a semiconductor-like resistivity close to a magnetic instability had been established. Two different models had been proposed to account for the unusual behavior. In analogy to strongly correlated $FeSi$, the first model proposed a Kondo-insulating scenario. On the other hand, an optical conductivity study provided evidence for a temperature independent pseudogap formation in the density of states at variance with a Kondo insulator picture. Given this contradictory experimental situation we performed a thorough structural and magnetic investigation of Fe_2VAl. In the course of this study, we establish the level of disorder and, more specifically, the type of disorder in this compound. Altogether, our findings on Fe_2VAl disprove the claims of a strongly correlated insulator state.

A characteristic feature of heavy fermion systems near a quantum critical point (QCP) is a very strong dependence of the physical properties to comparatively small levels of disorder. In dense Kondo systems, intersite magnetic interactions compete with the Kondo effect, leading to such a quantum phase transition. However, so far there has been no detailed investigation on how structural disorder affects the interplay between Kondo effect and RKKY interaction. Therefore, we have performed an extensive study on the disordered heavy fermion system $UPd_{2-x}Sn$, which exhibits a paramagnetic/magnetic ground state transition as result of a structural deformation, accompanied by a transition from metallic

($d\rho/dT$ >0) to non-metallic ($d\rho/dT$ >0) electronic transport. Specifically, for this system, we examine the type of disorder, and how it affects the magnetic ground state on a microscopic level. In addition, we discuss, in how far the non-metallic electronic transport behavior arises from Kondo scattering, with the coherent state suppressed by the disorder, or is governed by a tendency towards localization of the electrons. All in all, this study, presented in chapter 4, serves as a demonstration for the very strong influence of disorder in a heavy fermion compound on its physical properties.

In the last chapter, we will focus entirely on the anomalous properties due to crystallographic disorder in a heavy fermion compound, *i.e.*, in the first 3D metallic random-bond spin glass URh_2Ge_2. Utilizing the availability of single crystalline specimens, we have found that the magnetic irreversibility behavior in the frozen-in state in URh_2Ge_2 strongly deviates from classical theoretical predictions. Instead, it can be accounted for if the role of single ion anisotropy for the freezing in a m-vector spin glass is considered. Moreover, we have established the electronic transport properties of URh_2Ge_2 as function of field, disorder and anisotropy. Thus, for the first time the electronic transport properties of a moderately disordered heavy fermion compound have been thoroughly studied, hopefully forming the basis for future theoretical investigations.

Finally, we find that the Hall effect of the two disordered systems with anomalous, non-metallic resistivities, URh_2Ge_2 and cubic $UPd_{2-x}Sn$, scales with the susceptibility over the whole temperature range, this in contrast to ordinary, non-disordered heavy fermions. Probably, this is a more general feature of moderately disordered heavy fermion compounds, which so far, however, theoretically has not been fully explained.

2 Introduction

2.1 Theoretical Background

2.1.1 Heavy-fermion systems

Heavy fermion compounds belong to a class of strongly correlated electron systems (for general reviews see Grewe and Steglich [1]; experimental aspects are discussed by Steglich et al. [2, 3], Fisk et al. [4, 5], theoretical topics by Hewson [6], Fulde et al. [7, 8] and Zwicknagl [9, 10]). Typically, heavy fermion systems are intermetallic compounds of elements with partly occupied f-shells ($4f$: Cerium, Ytterbium and $5f$: Uranium, Plutonium, Neptunium) and transition metals (exceptions like LiV_2O_4 and $Nd_{2-x}Ce_xCuO_4$ [11]-[15] will not be considered here, as the mechanism of mass enhancement is different than that for the "classical" intermetallic heavy fermions).

Heavy fermion materials are characterized by f-orbitals, which energetically lie close to the Fermi level. In this situation, the interaction between localized f-electrons and delocalized conduction electrons controls the physics of such materials. In effect, it leads to very strong correlations within the electron system. These correlations are reflected in an enhanced effective mass m^* of the electrons, and thus non-magnetic heavy fermion materials behave as if they were free electron materials, but with largely enhanced values m^*. Within Fermi Liquid theory, the correspondence between the properties of a free electron gas and heavy fermion materials is taken as evidence for the existence of "quasi-particles", that is particles behaving like electrons, but being much heavier, hence the name "heavy fermion".

The huge effective mass of the electrons accounts for the unusual physical properties of heavy fermion materials. The specific heat c_p of a non-magnetic heavy fermion compound at low temperatures (far below the Debye temperature) contains two contributions:

$$c_p = \gamma T + \beta T^3 \tag{2.1}$$

with γT as electronic specific heat and βT^3 as lattice contribution. The γ - value, within the Sommerfeld model for free electrons, is proportional to the effective

mass of the electrons:

$$\gamma = \frac{\pi^2 k_B^2 N(E_F)}{3} = \frac{k_B^2 k_F m^*}{3\hbar^2} \tag{2.2}$$

with $N(E_F)$ as density of the electron states at the Fermi level, k_F as Fermi wave vector and m^* as effective mass of the electron. For heavy fermion systems the effective mass, as result of a largely enhanced density of states at the Fermi level, is much larger than for non-correlated metals, and consequently, the γ - value is increased by the same factor. In free electron metals like Na the value of γ is of the order of 1mJ/K^{2}mole, corresponding to $m^* \sim m_e$. In contrast, for heavy fermion compounds γ - values up to 1000 mJ/K^{2}mole are found, corresponding to effective masses m^* up to $1000 m_e$.

In the transport properties, Fermi liquid theory predicts the dominance of quasi-particle - quasi-particle scattering, implying for the electrical resistivity:

$$\rho(T) = \rho_0 + AT^2 \quad \text{with} \quad \sqrt{A} \propto m^* \tag{2.3}$$

As well, the spin susceptibility of free electrons in the paramagnetic state depends on the density of states at the Fermi level. Thus, according to Fermi liquid theory, a large Pauli susceptibility χ_0 reflects the huge mass enhancement in the limit $T \to 0$:

$$\chi_0 = \mu_B^2 N(E_F) = const \tag{2.4}$$

For simple metals, the proportionality between γ and χ is expressed through the Sommerfeld-Wilson coefficient:

$$R_{SW} = \frac{\chi}{\gamma} \frac{\pi^2 k_B^2}{\mu_0 \mu_{eff}^2} \quad \text{with} \quad \mu_{eff}^2 = g^2 \mu_B^2 j(j+1) \tag{2.5}$$

where μ_{eff} represents the effective magnetic moment, g is the Lande-factor with the total angular moment j. The value R_{SW} for heavy fermions is of the same order as for free electrons, $R_{SW} \simeq 1$ [16], implying that both γ and χ are enhanced by the same mechanism.

Often, in heavy fermion materials magnetically ordered ground states are observed. This is viewed as a result of a competition between Kondo effect and the Ruderman-Kittel-Kasuya-Yosida (RKKY) indirect magnetic coupling. The Kondo effect describes the tendency of conduction electrons to screen localized magnetic moments, thus suppressing magnetic order via spin compensation. In contrast, the RKKY interaction tends to generate long range magnetic order of f-moments through spin polarization of conduction electrons. Thus, both Kondo effect and RKKY coupling depend on the interaction between localized f and delocalized conduction electrons. This coupling is measured by the exchange interaction J, which is a function of the degree of hybridization of localized and delocalized electrons. As a result, depending on the exchange interaction J, different magnetic ground states are observed in heavy fermion materials, ranging from long-range magnetic order to a Kondo compensated Fermi Liquid state.

Qualitative insight into the competition is provided by the Doniach model [17]-[18]. Doniach considered a system with one local magnetic moment in each crystallographic unit cell. A one-dimensional array of these localized spins is coupled to the conduction electrons by the exchange interaction J. The main assumption of the model is that the characteristic temperature scales depend only on the exchange parameter J and the density of states $N(E_F)$. The Kondo interaction is taken as

$$T_K \propto \frac{1}{N(E_F)}\, e^{-\frac{1}{|JN(E_F)|}}, \tag{2.6}$$

while the magnetic RKKY exchange evolves as

$$T_{RKKY} \propto J^2 N(E_F). \tag{2.7}$$

From the two dependencies $T_K(JN(E_F))$ and $T_{RKKY}(JN(E_F))$ the Doniach phase diagram is derived and displayed in Fig. 2.1.

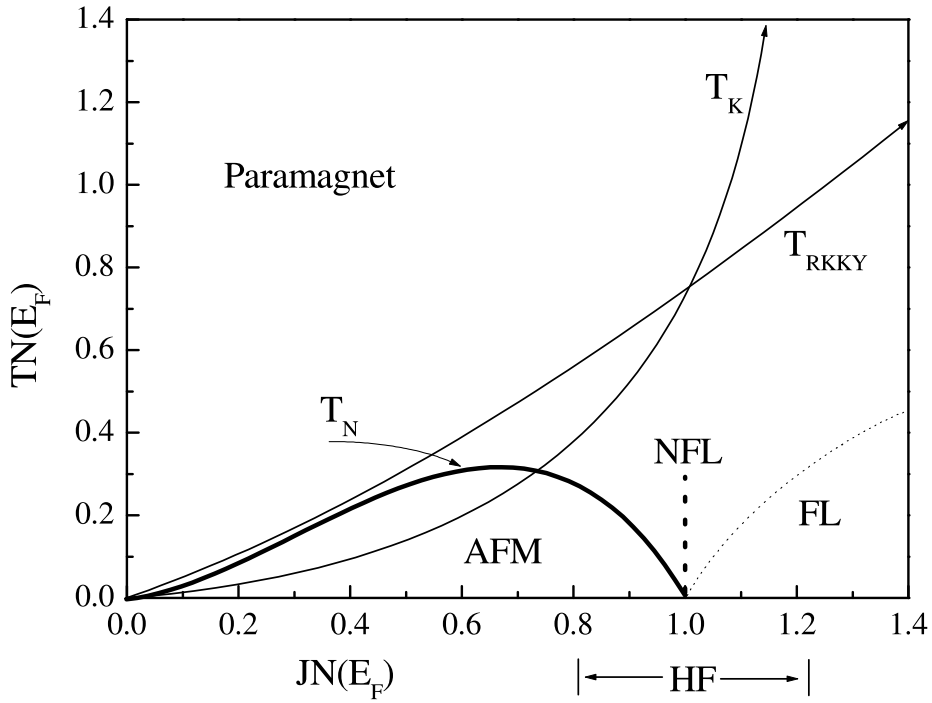

Figure 2.1: The Doniach phase diagram for a one-dimensional Kondo-lattice [18]. The dependencies of T_K and T_{RKKY} are shown schematically.

At $T = 0$, at a critical value $JN(E_F) := 1$, the phase diagram demonstrates a second-order phase transition from an antiferromagnetic to a Kondo-compensated ground state as function of the parameter $JN(E_F)$. The antiferromagnetic ordering temperature T_N, upon increasing $JN(E_F)$ from 0, first goes up, passes through

a maximum and subsequently goes to zero. Thus, in the phase diagram there are three qualitatively different regions:

1. $JN(E_F) \ll 1 \Leftrightarrow T_K \ll T_{RKKY}$: Magnetic coupling dominates over Kondo spin-compensation. In consequence, antiferromagnetic ordering (AFM) below a finite transition temperature T_N occurs.

2. $JN(E_F) \gg 1 \Leftrightarrow T_K \gg T_{RKKY}$: The magnetic moment is suppressed by Kondo screening, and no magnetic ordering occurs. Nevertheless, short range correlation between moments can happen. In this region, the system has a Kondo-singlet ground state and is well described by Fermi liquid theory.

3. $JN(E_F) \simeq 1 \Leftrightarrow T_K \simeq T_{RKKY}$: An intermediate state, which occurs close to an antiferromagnetic quantum critical point (QCP) [19]-[22]. Due to the coincidence of the two quantities T_K and T_{RKKY}, the magnetic transition temperature goes to zero. In this region, the properties of the system are extremely sensitive to small variations of the parameter $JN(E_F)$. Near the threshold to antiferromagnetic ordering, at the critical value $JN(E_F) = 1$, deviations from Fermi liquid behavior are commonly observed and referred to as Non-Fermi-Liquid (NFL) behavior.

2.1.2 Spin glasses

The term *spin glass* denotes a particular type of magnetic order, which is formed below a so called freezing temperature T_F (for general reviews see Mydosh [23], Maletta and Zinn [24], Moorjani and Coey [25] for experimental aspects; Binder and Young [26], Fischer and Hertz [27] for theoretical models). The magnetic state of a spin glass is characterized by the lack of translational invariance, this in contrast to the long-range ordered states of ferro- or antiferromagnets. Thus, the magnetic state of a spin glass is amorphous, with the spins frozen into locked positions and pointing in random directions. In order to produce such a state, two ingredients are necessary: There must be a competition among the different interactions between the magnetic moments, in a way that no single configuration of the spins is uniquely favoured by all the interactions (commonly called "frustration"), and these interactions must be at least partially random. An example for magnetic frustration is a regular triangle with antiferromagnetic exchange interaction between magnetic moments placed in the corners (Fig. 2.2). Here, for the spin on the lower right corner its direction is not well defined because of frustration. The second ingredient, the randomness of magnetic interactions, is induced by crystallographic disorder, either of the magnetic ions themselves (random site) or the non-magnetic ligands (random bond).

A material can be identified as a spin glass via different experimental methods. The following properties can be studied to establish typical spin glass behavior

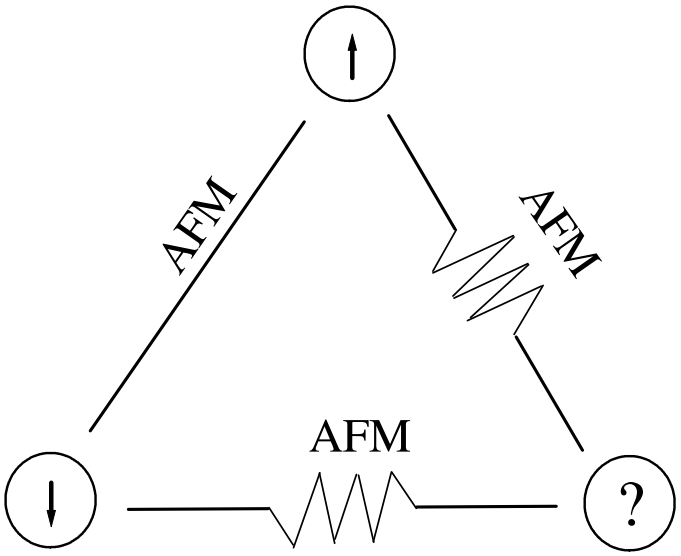

Figure 2.2: A schematic drawing illustrating magnetic frustration on AFM coupled triangle.

of a given system [23, 27]:

1. An indication for a spin glass is a sharp maximum in the temperature dependence of the magnetization, similar to a second-order phase transition from the disordered paramagnetic state.

2. The freezing temperature T_f, defined by the cusp in the ac susceptibility depends on frequency.

3. Magnetic irreversibility and remanence occurs below T_f. At low temperatures there is strong irreversibility between field cooled (FC) and zero field cooled (ZFC) measurements.

These properties of the spin glass state can be clearly observed only in comparatively small fields. Application of fields of a few hundred Gauss smear out the peak, with only a broad maximum remaining above a regime of magnetic irreversibility [23]. This behavior is schematically depicted for the dc-susceptibility $\chi_{dc} = M/B$ in Fig. 2.3 for a canonical spin glass system [28]. Here, the field-cooled (FC) and zero-field-cooled (ZFC) experiments are shown. In both cases χ_{dc} is measured as temperature increases in identical external fields B_{ext}. The difference reflects the history dependence of the spin glass state, as the system prior to the measurement is either cooled down in zero field ($\rightarrow$ ZFC) or the applied field B_{ext} ($\rightarrow$ FC). From the figure several temperatures which are characteristic for the crossovers traversed upon undergoing the spin glass freezing can be obtained. The irreversibility temperature T_{irr} is defined as the temperature, below

which the field-cooled measurement deviates from the zero-field-cooled experiment. The break temperature T_B represents the point, below which χ_{dc} deviates from Curie-Weiss behavior $\propto C/(T-\Theta_{CW})$. The freezing temperature T_F is obtained from the condition $d\chi/dT$=0. In the limit $B \rightarrow$0, T_f, T_{irr} and T_B coincide at the glass temperature, T_G^0 ($B \rightarrow$0) [28].

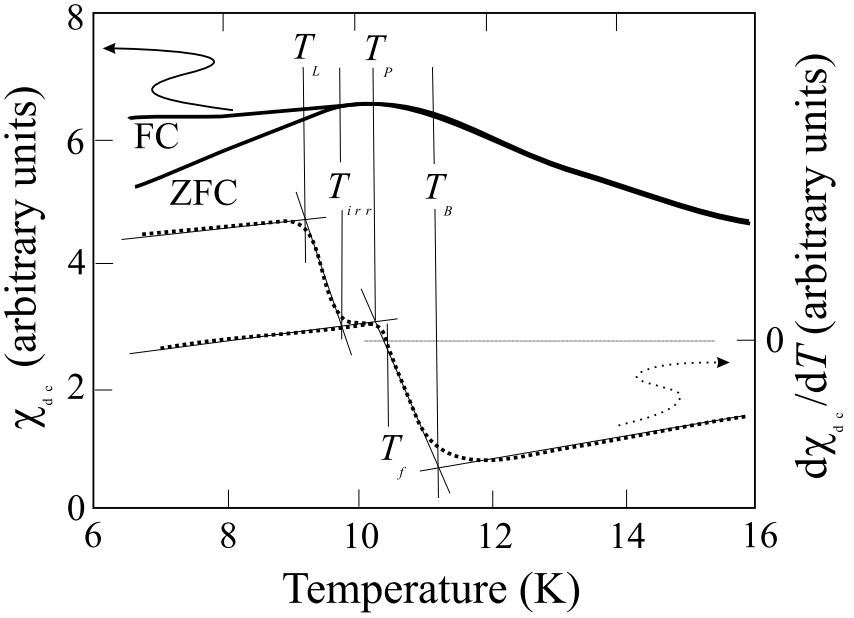

Figure 2.3: Dc susceptibility in the field cooled (FC) and zero field cooled (ZFC) mode (left scale) and its derivative (right scale) vs. temperature as illustration for the determination of the characteristic temperatures T_{irr}, T_f and T_B, as discussed in the text (from [28]).

The crossover temperatures depend on the applied magnetic field and can be summarized in a $B-T$ phase diagram (Fig. 2.4). The field dependence of the irreversibility temperature T_{irr} is associated with the Almeida-Thouless line [29]. In the corresponding theoretical models the Almeida-Thouless line, also referred to instability line, is defined by the following equation:

$$[1-\frac{T}{T_f^0}] \propto (\frac{\mu_B g B}{k_B T_f^0})^x \tag{2.8}$$

The exponent x depends on the spin model, *e.g.* for the Ising case x=2/3 [30, 31, 32].

The second line separates the high-temperature paramagnetic phase from the spin glass phase and is characterized by a freezing of spin components which are transverse with respect to applied field [32, 33] and determined from $T_f(B)$. In the limit of a model for m-component spins, the line, associated with the

Gabay-Toulouse crossover line, is derived as:

$$B^2 \propto 4\frac{m+2}{m+4}(1-\frac{T}{T_G^0}),\ \text{for}\ \frac{T}{T_G^0} \simeq 1 \tag{2.9}$$

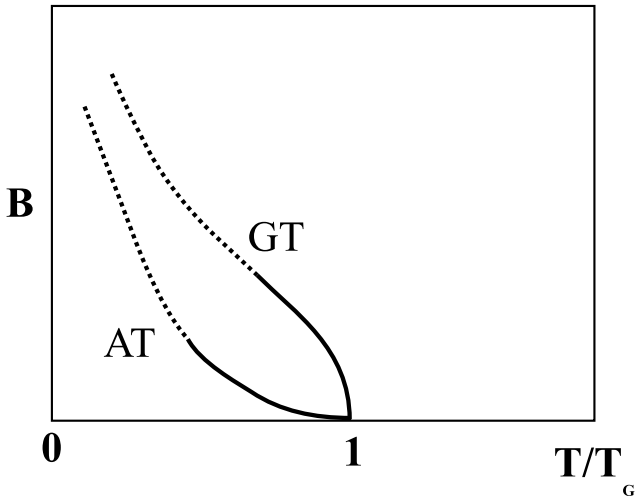

Figure 2.4: Phase diagram for classical vector spins (B magnetic field, T temperature). The line GT corresponds to the freezing of the transverse degrees of freedom (Gabay-Toulouse line), the line AT to the Almeida-Thouless line [29, 33] (for details see text).

2.2 Electric transport in solids

One of the basic approaches to describe the electronic transport in solids is the Bloch model. It is based upon the assumption of a gas of free and noninteracting electrons obeying to Fermi-statistic within the periodic potential of the crystal lattice (Bloch Electrons). Because of the strong electronic correlations, this model might not appear as a good starting point to describe the transport properties in heavy fermions. Yet, so far as the Fermi Liquid model holds for a heavy fermion, the matching between free electron approximation and the properties of the correlated electron systems renders applicability of the Bloch model. Only, for a microscopic description the enhanced effective mass m^* of the quasi-particles ought to be taken into account.

The Bloch concept expands the treatment of electronic transport beyond the Drude model. Hence, the electrical conductivity σ, defined via current density j and electric field E as $j = \sigma E$, is expressed in a Drude-like equation [34, 35, 36]:

$$\sigma = \frac{ne^2\tau(E_F)}{m^*}, \tag{2.10}$$

where $\tau(E_F)$ is the relaxation time of the electrons at the Fermi surface. The temperature dependence of the electrical resistivity $\rho = 1/\sigma$ follows from the temperature dependence of the relaxation time $\tau(E_F)$, and reflects a disturbance of the periodicity of the lattice.

Commonly, the temperature dependence of the resistivity of a metal containing impurities is written in the form:

$$\rho(T) = \rho_0 + \rho_{e-p}(T) + \rho_{e-e}(T), \tag{2.11}$$

with ρ_{e-p} and ρ_{e-e} as resistivities from electron-phonon and electron-electron scattering, and ρ_0 the residual resistivity from potential scattering off the impurities. This relationship with a temperature independent ρ_0 is known as Matthiessen's rule. For common metals, at sufficiently high temperatures electron-phonon scattering is the dominant resistive contribution, yielding $\rho_{e-p} \propto T$ at $T \gg \Theta_D$ and $\rho_{e-p} \propto T^5$ at $T \ll \Theta_D$, with Θ_D as the Debye temperature. In contrast, the contribution from electron-electron scattering follows a T^2-dependence at low temperatures.

Now, various metallic disordered systems exhibit pronounced deviations from this type of transport. For instance, irradiated $LuRh_4B_4$ [37] or heavy fermion $UPd_{1.85}Sn$ [38] and URh_2Ge_2 [39] exhibit a negative temperature coefficient $d\rho/dT < 0$ below room temperature, that is a non-metallic resistivity. The absolute value of the resistivity for these systems is of the order of 100-1000$\mu\Omega$cm, which is very large for a metal, but too small for a semiconductor or insulator.

Up to now, this behavior is not well understood. In particular for the heavy fermion representatives there are three basic concepts to account for a non-metallic electronic transport. The first model is the concept of electronic localization. Its principles have been introduced by Anderson, who demonstrated that in random electronic potentials from disorder "localization" of the one-electron wave functions can occur if the random component is large enough [40]. In consequence, the electronic transport properties of a material can show a transition from a metallic to a non-metallic behavior upon increasing the disorder.

Alternatively, in heavy fermion systems it could be argued that anomalous electronic transport is a consequence of a gapped Fermi surface in the presence of a strongly correlated electrons. In heavy fermion compounds, the high temperature state is believed to consist of a lattice of uncorrelated f ions, each independently scattering conduction electrons via the Kondo mechanism. At low temperatures intersite correlations develop, and one of two different types of a coherent ground state can occur. In most cases the ground state is metallic (paramagnetic, antiferromagnetic or superconducting), but in some cases like SmB_6 [41], YbB_{12} [42], $CeFe_4P_{12}$ [43], $Ce_3Bi_4Pt_3$ [44], the ground state is insulating with a small energy gap. The energy gap, leading to a non-metallic electronic transport, is believed to originate from the hybridization of the localized f-state with a half-filled conduction band. The strong electronic correlations then persist in the non-gapped

regimes of the density of states. This class of materials has been labelled Kondo insulators. Often, crystallographic disorder in these materials generates electronic states in the gap, and thus its closure. In consequence, similar to semiconductors a "doping-induced" transition from non-metallic to metallic behavior might be observed under these circumstances.

There is a third aspect to be considered for strongly correlated electron systems, that is the Coulomb repulsion between electrons. A number of compounds with partially filled $f(d)$-electron bands exhibit an isolating behavior (a typical example is NiO [45]). The origin of the non-conducting state was attributed by Mott [46] to strong electron-electron correlations via the Coulomb repulsion. This insulating state received the name of *Mott insulator* and a transition into this non-conducting phase is called a $metal - insulator\ transition$ (MIT). Mott considered a lattice model with a single electronic orbital on each site. Without electron-electron interactions, a single band would be formed from the overlap of the atomic orbitals in this system, where the band is filled when two electrons with spin-up and spin-down occupy each site. Now, because of the Coulomb repulsion, energetically it is less favorable for two electrons to sit on the same site, which Mott argued would split the band in two: The lower band formed from electrons that occupy an empty site and the upper one from electrons that occupy a site already taken by another electron. In this situation, the electronic transport properties (metallic or non-metallic) of a given material will depend on the site occupation and Coulomb repulsion. The effect of crystallographic disorder on the properties of a Mott insulator is essentially unsolved, as is the relationship between the Anderson model of electronic localization and the Mott concept of electronic correlation.

In order to establish which of the three concepts should be applied to disordered heavy fermion systems a very thorough characterization of the electronic transport properties has to be carried out. Here, one central transport quantity is the carrier density, which for a material is commonly determined via a Hall effect measurement.

When a magnetic field is applied at right angles to the current flow, an electric field E_H perpendicular to current and magnetic field is generated because of the Lorentz force (Fig. 2.5). The corresponding voltage V_H across the sample of thickness d is proportional to the product of current density I and magnetic induction B,

$$V_H = \frac{R_H I B}{d}, \tag{2.12}$$

where R_H is the Hall coefficient.

In case of electrons and holes contributing to the transport, the contributions from each band and carrier type need to be taken into account. Specifically, for a simple spherical Fermi surface in small magnetic fields for the Hall coefficient

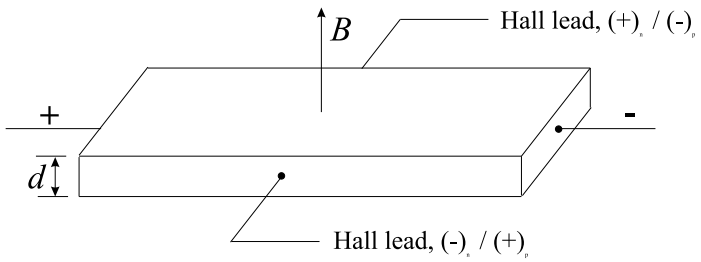

Figure 2.5: A sketch for the measurement of the Hall effect. The indexes (+) and (-) imply n and p type materials.

we find

$$R_H = \frac{(1/e)(\mu_h^2 n_h - \mu_e^2 n_e)}{(\mu_h n_h + \mu_e n_e)^2}. \tag{2.13}$$

Here, μ_e and μ_h represent the mobilities of holes and electrons, and n_e, n_h the corresponding carrier densities. If one carrier type dominates electronic transport, say the electrons, the relationship simplifies to

$$R_H = -\frac{1}{en_e}. \tag{2.14}$$

In this situation for the Hall mobility it is found

$$\mu_e = \frac{e\tau}{m^*}. \tag{2.15}$$

Commonly, to analyze the temperature dependence of the Hall constant in heavy fermion materials it is decomposed into ordinary and skew scattering contribution [47]:

$$R_H = R_0 + \chi\rho_{mag}R_{S,Kondo}. \tag{2.16}$$

Here, R_0 represents the ordinary Hall constant and measures the carrier density. The second term $\chi\rho_{mag}R_{S,Kondo}$ arises from anomalous Skew scattering in heavy fermions (ρ_{mag} magnetic resistive contribution, χ magnetic susceptibility).

Beyond the simple theoretical picture of the Hall effect sketched so far, in the real experiment several related galvanomagnetic effects will be encountered. Hence, to extract the Hall contribution from the experimental result care has to be taken that accompanying effects will be separated out. As the determination of the Hall effect represents a central experimental result of this thesis, in the following a more detailed account of the experimental procedure will be given. We will only discuss Hall effect measurements of bulk samples with a simple, rectangular shape. The Hall measurements of samples of irregular shape or thin films will not be considered (see, for example, van der Pauw method [48]).

In a real experiment following the sketch in Fig. 2.5 there will be two distinct contributions to the output signal. The first one is from the Hall voltage, but

in addition there will be a magnetoresistance contribution because of the non-perfection of the voltage contacts. First of all, the two voltage leads might not be arranged perfectly opposite to each other, thus giving rise to a magnetoresistive voltage. Further, the shape of the contacts play an important role. Since the thickness of the sample is inversely proportional to the Hall voltage, the contact spot should cover the full height of the sample. At the same time, the width of the spot should be as narrow as possible, because the broadening of the contacts gives rise to a magnetoresistive signal.

To suppress the magnetoresistive signal completely the 5-point or balance method can be employed. Similar to the arrangement in Fig. 2.5, the current leads and one voltage A lead will be attached. In addition, two (B and C) instead of one second voltage lead should be attached to the side opposite to voltage lead A such that the magnetoresistive signal A-B is positive and A-C negative. By means of an electrical divider a balance at zero magnetoresistive potential can be attained between the two leads B and C. This way, the output signal is directly the Hall voltage.

Still, there are some disadvantages. In small samples the method is prone to experimental errors arising from curvature of the current flow. Moreover, the third voltage lead triggers extra noise. This might be problematic especially for low temperature measurements, when the electrical divider cannot be positioned close to the sampleholder. Then, in particular for metallic samples the noise level might exceed the low field Hall signal. It can be an obstacle for experiments with systems like spin glasses, where high fields alter the magnetic state or induce magnetic irreversibility, making it hard to analyze the data because of the anomalous Hall component being proportional to the susceptibility χ.

All in all, the results presented in this thesis were obtained by means of a standard 4-point method and using ac-currents. Experimentally, it was necessary to reduce the signal-to-noise ratio by long-time averaging (300 seconds) of the signal. To separate magnetoresistive and Hall contribution the experiments have been carried out by measuring the signal for opposite fields. Here, it is utilized that upon switching the field direction the Hall voltage changes its sign, while the magnetoresistance does not. Hence, by extracting symmetric and antisymmetric voltage contributions the two components can be separated.

2.3 Basic aspects of crystallographic disorder

The effect of crystallographic disorder on the properties of strongly correlated electron systems has scarcely been studied so far. However, this issue in particular concerns heavy fermion compounds, as here both competing interactions – the RKKY magnetic exchange and the Kondo effect – strongly depend on the level of crystallographic disorder. In consequence, the ground state properties of a heavy fermion system as result of the competition between the two interactions

also depend on the disorder level. Still, a detailed understanding of the effect of disorder on the properties of heavy fermion compounds is lacking.

So far, only a handful theoretical and experimental studies on disorder effects in heavy fermions have been presented. From the theoretical side, within dynamical mean field theory it was shown that sufficient disorder can cause substantial modifications of the low temperature properties of a heavy fermion system, resulting in a breakdown of conventional Fermi liquid behavior [49, 50]. Correspondingly, it has been shown experimentally that certain heavy fermion related systems like $UCu_{5-x}Pd_x$ [51]-[53] or $U_{1-x}Th_xPd_2Al_3$ [54] in the presence of disorder exhibit NFL behavior at low temperatures. Specifically, for $UCu_{5-x}Pd_x$ this had been attributed to a disorder induced local distribution of the Kondo temperature T_K [49], or the combined effect of a distribution of T_K and a locally varying RKKY coupling strength [50]. Neither proposal, however, is generally accepted from theoretical side, nor has been clearly demonstrated as valid model in experimental investigations.

In particular, treating the RKKY interaction in the presence of crystallographic disorder is a complex task. As yet, it has only been done in the limit of weak disorder, which corresponds to a case like that of the dilute spin glass, *i.e.*, one percent of a magnetic impurity diluted in a non-magnetic matrix [55, 56, 57]. It is unclear, in how far the results obtained in this limit can be extrapolated to moderate levels (10 %) of crystallographic disorder. In addition, it has been shown that in strongly correlated electron systems the "efficiency" of the disorder is enhanced by electronic correlations [58], possibly indicating that the weak disorder limit is not adequate for archetypical strongly correlated systems like heavy fermions.

In this situation, phenomenological approaches have been put forward, one of which schematically is illustrated in Fig. 2.6. Here, a "Doniach-style" phase diagram of the ground state properties of heavy fermion compounds is plotted, only the tuning parameter now is the level of crystallographic disorder. This phase diagram was presented by S. Süllow, and is based on various experimental observations. It reflects that as function of disorder the type of the magnetic ground state can be altered from long range antiferomagnetically ordered to a spin glass to NFL behavior. Moreover, now the NFL regime, because of the distribution of local interaction parameters, extends over some range of the tuning parameter. The change of the magnetic ground state is accompanied by a transition from a metallic to a non-metallic electronic transport. In the chapters 4 and 5 of this thesis we will present experimental observations in line with the basic concepts of this phenomenological phase diagram.

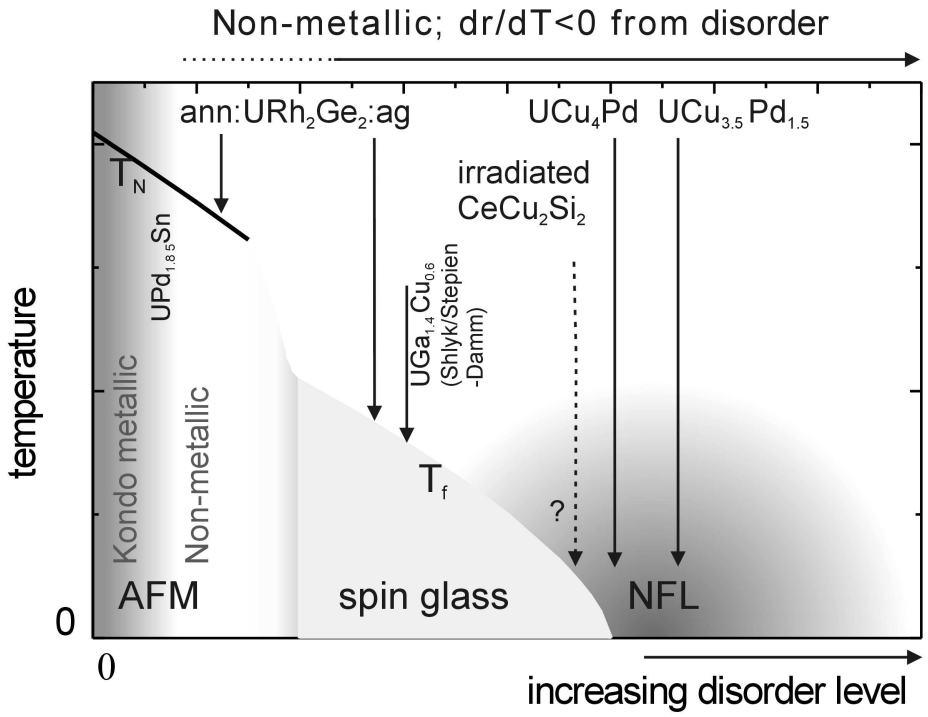

Figure 2.6: The schematic phase diagram depicting the ground state properties of heavy fermion systems as function of the level of crystallographic disorder, as presented by S. Süllow at the DPG-meeting in Regensburg (2002).

Bibliography

[1] N. Grewe and F. Steglich. Heavy Fermions. In: Gschneider K.A., Eyring L. (eds.) *Handbook on the physics and Chemistry of the Rare Earth*, Vol. **14**, Elsevier, Amsterdam, (1991) 343-474.

[2] F. Steglich et al., *Heavy fermion superconductivity*, Physica B **126** (1984) 82.

[3] F. Steglich et al., *Classification of strongly correlated f-electron systems*, J. Low Temp. Phys. **99** (1995) 267.

[4] Z. Fisk et al., *Heavy-electron metals*, Nature **320** (1986) 124.

[5] Z. Fisk et al., *Heavy-electron metals: new highly correlated states of matter*, Science **239** (1988) 33.

[6] A.C. Hewson. *The Kondo Problem to Heavy Fermions*. Cambridge University Press, Cambridge, 1993.

[7] P. Fulde, J. Keller und G. Zwicknagl, *Theory of heavy fermion systems*, Solid State Phys. **41** (1988) 1.

[8] P. Fulde. *Electron Correlations in Molecules and Solids*, Springer, Berlin, 1993.

[9] G. Zwicknagl, *Quasi-particles in heavy-fermion-systems*, Adv. Phys. **41** (1992) 203.

[10] G. Zwicknagl, *Quasiteilchen in Schwere-Fermionen-Verbindungen*, Phys. Bl. **49** (1993) 657.

[11] T. Brugger et al., Phys. Rev. Lett. **71** (1993) 2481.

[12] S. Kondo et al., Phys. Rev. Lett. **78** (1997) 3729.

[13] S.I. Woods et al., Phys. Rev. B **66** (2002) 014538.

[14] J.T. Markert et al., Physica C **158** (1989) 178.

[15] S. Ghamaty et al., Physica C **160** (1989) 217.

[16] Z. Fisk, H.R. Ott und G. Aeppli, *Experimental perspectives on heavy-electron metals*, Jpn. J. Appl. Phys. 26 Suppl. **3** (1987) 1882.

[17] S. Doniach, Physica B **91** (1977) 231

[18] S. Doniach, *in Valence Instabilities and Related Narrow-Band Phenomena*, edited by R.D. Parks, Plenum Press, New York (1993) 435.

[19] J. Hertz, Phys. Rev. B **14** (1976) 1165.

[20] A. Millis, Phys. Rev. B **48** (1993) 7183.

[21] T. Moriya and T. Takimoto, J. Phys. Soc. Jpn. **64** (1995) 960.

[22] S. Kambe et al., J. Phys. Soc. Jpn. **65** (1996) 3294.

[23] J.A. Mydosh, *Spin Glasses: An Experimental Introduction* (Taylor&Francis, London, Washington, 1993).

[24] H. Maletta und W. Zinn, *Spin glasses*. In: K.A. Geschneider und L. Eyring, *Handbook of the Physics and Chemistry of Rare Earths*. Elsevier, Amsterdam (1989).

[25] K. Moorjani and J.M.D. Coey. *Magnetic Glasses*. Elsevier, Science, Amsterdam (1984).

[26] K. Binder and A.P. Young. *Spin glasses : experimental facts, theoretical concepts and open questions*, Rev. Mod. Phys. **58** (1986) 801.

[27] K.H. Fischer and J.A. Hertz, *Spin glasses* Cambridge University Press, Cambridge (1991).

[28] R.V. Chamberlin et al., Phys. Rev. B **25** (1982) 6720.

[29] J.R.L. de Almeida and D.J. Thouless, J. Phys. A **11** (1978) 983

[30] G. Parisi and G. Toulouse, J. Phys. Lett. **41** (1980) L361.

[31] J. Vannimenus, G. Toulouse and G. Parisi, J. Phys. **42** (1981) 565.

[32] G. Toulouse and M. Gabay, J. Phys. Lett. **42** (1981) L103.

[33] M. Gabay and G. Toulouse, Phys. Rev. Lett **47** (1981) 201

[34] N.W. Ashcroft and N.D. Mermin, *Solid State Physics*, Saunders College Publishing, New York (1976).

[35] C. Kittel, *Introduction to Solid State Physics*, John Wiley & Sons, New York, London, Sydney (1967).

[36] P.L. Rossiter, *The Electrical Resistivity of Metals and Alloys*, Cambridge University Press, Cambridge (1991)

[37] R.C. Dynes, J.M. Rowell and P.H. Schmidt, in *Ternary Superconductors*, North-Holland, Amsterdam (1981) 169.

[38] I. Maksimov et al., Physica B **312-313** (2002) 283.

[39] S. Süllow et al., Phys. Rev. Lett. **78** (1997) 354; Phys. Rev. B **61** (2000) 8878.

[40] P.W. Anderson, Phys. Rev. **109** (1958) 1492.

[41] J. Allen, B. Batlogg and P. Wachter, Phys. Rev. B **20** (1979) 4807.

[42] M. Kasaya et al., J. Magn. Magn. Mater. **31-34** (1983) 437. M. Kasaya et al., J. Magn. Magn. Mater. **47-48** (1985) 429. F. Iga, M. Kasaya and T. Kasaya, J. Magn. Magn. Mater. **76-77** (1988) 156.

[43] G. Meisner et al., J. Appl. Phys. **57** (1985) 3073.

[44] M. Hundley et al., Phys. Rev. B **42** (1990) 6842.

[45] J.H. de Boer and E.J.W. Verwey, Proc. Phys. Soc. (London) **49** (1937) 59.

[46] N.F. Mott, Rev. Mod. Phys. **40** (1968) 677.

[47] P. Levy and A. Fert, Phys. Rev. B **36** (1987) 1907.

[48] L.J. van der Pauw, Philips Res. Rep. **13** (1958) 1.

[49] E. Miranda, V. Dobrosavljević and G. Kotliar, Phys. Rev. Lett. **78** (1997) 290.

[50] A.H. Castro Neto, G. Castilla, and B.A. Jones, Phys. Rev. Lett. **81** (1998) 3531.

[51] B. Andraka and G.R. Stewart, Phys. Rev. B **47** (1993) 3208.

[52] M.C. Aronson et al., Phys. Rev. Lett. **75** (1995) 725.

[53] O.O. Bernal et al., Phys. Rev. Lett **75** (1995) 2023.

[54] M.B. Maple et al., J. Low Temp. Phys. **99** (1995) 223.

[55] I. Lerner, Phys. Rev. B **48** (1993) 9462.

[56] M. Hitzfeld and P. Ziemann, Phys. Rev. B **32** (1985) 3026.

[57] D. Vier and S. Schultz, Phys. Rev. Lett. **54** (1985) 150.

[58] K.I. Wysokinski, Phys. Rev. B **60** (1999) 16376.

3 Structure and magnetic order in $Fe_{2+x}V_{1-x}Al$

3.1 Introduction

Recently, the magnetic phase diagram of the alloying series $(Fe_{1-x}V_x)_3Al$ has been the focus of various detailed studies [1, 2]. In particular, Heusler-type Fe_2VAl has been reported to exhibit a very unusual behavior for an intermetallic compound, namely a semiconductor-like resistivity close to a magnetic instability [1]. This was interpreted in terms of Kondo-insulating behavior, analogous to the system $FeSi$ [3, 4]. In contrast, optical conductivity studies provided evidence for a pseudogap in the density of states of Fe_2VAl of 0.1-0.2eV [5], a view supported by various band structure calculations [6]-[8]. Notably, no temperature dependence of the gap features has been detected in these studies, apparently contradicting a Kondo insulator scenario for Fe_2VAl. However, the pseudogap scenario itself does not account for the unusual resistivity of Fe_2VAl, as in the absence of magnetic correlations it should predict no or a positive, metallic magnetoresistance, in conflict with experimental observations [2, 9]. Therefore, tentatively, in Ref. [5] it has been speculated that the (magneto)resistivity of Fe_2VAl reflects a mixture of electron excitation processes over the pseudogap and spin dependent scattering from impurities.

Independently, on basis of specific heat and NMR-experiments it has been demonstrated that in Fe_2VAl crystallographic disorder, assumed to be present in form of atomic site exchange between Fe and V atoms, substantially affects the ground state properties of this compound [10, 11]. In particular, the anomalous low temperature specific heat has been attributed to ferromagnetic clusters with a density of 0.003-0.004/unit cell, consistent with the results from NMR experiments. These works, as well, are in broad agreement with the results from band structure calculations, which predict that via Fe/V site exchange or crystallographic superstructure formation ferromagnetic clusters or long-range order might be generated in Fe_2VAl [6]-[8]. Recently, it has been claimed that such impurity induced ferromagnetism was observed in the related Heusler compound Fe_2TiSn [12].

Matsushita and Yamada [13] found that the bulk properties of Fe_2VAl exhibit a very strong dependence on the applied heat treatment. They demonstrated

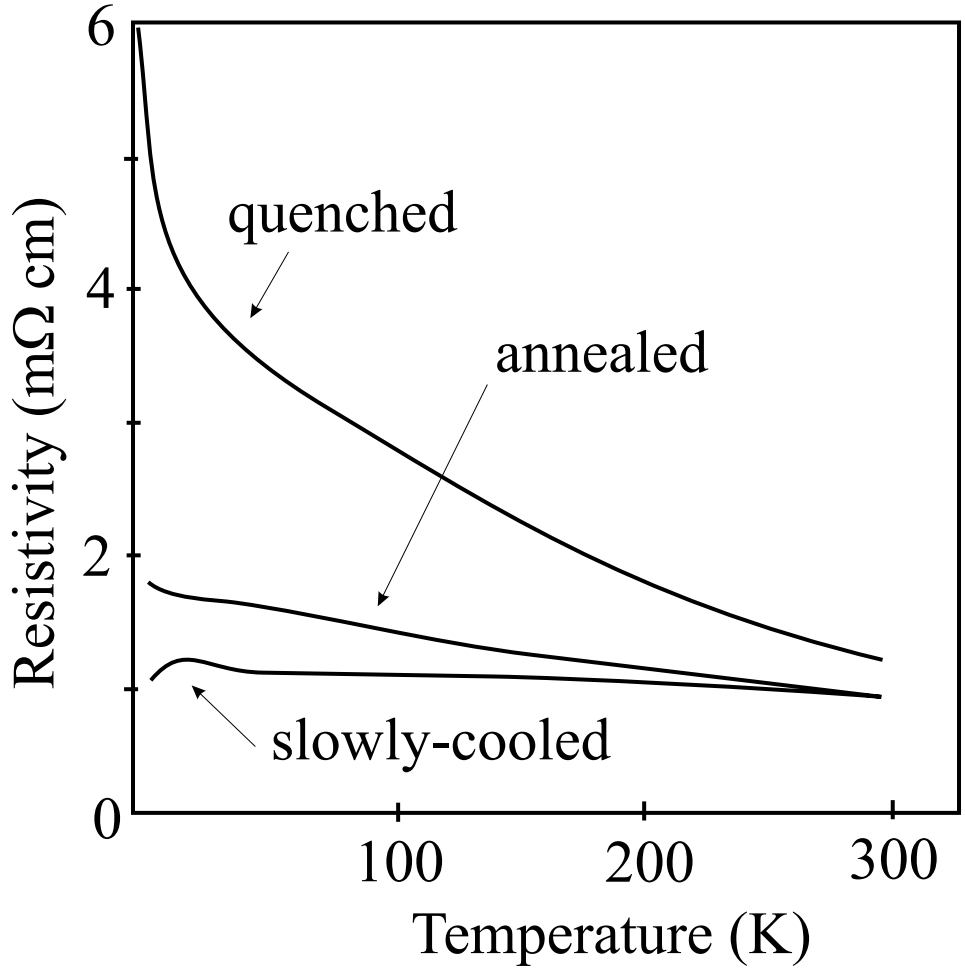

Figure 3.1: Effect of the heat treatment on the electrical resistivity of Fe_2VAl. The sketch is reploted from Ref. [13].

that by way of different cooling procedures after an annealing stage the nature of the ground state of Fe_2VAl can be tuned: while quenched material exhibits the previously reported semiconducting-like, non-magnetic behavior [1], a sample slowly cooled down to room temperature after a heat treatment shows almost metallic transport and a ferromagnetic transition at $T_C = 13$K (Fig. 3.1). Specific heat measurements assert the bulk nature of the magnetic transition in the slowly cooled samples. However, X-ray experiments do not show a significant difference between quenched and slowly cooled samples.

In this context, the question arises if any or which material - slowly cooled or quenched Fe_2VAl - represents the intrinsic behavior of this compound. Based on the band structure, specific heat and NMR results, it would have to be argued that in slowly cooled material either a crystallographic superstructure has been formed [6] or that a larger level of Fe/V site exchanges is present [7, 8], both

which might generate long-range magnetic order. Metallurgically, this is counter-intuitive, as the slow cooling procedure should allow the system a more complete relaxation from internal strain and non-equilibrium site occupations, compared to the freezing in of such forms of crystallographic disorder in the quenched material. Further, since ferromagnetism in slowly cooled Fe_2VAl is a bulk phenomenon, in the absence of a crystallographic superstructure it requires a drastic increase of the number of Fe/V site exchanged positions from the value in the quenched material, 0.003-0.004/unit cell, probably up to the level of the percolation limit, *i.e.*, ∼10-20%, in slowly cooled samples. Such a strong dependence of the number of Fe/V site exchanges on the cooling procedure would require a critical re-examination of previous results on Fe_2VAl. Finally, if the resistivity, as suggested in Ref. [5], largely arises from spin dependent scattering, then the very strong reduction of the resistivity in the slowly cooled sample rather indicates a reduction of disorder scattering, in conflict with a view of impurity induced ferromagnetism.

Given this contradictory experimental situation we decided to perform a thorough structural and magnetic investigation of slowly cooled Fe_2VAl, concentrating here on microscopic experimental techniques, complementary to the bulk experiments executed so far [13]. In particular, we performed a high resolution neutron diffraction study and Mössbauer spectroscopy on slowly cooled and quenched Fe_2VAl. In addition, we performed similar investigations on other samples from the alloying series $Fe_{2+x}V_{1-x}Al$, $x > 0$, in order to obtain reference data. Further, we present a study of slowly cooled Fe_2VAl by means of muon spin relaxation. We have chosen these techniques for the following reasons:

1. If a crystallographic superstructure is formed in slowly cooled Fe_2VAl, it should be detectable in diffraction experiments. The contrast between Fe, V and Al in X-ray diffraction, because of similar atomic weights, is weak, and might hinder an observation of a superstructure. Therefore, neutron diffraction experiments are more suitable, as Fe, Al and V have very different neutron scattering lengths yielding a bright contrast (Fe: 9.45*10^{-15}m; Al: 3.45*10^{-15}m; V: -0.38*10^{-15} m). Further, a superstructure might give rise to different local environments resolvable in Mössbauer spectra, that is in form of a double peak spectrum resulting from different isomer shifts at inequivalent lattice sites.

2. ^{57}Fe-Mössbauer spectroscopy and muon spin relaxation are used to characterize the magnetic properties microscopically. In addition to long range magnetic order these local probe techniques allow to examine inhomogeneous magnetic states caused by crystallographic disorder. However, the expected size of the average magnetic moment in Fe_2VAl ($\sim 0.1\mu_B$) is at the sensitivity limit of Mössbauer-spectroscopy. Therefore, muon spin relaxation has been used as the most sensitive microscopic method to examine static magnetic order.

3. If magnetic order stems from a large number (∼10%) of Fe/V site exchanged positions, with the bright Fe/V contrast this should be resolved in a neutron diffraction experiment, and possibly in Mössbauer spectroscopy and muon spin relaxation studies.

4. Repeating similar experiments for a number of samples $Fe_{2+x}V_{1-x}Al$, $x > 0$, enables us to compare the results on nominally ordered Fe_2VAl to those deliberately containing crystallographic disorder, thus allowing us to assess the relevance of disorder for the magnetic ground state of the systems.

We note that previously Mössbauer experiments have been performed on $Fe_{2+x}V_{1-x}Al$, -0.1 $\leq x \leq$ 1 [14, 15]. In these works broad field distributions in the magnetically ordered state have been observed, which however have been interpreted in terms of magnetic fluctuations, in variance with the present view of long-range magnetic order. Further, the magnetic phase diagram determined in Ref. [15] differs greatly from that in [1, 16], thus adding to the inconsistencies, and Fe_2VAl was not specifically considered in these works.

3.2 Metallurgy

The polycrystalline samples $Fe_{2+x}V_{1-x}Al$ have been supplied by A. Matsushita, Institute of Metals Research, Tsukuba, Japan. For preparation, the stoichiometric mixtures of the constituent elements Fe (4N), V (3N) and Al (5N) have been arc-melted in a copper crucible under argon (5N) atmosphere and simultaneous Ti-gettering [13]. The weight loss during this process was less then 0.5%. The specimens were cut from the polycrystalline ingot and sealed in evacuated quartz ampoules for the heat treatment. Initially, the two samples Fe_2VAl were homogenized at 1273K for 24h. The first sample (referred to as "q-Fe_2VAl") was quenched in water after the heat treatment. The second one (referred to as "sc-Fe_2VAl") was slowly cooled to 553K at a rate of 6K/h, and subsequently furnace cooled. Other samples $Fe_{2+x}V_{1-x}Al$ (x=0.5, 0.1, 0.02, 0.01) were cooled down to 373K at a rate of -60K/h after homogenization at 1273K during 15h. Scanning electron microscopy (SEM) pictures have been taken on the samples, indicating that the materials consist of a homogeneous majority phase, with small inclusions of pure Al or Al oxides.

The samples have been characterized via resistivity and susceptibility, and for $Fe_{2+x}V_{1-x}Al$, x=0.5, 0.1, 0.02, 0.01 and q-Fe_2VAl they exhibit the previously reported behavior [1, 16], with a suppression of magnetic order and a tendency towards semiconductivity as $x = 0$ is approached. In contrast, sc-Fe_2VAl has a ferromagnetically ordered ground state and a more metallic resistivity, as reported in Ref. [13]. The transition temperatures, determined from the resistivity experiments, are: $x = 0.5$: $T_C > 300$K; 0.1: $T_C = 28$K, $x = 0.02$, 0.01 and q-Fe_2VAl: $T_C < 2$K; sc-Fe_2VAl: $T_C = 13$K.

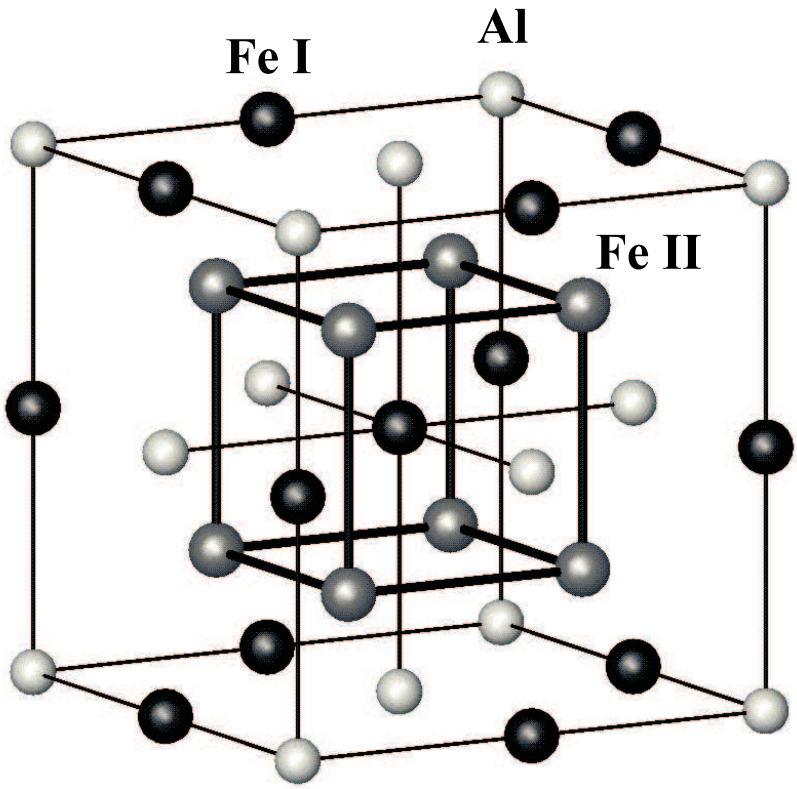

Figure 3.2: The cubic DO_3 lattice of Fe_3Al, with the two inequivalent Fe sites at Fe I: $(\frac{1}{2}\ \frac{1}{2}\ \frac{1}{2})$, and Fe II: $(\frac{1}{4}\ \frac{1}{4}\ \frac{1}{4})$ and $(\frac{3}{4}\ \frac{3}{4}\ \frac{3}{4})$.

3.3 Neutron scattering

The structure of $Fe_{2+x}V_{1-x}Al$, 0 ≤ x ≤ 1, derives from the cubic DO_3 lattice of Fe_3Al. In this lattice Fe occupies two crystallographically inequivalent sites (Fig. 3.2): Fe I on $(\frac{1}{2}\ \frac{1}{2}\ \frac{1}{2})$, and Fe II on $(\frac{1}{4}\ \frac{1}{4}\ \frac{1}{4})$ and $(\frac{3}{4}\ \frac{3}{4}\ \frac{3}{4})$, respectively. It is assumed that for $x \leq 1$ the V ion almost entirely replaces Fe on the Fe I site [1]. For $x = 1$, that is for Fe_2VAl, this leads to a fully ordered Heusler lattice, with Fe, V and Al each occupying separate cubic sublattices. Band structure calculations [6]-[8] indicated that in Fe_2VAl each Fe ion occupying an Fe I site carries a magnetic moment. This requires a site exchange of V with an Fe II ion, which might cause, either via superstructure formation (*i.e.*, V occupying exclusively one Fe II site) or a sufficiently large level of random Fe II/V site exchanges, a magnetically ordered state or anomalous behavior from diluted magnetic clusters.

In Fig. 3.3 we plot the calculated neutron diffraction intensities for above three structural modifications of Fe_2VAl: the fully ordered Heusler lattice, 10% random Fe II/V site exchange and a superstructure with V entirely occupying one Fe II site. Qualitative and quantitative differences between the calculated spectra are

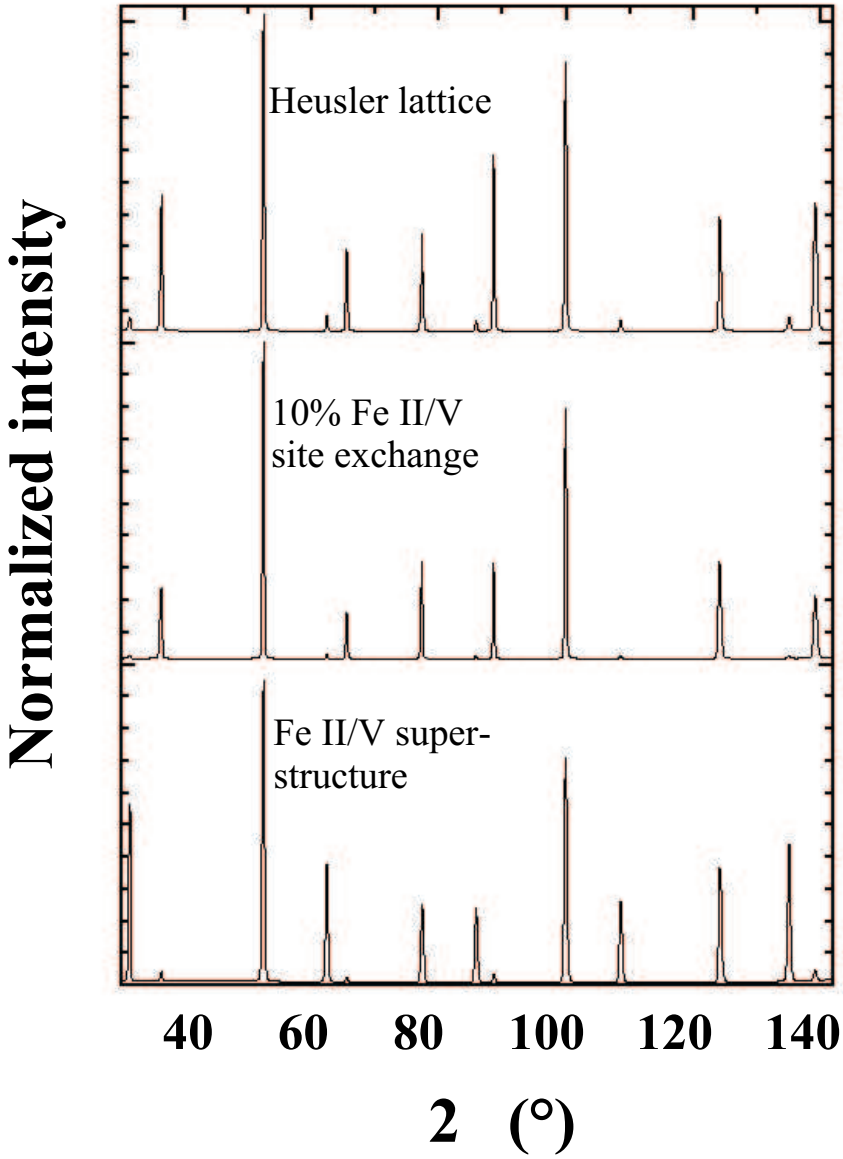

Figure 3.3: The calculated normalized neutron diffraction intensities for three different structural modifications Fe_2VAl: the fully ordered Heusler lattice (V on Fe I site), 10% Fe II/V site exchange and V entirely occupying one Fe II site, giving rise to a superstructure.

clearly visible, indicating that in a high resolution neutron diffraction experiment the level of Fe II/V site exchanged positions should be resolvable down to about 3% Fe on V sites.

Powder neutron diffraction data on $Fe_{2+x}V_{1-x}Al$, $0 \leq x \leq 0.5$, have been taken on the Fine-Resolution-Powder-Diffractometer E9 [17] at the Berlin Neu-

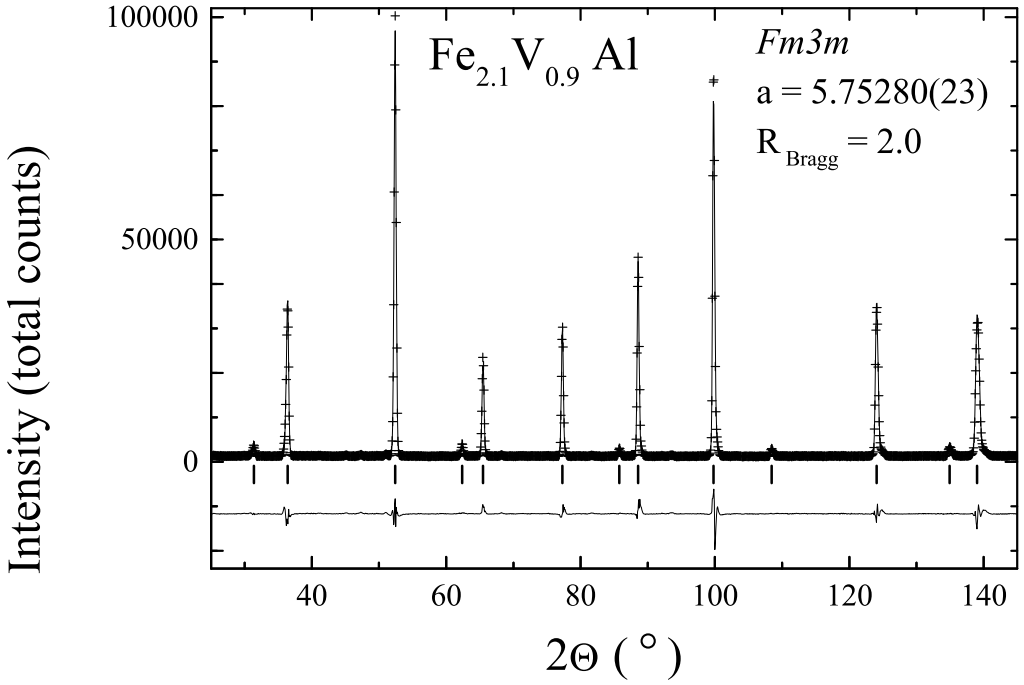

Figure 3.4: The neutron diffraction spectrum of $Fe_{2.1}V_{0.9}Al$, measured at 50K (+). Included is a refined fit to the data, the difference between fit and data, and tics indicating Bragg peak positions.

tron Scattering Center, HMI, Berlin. The diffractograms have been recorded in the region 2Θ = 5 - 155°, with an incident neutron wavelength λ = 1.7964(1) Åat temperatures T = 50K. Full Rietveld structure refinements of the diffraction data were performed employing the program WinPLOTR/FULLPROF [18]. Typical results are presented in Fig. 3.4, where we plot the data for the sample with nominal composition $Fe_{2.1}V_{0.9}Al$. In the plot we include the refined fit, Bragg peak positions and the difference between fit and data. Spectra of similar high statistics have been taken for both samples (q- and sc-) Fe_2VAl, and for $Fe_{2+x}V_{1-x}Al$, x = 0.02, 0.5 (see Appendix).

All spectra correspond to the fully ordered cubic $Fm\bar{3}m$ Heusler structure with some site disorder; a formation of a crystallographic superstructure has not been detected for any sample. In addition, for all samples between one and five Bragg peaks from an impurity phase, aside from those reflections coming from the $Fm\bar{3}m$ lattice, have been observed. In view of the SEM results, the second phase probably is pure Al or Al oxides; the relative intensity of the corresponding Bragg peaks is low (between 0.3 to 1.3% for the largest peak), implying a small volume amount of this second phase (about 1%). We have tested if the refinements depend upon taking the secondary phase into account, but did not find a significant influence on the results. This reflects that the residual value of R_{Bragg} is almost completely determined by the mismatch between the fitted profile functions and

	Lattice parameter a(Å)	B_{iso-Fe} (Å)^2	$B_{iso-V/Al}$ (Å)^2	Measured composition	R_{Bragg} (%)
$Fe_{2.5}V_{0.5}Al$	5.7604(3)	0.15(8)	0.9(2)	$Fe_{2.5}V_{0.5}Al$	4.3
$Fe_{2.1}V_{0.9}Al$	5.7528(2)	0.15(6)	0.3(2)	$Fe_{2.1}V_{0.9}Al_{1.01(5)}$	2.0
$Fe_{2.02}V_{0.98}Al$	5.7521(2)	0.13(6)	0.4(2)	$Fe_{2.02}V_{0.98}Al_{1.01(4)}$	2.1
sc-Fe_2VAl	5.7523(2)	0.25(6)	0.4(3)	$Fe_2VAl_{0.99(4)}$	1.9
q-Fe_2VAl	5.7514(2)	0.23(6)	0.4(3)	$Fe_2VAl_{0.94(4)}$	2.3

Table 3.1: Summary of the refinement results of the neutron diffraction data on $Fe_{2+x}V_{1-x}Al$, $0 \leq x \leq 0.5$, with the cubic lattice parameter a, the isotropic thermal displacement parameter B_{iso} of Fe and V/Al, the measured composition and the value of R_{Bragg}.

the experimental data for the Bragg peaks of the cubic $Fm\bar{3}m$ phase.

More specifically, to refine our data we used as input the cubic Heusler lattice, but modified it to incorporate different types of disorder:

1. assuming nominal composition;
2. allowing for off-stoichiometry of Fe, V and Al;
3. considering possible site exchange between Fe, V and Al.

Consistently, for all samples except for $Fe_{2.5}V_{0.5}Al$ the closest agreement between refinement and experimental data has been observed for models assuming Al off-stoichiometry. For $Fe_{2.5}V_{0.5}Al$ the models (2) and (3) did not yield a significantly improved solution compared to (1) [19]. Since $Fe_{2.5}V_{0.5}Al$ is ferromagnetically ordered ($\mu_{ord} = 0.85\mu_B$), magnetic scattering contributes to the spectrum. Yet, including a ferromagnetic contribution in the refinement only marginally improved the fit. We stress that we could not find for any of our samples evidence for a significant level ($> 3\%$) of Fe II/V site exchange.

In Table 4.2 we summarize the results of our refinements of the neutron diffraction data on $Fe_{2+x}V_{1-x}Al$, $0 \leq x \leq 0.5$. Overall, the refinements yield very good agreement with the experimental data, with R_{Bragg} values $\sim$2% for $0 \leq x \leq 0.1$. The isotropic thermal displacement parameters B_{iso} exhibit hardly any x dependence [20]. In particular, no significant difference of the B_{iso} parameters for sc- and q-Fe_2VAl has been detected. However, lattice parameters and the measured compositions both show significant differences between the two samples Fe_2VAl.

Previously, it has been reported that the lattice parameters of $Fe_{2+x}V_{1-x}Al$ are decreasing for decreasing x [1]. Specifically, while for x varying from 1 to 0.5 a linear variation of the lattice parameter with x has been found, subsequently a levelling off occurs as x approaches 0, until finally for $x < 0$ the lattice expands with x. This result is reflected in our experiments: upon reduction of x from 0.5 to 0.02 we observe a non-linear suppression of the lattice parameter a with x. This

is illustrated in Fig. 3.5, where we plot the lattice parameters of $Fe_{2+x}V_{1-x}Al$ as function of x. Remarkably, at $x = 0$, *i.e.*, for Fe_2VAl, we find two significantly different values of a for slowly cooled and quenched material: for sc-Fe_2VAl it is about 0.02% larger than for q-Fe_2VAl. The relevance of this difference is indicated in Fig. 3.5: the construction with the dashed lines demonstrates that the value of the lattice parameter for sc-Fe_2VAl corresponds to that of $Fe_{2.05}V_{0.95}Al$. According to the phase diagram from Ref. [16] $Fe_{2.05}V_{0.95}Al$ is ferromagnetically ordered below $T_C = 15$K. Therefore, we argue that the slow cooling procedure causes an expansion of the lattice in sc-Fe_2VAl, thus generating negative applied pressure and the onset of ferromagnetic order below $T_C = 13$K.

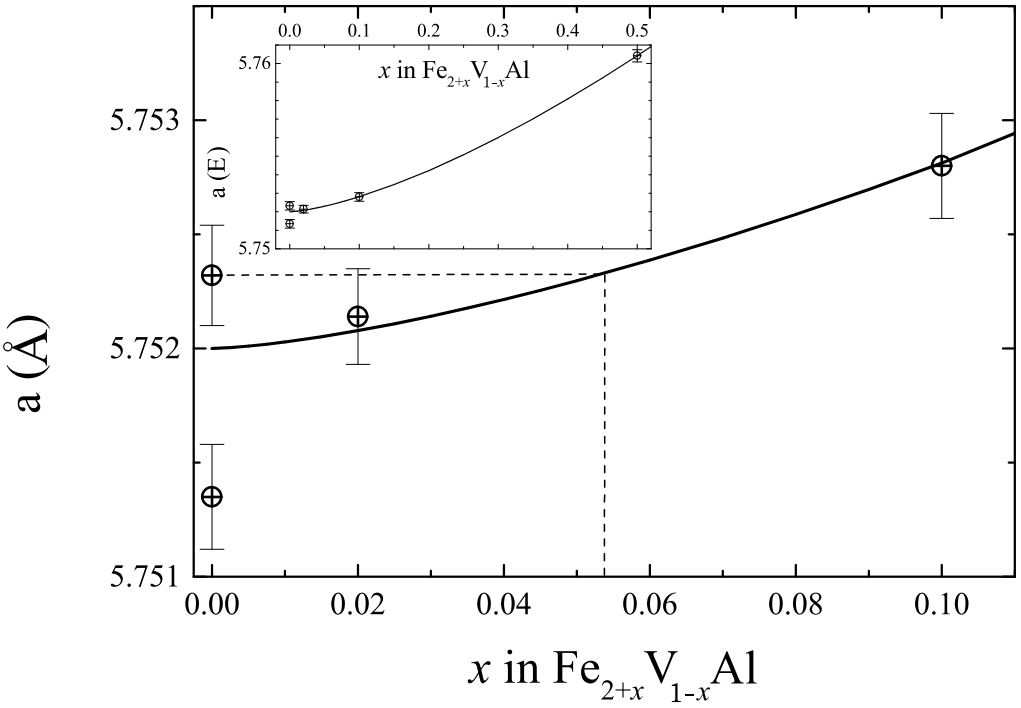

Figure 3.5: The lattice parameters of different samples $Fe_{2+x}V_{1-x}Al$, $0 \leq x \leq 0.1$, as a function of x. The inset depicts the data for $0 \leq x \leq 0.5$. Lines are guides to the eye.

The lattice parameter of q-Fe_2VAl falls out of the range of the other, more slowly cooled samples. We believe that this reflects the significant *Al* off-stoichiometry of this sample. According to our data the actual composition is $Fe_2VAl_{0.94(4)}$, well out of the range of nominal stoichiometry. In contrast, for all other samples nominal and actual compositions are identical within experimental uncertainty. More specifically, we directly compare the Bragg spectra measured for sc- and q-Fe_2VAl, after normalizing them for their overall intensities and correcting the latter for the angular shift from the difference in the lattice parameters. This procedure yields a matching of the positions of the Bragg peaks of

sc- and q-Fe_2VAl, as demonstrated in Fig. 3.6 for part of the spectra. We then can directly determine the intensity difference between the two spectra I_{sc-Fe_2VAl} - I_{q-Fe_2VAl}, which is included in Fig. 3.6. Variations of the intensities for different Bragg peaks are resolvable for the two spectra. We quantify the intensity variations by calculating the relative difference of the areas,

$$1 - \sum \frac{I_{q-Fe_2VAl}(\Theta)}{I_{sc-Fe_2VAl}(\Theta)} \Delta\Theta \tag{3.1}$$

under each Bragg peak. In Fig. 3.7 we present the result of this analysis, with the relative Bragg peak intensities for sc-Fe_2VAl in the lower panel, and the intensity variation in the upper one.

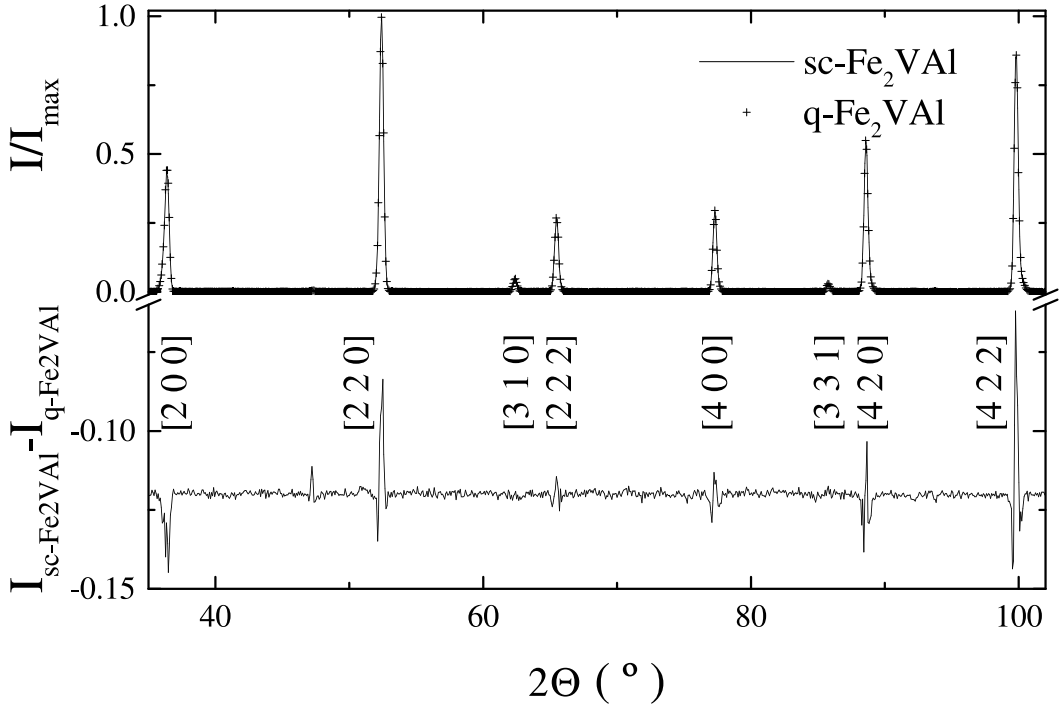

Figure 3.6: The normalized neutron spectra of sc- (solid line) and q-Fe_2VAl (+), and the difference $I_{sc-Fe_2VAl} - I_{q-Fe_2VAl}$ between the two spectra.

The $Fm\bar{3}m$ Heusler lattice consists of four interpenetrating fcc sublattices with origins at A(0 0 0), B($\frac{1}{4}$ $\frac{1}{4}$ $\frac{1}{4}$), C($\frac{1}{2}$ $\frac{1}{2}$ $\frac{1}{2}$) and D($\frac{3}{4}$ $\frac{3}{4}$ $\frac{3}{4}$). Bragg reflections are produced by either all even or all odd Miller indices with the three structure amplitudes:

F$_1$ $\sim$ $[(f_A - f_C)^2+(f_B - f_D)^2]^{\frac{1}{2}}$ for h,k,l all odd,
F$_2$ $\sim$ $f_A - f_B + f_C - f_D$ for $\frac{1}{2}(h+k+l) = 2n + 1$
F$_3$ $\sim$ $f_A + f_B + f_C + f_D$ for $\frac{1}{2}(h+k+l) = 2n$

with n an integer, and $f_{A,B,C,D}$ as average scattering factors for the atoms A, C = Fe, B = V and D = Al, respectively. For identical stoichiometry of I_{sc-Fe_2VAl}

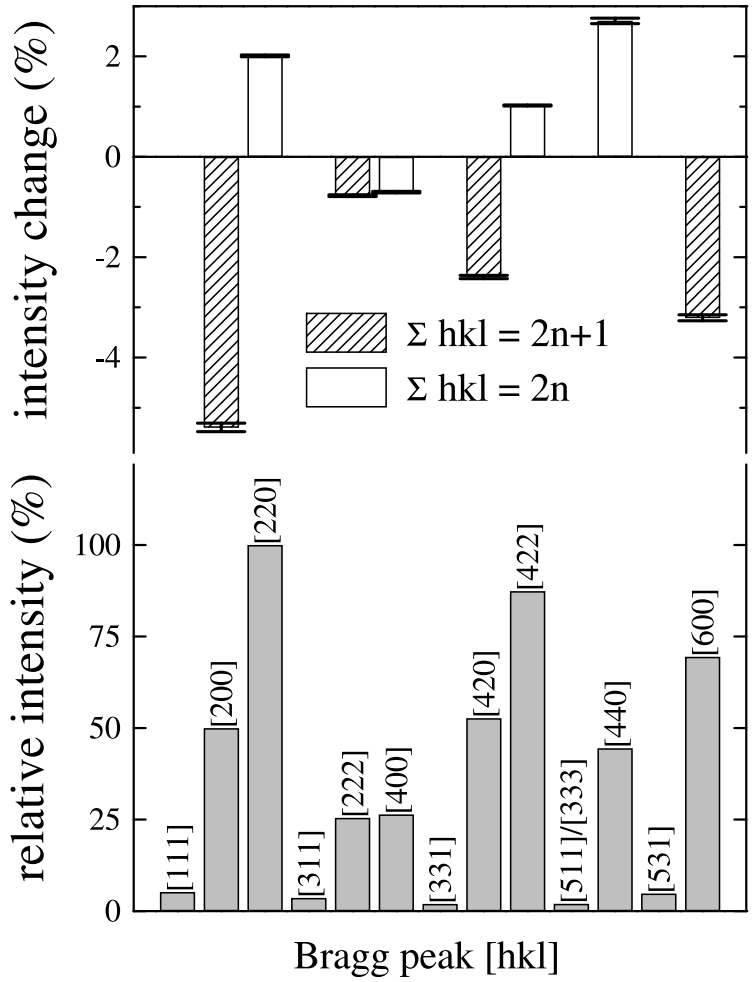

Figure 3.7: The relative Bragg peak intensities of sc-Fe_2VAl and the intensity variations, calculated from 1-$\Sigma(I_{q-Fe_2VAl}(\Theta)/I_{q-Fe_2VAl}(\Theta))\Delta\Theta$.

and I_{q-Fe_2VAl} no variation of the peak intensities $\frac{1}{2}(h+k+l)) = 2n$ is expected. In contrast, experimentally we find for these peaks on average a larger intensity in sc-Fe_2VAl than in q-Fe_2VAl. This proves that a stoichiometry difference exists between the two samples. Further, for $\frac{1}{2}$(h+k+l) = 2n +1 we find consistently that $I_{sc-Fe_2VAl} < I_{q-Fe_2VAl}$, which in view of the different F3 reflects that $f_{D:q-Fe_2VAl} < f_{D:sc-Fe_2VAl}$, *i.e.*, a smaller Al concentration in the quenched sample compared to sc-Fe_2VAl. Because of the comparatively small intensities of peaks $[h\ k\ l]$ = all odd, it yields a large error in the difference I_{sc-Fe_2VAl} - I_{q-Fe_2VAl}, prohibiting conclusions on the structural properties from the intensity variations of these peaks.

A refinement of the neutron spectra assuming stoichiometric composition $Fe : V : Al$ = 2:1:1 yields for sc-Fe_2VAl a value R_{Bragg} = 1.9%, which is significantly smaller than the corresponding value for q-Fe_2VAl, R_{Bragg} = 2.7%.

Therefore, on basis of our neutron diffraction study of differently heat treated samples $Fe_{2+x}V_{1-x}Al$ we conclude that sc-Fe_2VAl, which is magnetically ordered below $T_C = 13$K, structurally is much better ordered than q-Fe_2VAl. Primarily, the disorder in q-Fe_2VAl arises from Al vacancies, while Fe/V site exchange is not observable for any sample within the resolution of our experiment.

In addition to our structural investigation we attempted to study the magnetically ordered phases of sc-Fe_2VAl and $Fe_{2.1}V_{0.9}Al$ using the focusing diffractometer E6 at the HMI. We were unable to resolve intensity differences between measurements taken above and below T_C in our powder neutron diffraction experiments, indicating that for both sc-Fe_2VAl and $Fe_{2.1}V_{0.9}Al$ the ground states are ferromagnetically ordered with magnetic moments smaller than the resolution limit at E6 of about $0.5\mu_B$.

3.4 μSR-experiments

In collaboration with H.H. Klauss, D. Baabe and D. Mienert time-differential muon spin relaxation experiments in zero external field (ZF-μSR) on the above powdered specimen of slowly cooled sc-Fe_2VAl in the temperature range 3 - 225K at the GPS spectrometer of the Paul Scherrer Institute, Switzerland, have been performed. The sample was mounted with ultra-thin aluminium tape in a gas flow cryostat and an electronic veto logic was used to register only the decay positron signals from muons stopped in the sample.

The muon spin polarization as a function of time is reconstructed by forming the asymmetry between the numbers of positrons emitted parallel and antiparallel to the original muon spin polarization direction. As described in [19] the experimentally determined asymmetry $A(t)$ is given as $A(t) = A_0G(t)$, where $A_0 \sim 0.21$ is the experimentally determined intrinsic asymmetry of the positron detectors and $G(t)$ the normalized polarization function of the muon ensemble implanted in the sample.

In zero external field a possible source for a relaxation of the muon spin ensemble are static local magnetic fields at the muon site, B_{loc}, due to finite electronic magnetic moments. The individual muon spin shows a Larmor precession around B_{loc} at a frequency $\omega_\mu = \gamma_\mu B_{loc}$, with $\gamma_\mu/2\pi = 13.55$MHz/kG. For a magnetically ordered polycrystalline sample an isotropic spatial averaging over all angles between B_{loc} and the initial muon polarization $P_\mu(0)$ yields a polarization function $G(t) = 1/3 + 2/3\ \cos(\omega_\mu t)\ \exp(-(\lambda_{stat}t)^\beta)$ [20]. The relaxation of the oscillating part describes an inhomogeneous distribution of B_{loc} for the total muon ensemble. If the average value of B_{loc} is zero and the form of the distribution is Gaussian, $G(t)$ is given by the Kubo-Toyabe function $G(t) = 1/3 + 2/3\ (1-\Delta^2t^2)\ \exp(-\frac{1}{2}\ \Delta^2t^2)$ [20]. In general, a static local field distribution in a polycrystalline sample will always lead to a longitudinal non-relaxing 1/3-tail and a transverse relaxing 2/3-signal fraction. If the field distribution becomes dynamic with a slow fluctu-

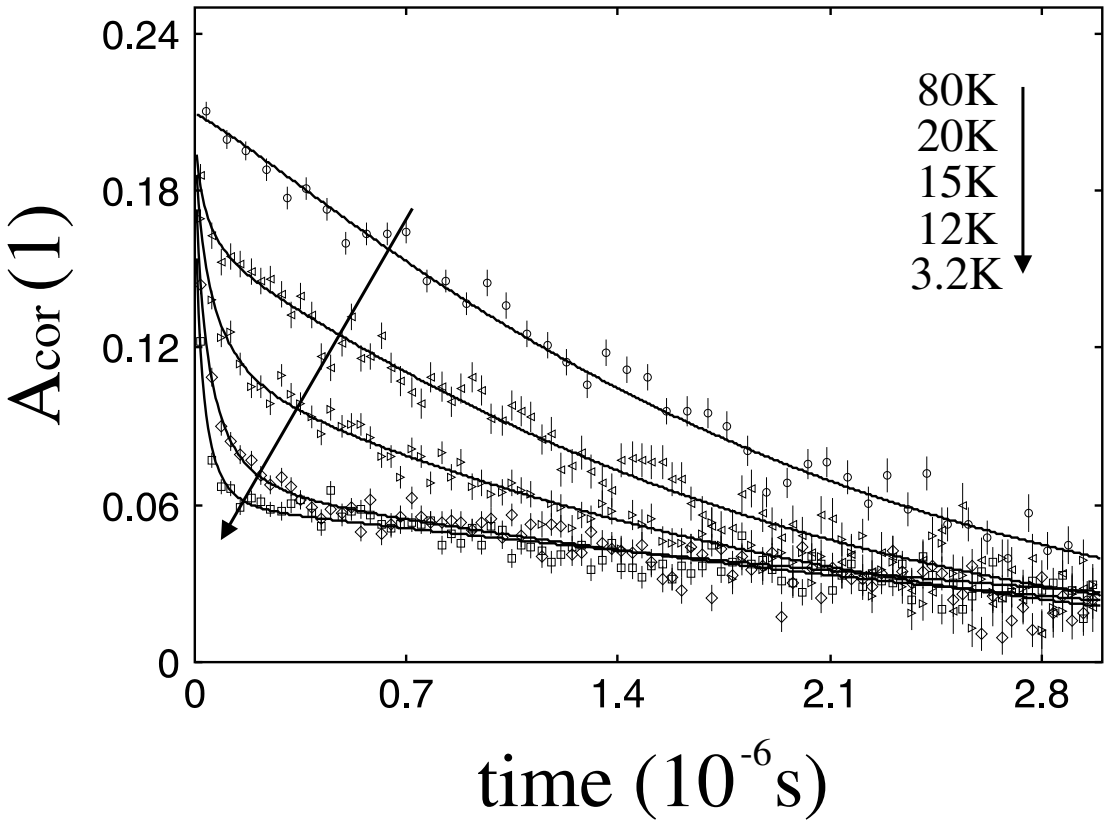

Figure 3.8: Zero field μSR spectra of sc-Fe_2VAl at different temperatures. The fit functions (solid lines) are described in the text.

ation rate $\nu \ll (\lambda_{stat}$ or $\Delta)$, the 1/3-tail will exhibit a relaxation $\sim$ exp(-$\lambda_{long}t$). For fast fluctuations ($\nu \gg (\lambda_{stat}$ or $\Delta)$) a single component relaxation function $G(t) = exp(-(\lambda_{dyn}t)^{\beta})$ can be employed.

Typical ZF-μSR spectra of Fe_2VAl are depicted in Fig. 3.8. At temperatures below 13K a two component structure of a quasi-static spectrum exists: a fast relaxing transversal part of nearly 2/3 total signal amplitude and a slowly relaxing longitudinal part. No oscillating signal fraction is detected. Between 13 and 40K the fast relaxing signal fraction gradually disappears and above 40K only a single, slowly relaxing signal is observed.

The data sets can be described by a phenomenological polarization function of the form

$$A(t) = A_0(F_{slow}exp(-(\lambda_{long}t)^{\alpha}) + (1 - F_{slow})exp(-(\lambda_{trans}t)^{\beta}).$$

Common parameters at all temperatures are the spectrometer asymmetry $A_0 = 0.21$ and the generalised exponents $\alpha = 1.15(2)$ and $\beta = 0.64(3)$ describing the shape of the relaxation functions of the slow and fast components, respectively. The temperature dependence of the relative asymmetry F_{slow} of the slow com-

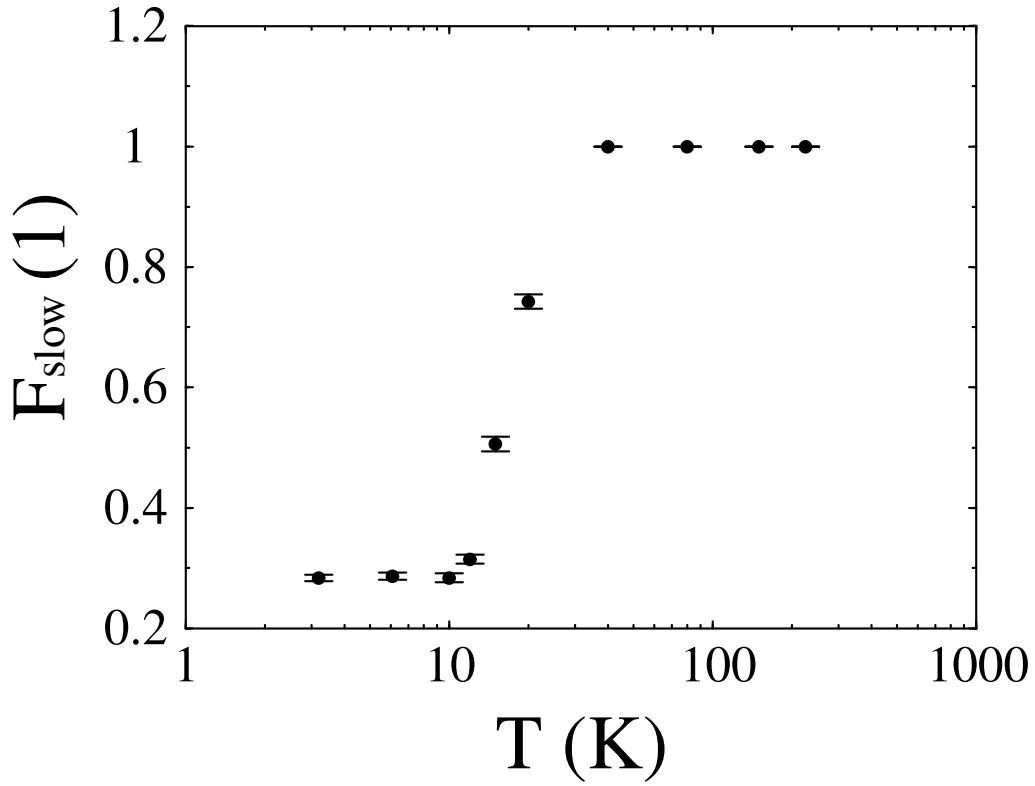

Figure 3.9: Temperature dependence of the slowly relaxing signal fraction F_{slow} in zero field μSR of sc-Fe_2VAl.

ponent is plotted in Fig. 3.9, the resulting muon spin relaxation rates λ_{long} and λ_{trans} in Figs. 3.10 and 3.11.

The full signal amplitude in the temperature regime above 40K reflects a paramagnetic relaxation of the muon spin. An additional 10% signal amplitude increase between 40K and higher temperatures is attributed to a change of the experimental set-up (*i.e.*, time resolution). The increase of the relaxation rate with decreasing temperature (Fig. 3.10) arises from the slowing down of the paramagnetic moments. Between 40 and 12K the amplitude of this signal is gradually reduced and a strongly relaxing component appears, reflecting a sample volume fraction with quasi-static magnetic moments on a time scale of $\sim 10^{-7}$s, e.g. inhomogeneous short range magnetic order. The ordered volume fraction continuously increases from zero at ∼40K to 100% at 12K. The μSR data confirm a magnetic transition between 15 and 12K, since the low temperature value of $F_{slow} = 0.29(2)$ clearly proves that below 13K the sample is fully magnetically ordered. The 10% deviation of F_{slow} from the theoretical value 1/3 is due to the constant sample amplitude fixed to the high temperature value above 40K. The reduction of λ_{long} between 40 and 12K reflects the change of the nature of the relaxation mechanism from dynamic in the paramagnetic regime above 40K to a quasi-static

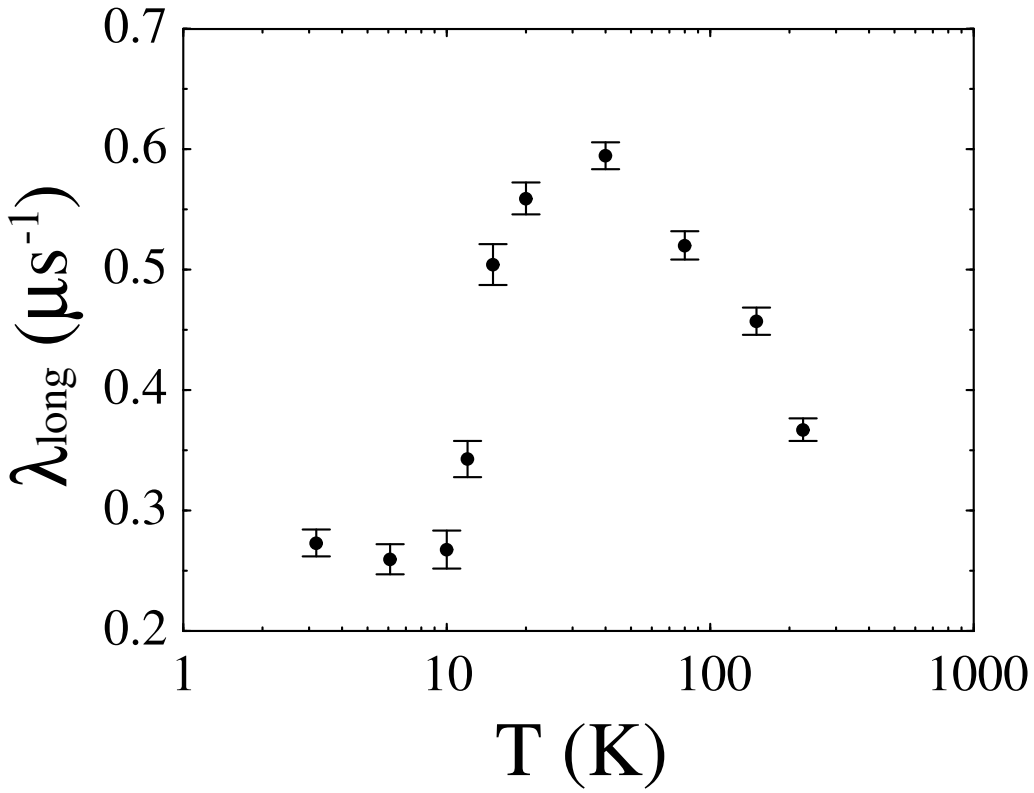

Figure 3.10: Temperature dependence of the longitudinal muon spin relaxation rate λ_{long} in zero field μSR of sc-Fe_2VAl.

one of the longitudinal muon spin component in the magnetically ordered state. The saturation value of $\lambda_{long} \sim 0.27(2)\mu s^{-1}$ below 12K corresponds in a strong collision model to an effective spin fluctuation rate of the same order. The very strong transversal relaxation rate λ_{trans} in the ordered state and the absence of a coherent muon spin precession indicate a rather inhomogeneous magnetic state with a broad local field distribution at the muon site. The increase of λ_{trans} with decreasing temperature is compatible with the increase of the magnetization at low temperatures. The value at 20K corresponds to a strongly reduced signal asymmetry in the intermediate regime between paramagnetic and ferromagnetic state and is not directly comparable with those at lower temperatures.

The fitted value of the shape exponent α is close to 1, the expected value for a quasi-static relaxation of the longitudinal signal fraction in the magnetically ordered state. In the paramagnetic regime this value is consistent with a homogeneous relaxation process with a gaussian local field distribution and a well defined spin fluctuation rate. In the ordered state below 13K the exponent β is significantly smaller than 1. This is usually observed in inhomogeneous magnets without spontaneous spin precession. In Fe_2VAl the main source of the static

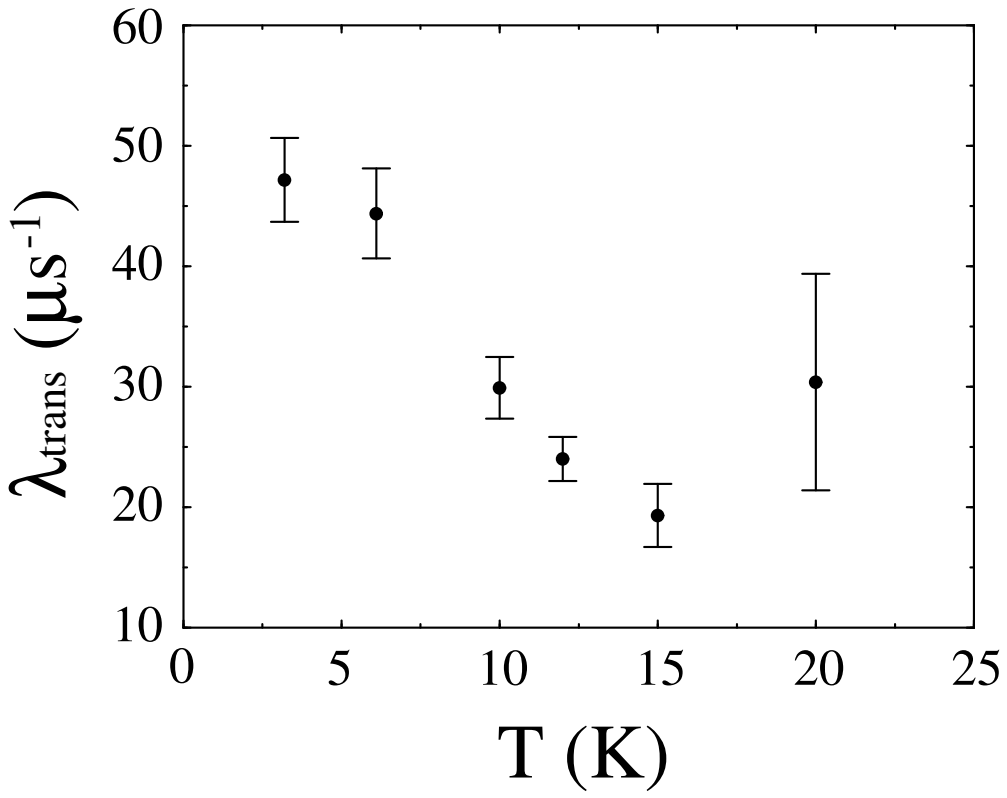

Figure 3.11: Temperature dependence of the transversal muon spin relaxation rate λ_{trans} in zero field μSR of sc-Fe_2VAl.

field distribution are imperfections of the magnetic lattice caused by diluted lattice imperfections and impurities. In this case a Lorentzian field distribution (exponent $\beta = 1$) is expected for dominant dipolar or RKKY-type hyperfine coupling between the muon and the local moments [21]. The observed behavior is an indication of an inhomogeneous magnetic state causing a superposition of more than one lorentzian field distribution with different static widths. The μSR data cannot unambiguously clarify the cause for this inhomogeneity. Either size and orientation variations of small magnetic moments on each Fe site or diluted moments like in a spin glass might be possible. Assuming the latter to be the case, we can compare the low temperature saturation value of $\lambda_{trans} \sim 47(3)\mu s^{-1}$ with those in canonical spin glasses like $(Au)Fe$ [22], where a linear scaling of λ_{trans} with the impurity spin concentration has been observed. From this comparison we obtain an impurity spin concentration of 8(2)% in sc-Fe_2VAl. This value is consistent with the Mössbauer results presented below but incompatible with the upper bound for $FeII/V$ site exchange from neutron scattering.

3.5 Mössbauer spectroscopy

^{57}Fe-Mössbauer-spectroscopy experiments were performed on all samples $Fe_{2+x}V_{1-x}Al$, $0 \leq x \leq 0.5$, in a standard low-temperature Mössbauer set-up (source: ^{57}Co in Rh matrix) at temperatures ranging from 8 to 300K. Here, we address two aspects of our Mössbauer studies on $Fe_{2+x}V_{1-x}Al$.

In Fig. 3.12 we present the Mössbauer spectra of $Fe_{2.1}V_{0.9}Al$ measured at 50 and 10K, together with the corresponding spectra of sc-Fe_2VAl at 50 and 8K. The experiments at 50K probe the paramagnetic state, while at 8/10K the systems are ferromagnetically ordered. For both compounds similar Mössbauer spectra are observed: at 50K we detect single lines with small isomer shifts of about 0.02-0.03mm/s, relative to $^{57}Co(Rh)$ and linewidths (FWHM) $\Gamma = 0.51$mm/s (fits represented by solid lines in Fig. 3.12). Upon lowering the temperature below T_C a broadening of these lines and a reduction of their depth occurs. The close quantitative and qualitative similarity between the temperature dependence of the Mössbauer spectra of $Fe_{2.1}V_{0.9}Al$ and sc-Fe_2VAl is emphasized by plotting the difference between the spectra at 50 and 8/10K for both compounds (Fig. 3.12). It reinforces the notion of ferromagnetism in sc-Fe_2VAl as result of the same mechanism as in $Fe_{2.1}V_{0.9}Al$ and is consistent with our view that it arises from negative chemical pressure.

For both $Fe_{2.1}V_{0.9}Al$ and sc-Fe_2VAl the observed behavior is not the expected one for an archetypical bulk ferromagnet, since no well-defined Zeeman splitting is visible. Previously, the Mössbauer-spectra of $Fe_{2+x}V_{1-x}Al$ have been interpreted in terms of fluctuating spins [14, 15] and on basis of a "shell model" of magnetic ions immersed in a non-magnetic matrix [10]. The first model is inconsistent with the observation of bulk ferromagnetic ordering for $Fe_{2.1}V_{0.9}Al$ and sc-Fe_2VAl.

The shell model has been successfully applied to disordered metallic ferromagnets like $Fe - Al$ alloys [24]. It assumes that the hyperfine field at a given Fe ion results from a superposition of the contributions of magnetic ions sited in the nearest neighbour, next-nearest neighbour etc. shell around the Fe ion. In $Fe_{2+x}V_{1-x}Al$ the magnetic ions are thought to be $FeII$ on V sites, which on basis of band structure calculations are predicted to carry a large ($2\mu_B$) magnetic moment [6]-[8]. From our Mössbauer data we can estimate for sc-Fe_2VAl the required number of site exchanged $FeII/V$ pairs. To account for the broadening of the Mössbauer-line below T_C it would require at least 6% $FeII$ on V sites. This value, which is more than one order of magnitude larger than the estimated level of Fe/V site exchanges for q-Fe_2VAl of 0.3 - 0.4% [10, 11], is inconsistent with the result of our neutron diffraction experiments, which sets an upper limit of 3% $FeII$ on V sites. Therefore, we conclude that neither model proposed so far properly accounts for the Mössbauer spectra of $Fe_{2+x}V_{1-x}Al$, $x \approx 0$.

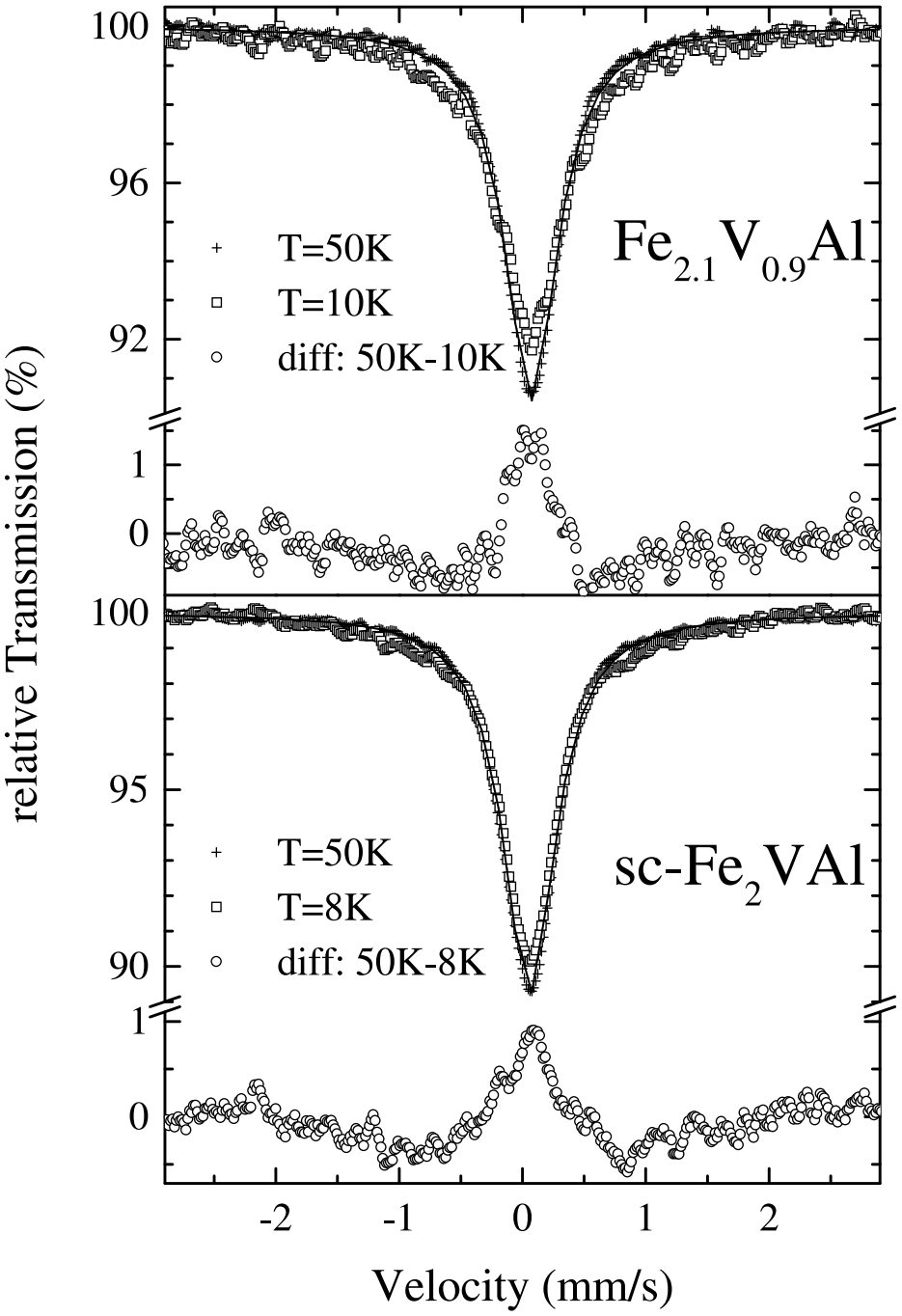

Figure 3.12: Mössbauer-transmission-spectra of $Fe_{2.1}V_{0.9}Al$ and sc-Fe_2VAl taken at 50 (+) and 10/8K. Solid lines indicate single lorentzian fits to the 50K data. Included in the plot are the differences between the spectra at 50 and 10/8K (o), respectively.

3.6 Conclusion

We have presented powder neutron diffraction, μSR and Mössbauer-experiments on $Fe_{2+x}V_{1-x}Al$, and in particular on differently heat treated samples Fe_2VAl. Our structural investigation proves that slowly-cooled Fe_2VAl, which we established on a microscopic scale to be ferromagnetically ordered below $T_C = 13$K, is structurally better ordered than quenched material, for which we found evidence for substantial Al off-stoichiometry. For the quenched material the bulk properties [13] resemble the behaviour of "Kondo-insulating like" or "pseudo gap" Fe_2VAl [1, 2, 5, 9, 10, 11, 16]; this suggest that the materials investigated in those works are Al deficient.

As pointed out in Ref. [5], because of the electron count Al deficiency might have a strong effect on the actual position of the Fermi level E_F in a pseudo-gap system. Specifically, it was argued that Al deficiency moves E_F out of the center of the pseudo gap into the slopes, implying that Al deficient material should be more metallic than non-deficient one. This hypothesis is in conflict with the observation that the resistivity of sc-Fe_2VAl is lower than that of q-Fe_2VAl, indicating less metallicity and E_F in the center of the gap for the latter sample.

Another explanation for the smaller resistivity of sc-Fe_2VAl might be based upon the ability of Al vacancies to localise conduction electrons. Then, the resistivity of Fe_2VAl would depend strongly on disorder induced (*i.e.*, from Al vacancies) localisation of electrons in states close to the gap; with the larger degree of disorder in q-Fe_2VAl its resistivity will be larger than that of sc-Fe_2VAl. Unfortunately, quantitative predictions are very difficult for this scenario, as it depends both on the actual position of E_F because of the number of charge carriers from Al, and the strength and number of localising potentials from Al vacancies. In addition, E_F might depend on the lattice parameter, *i.e.*, the chemical pressure, which in turn is a function of the Al stoichiometry.

Altogether, we conclude that the physical properties, in particular the anomalous resistivity, of non-magnetic Fe_2VAl are dominated by crystallographic disorder. Kondo-insulating behaviour seems not to play a role; specifically, Fe_2VAl can be easily tuned into a ferromagnet, which is not expected for inherently non-magnetic Kondo insulators [25]. Further, we conclude that sc-Fe_2VAl is "more representative" of the intrinsic behavior of ambient pressure Fe_2VAl than quenched material, as it is closer to perfect stoichiometry. Hence, while the closeness to a pseudo gap state predicted in band structure calculations [6, 8] is found for both sc- and q-Fe_2VAl, the prediction of a non-magnetic ground state for stoichiometric, perfectly Heusler-ordered Fe_2VAl must still be considered a matter of debate. In particular, we note that, given our Mössbauer- and μSR-experiments, the simple view of "Fe on the wrong (V) site" generating magnetism does not account for magnetic order in sc-Fe_2VAl, in so far as the measured number of "wrong sited" Fe is too low.

Since the properties of Fe_2VAl are so sensitively dependent on the actual

stoichiometry, which is hard to control in the limits relevant to Fe_2VAl, we believe that pressure experiments on either sc-Fe_2VAl or q-Fe_2VAl represent a more fruitful route to study this material. Based on our experiments, for sc-Fe_2VAl we would expect a suppression of magnetic order upon application of pressure. For q-Fe_2VAl a pressure experiment might yield insight in the relevance of Al vacancies for electronic localisation and the position of the Fermi level. Furthermore, pressure experiments might be very useful in combination with band structure calculations, as we would expect that the result of these calculations should sensitively depend on the value of the lattice constant.

Independently from our study, researchers from Iowa State University and Cornell University have investigated the metallurgical properties of Fe_2VAl. Similarly to our results, they concluded that disorder controls the properties of Fe_2VAl. However, basing on x-ray diffraction data they argued that the disorder in the Heusler lattice is realized by Fe/V site exchange. As pointed out, x-ray diffraction does not provide a large contrast between Fe, V and Al ions, and thus is unlikely to unambiguously establish such site exchange disorder. Moreover, our neutron scattering data do not yield evidence for such disorder. In consequence, our study disproves the presence of antisite disorder proposed in Ref. [26].

3.7 Appendix

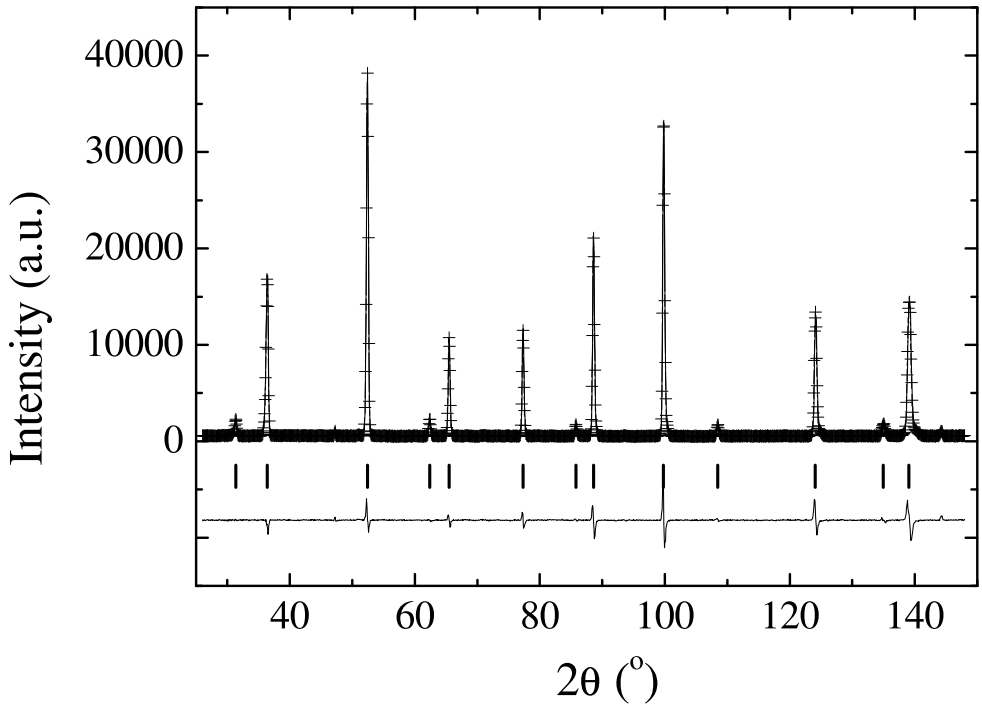

Figure 3.13: The neutron diffraction spectrum of slowly cooled Fe_2VAl, measured at 50K (+). Included is a refined fit to the data, the difference between fit and data, and tics indicating Bragg peak positions.

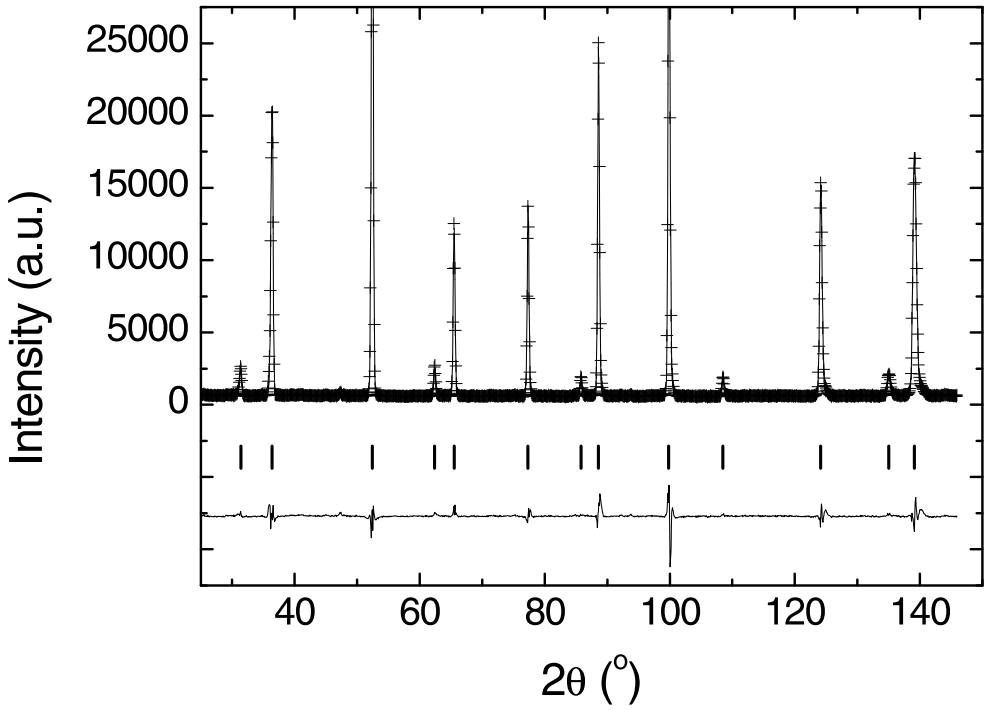

Figure 3.14: The neutron diffraction spectrum of quenched Fe_2VAl, measured at 50K (+). Included is a refined fit to the data, the difference between fit and data, and tics indicating Bragg peak positions.

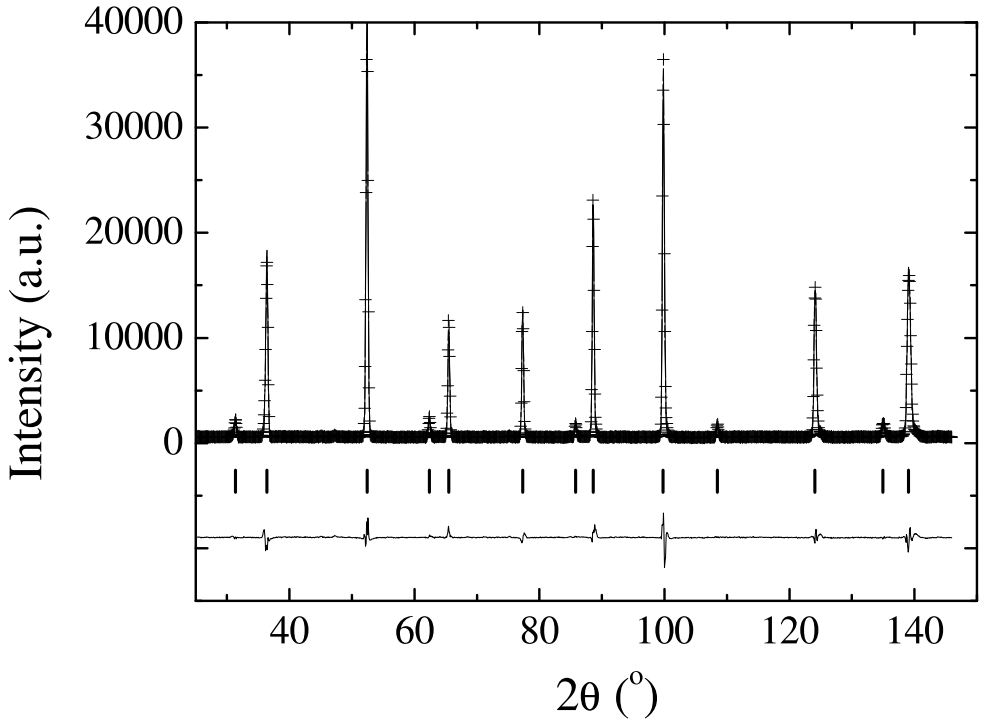

Figure 3.15: The neutron diffraction spectrum of $Fe_{2+x}V_{1-x}Al$, x=0.02, measured at 50K (+). Included is a refined fit to the data, the difference between fit and data, and tics indicating Bragg peak positions.

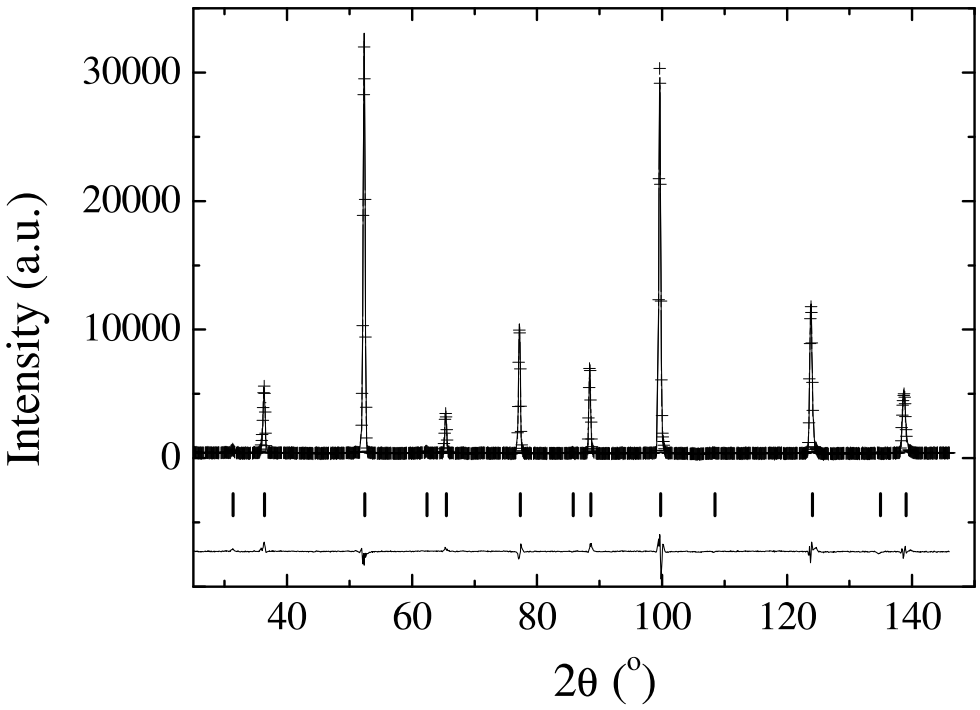

Figure 3.16: The neutron diffraction spectrum of $Fe_{2+x}V_{1-x}Al$, x=0.5, measured at 50K (+). Included is a refined fit to the data, the difference between fit and data, and tics indicating Bragg peak positions.

Bibliography

[1] Y. Nishino et al., Phys. Rev. Lett. **79** (1997) 1909.

[2] K. Endo et al., J. Magn. Magn. Mater. **177-181** (1998) 1437.

[3] Z. Schlesinger et al., Phys. Rev. Lett. **71** (1993) 1748.

[4] Z. Schlesinger et al., Physica B **237 &** **238** (1997) 460.

[5] H. Okamura et al., Phys. Rev. Lett. **84** (2000) 3674.

[6] G. Guo, G. Botton and Y. Nishino, J. Phys.: Condens. Matter. **10** (1998) L119.

[7] D.J. Singh and I.I. Mazin, Phys. Rev. B **57** (1998) 14352.

[8] R. Weht and W.E. Pickett, Phys. Rev. B **58** (1998) 6855.

[9] H. Matsuda et al., J. Phys. Soc. Japan **69** (200) 1004.

[10] C.-S. Lue and J.H. Ross, Phys. Rev. B **58** (1998) 9763.

[11] C.-S. Lue et al., Phys. Rev. B **60** (1999) R13941.

[12] A. Slebarski et al., Phys. Rev. B **62** (2000) 3296.

[13] A. Matsushita and Y. Yamada, J. Magn. Magn. Mater. **196/197** (2000) 669.

[14] E.S. Popiel et al., J. Less-Common Met. **146** (1989) 127.

[15] E.S. Popiel, W. Zarek and M. Tuszynski, Hyperfine Interact. **51** (1989) 981.

[16] M. Kato et al., J. Phys. Condens. Matter **12** (2000) 1769.

[17] D.M. Többens et al., Proc. 7th Eur. Powder Diffraction Conf. EPDIC 2000. (2000)

[18] J. Rodriguez-Carvajal, 1998 WinPLOTR/FULLPROF version 3.5d, Laboratory Leon Brillouin-CEA-CNRS Oct98-LLB-JRC.

[19] B. Nachumi et al., Phys. Rev. B **58** (1998) 8760.

[20] P. Dalmas de Réotier and A. Yaouanc, J. Phys. Condens. Matter **9** (1997) 9113.

[21] R.E. Walstedt and L.P. Walker, Phys. Rev. B **9** (1974) 4857.

[22] Y.J. Uemura and T. Yamazaki, J. Magn. Magn. Mater. **31-34** (1983) 1359.

[23] D. Baabe et al., Hyperfine Inter., in print (2003).

[24] V. Niculescu et al., Phys. Rev. B **14** (1976) 4160.

[25] G. Aeppli and Z. Fisk, Comments Condens. Matter Phys. **16** (1992) 155.

[26] Y. Feng et al., Phys. Rev. B **63** (2001) 165109.

4 Disorder effects in $UPd_{2-x}Sn$

4.1 Introduction

In recent years, cubic Heusler compounds attracted much attention due to a rich variety of physical phenomenon found in these materials [1]-[7]. For instance, a number of compounds of composition 1-2-1 have been reported to exhibit instabilities of the ground state and the crystal structure. In the context of disorder, Heusler structured heavy fermion compounds seem to play a special role. Several of the heavy fermion representatives undergo structural transitions from the cubic Heusler structure into lower symmetries. Thus, in UPd_2In Takabatake at el. [6] observed a martensitic phase transition accompanied by a lowering of the cubic symmetry below a transition temperature T_S=180K. The transition was associated with a significant change of the magnetic susceptibility and thermoelectric power. Analogously, the Heusler alloy UNi_2Sn [5, 7] undergoes a structural symmetry-lowering transition at around 220K, which strongly influences the susceptibility and resistivity. Moreover, it was shown that the temperature of the transition strongly depends on the Ni stoichiometry. Judging from the low temperature resistivity ρ of these compounds, it appears that they are moderately disordered, as ρ is comparatively large (a few hundred $\mu\Omega$cm) and the temperature derivative $d\rho/dT$ is negative below room temperature. However, so far crystallographic disorder has not directly been established (as a reference concerning disorder in Heusler systems see the case of Co_2NbSn [8]).

Similar to UNi_2Sn, isoelectronic UPd_2Sn exhibits a strong dependence of its structural and physical properties on the stoichiometry. Here, it was found that off-stoichiometric $UPd_{1.85}Sn$ crystallizes in the cubic $Fm\bar{3}m$ Heusler structure, instead of the orthorhombic $Pnma$ lattice established for stoichiometric UPd_2Sn [2, 9]. The $Pnma$ lattice represents a superstructure of the $Fm\bar{3}m$ lattice, that is in form of an orthorhombic distortion [5]. The structural transition is accompanied by a non-magnetic/magnetic transition: UPd_2Sn has been reported as a typical heavy fermion system, while $UPd_{1.85}Sn$ is antiferromagnetically (AFM) ordered at low temperatures [2, 9, 10, 11]. Resembling the situation in UPd_2In or UNi_2Sn [6, 7], the physical properties of $UPd_{1.85}Sn$ point to the presence of disorder. The magnetization exhibits irreversibility in the antiferromagnetic state, the resistivity is comparatively large, and $d\rho/dT$ negative to lowest temperatures.

A number of topics remain elusive: Is the structural disorder arising from the Pd

vacancies, or are there other sources for disorder? How does the structural disorder affect the magnetic ground state on a microscopic scale? Is the resistivity arising from Kondo scattering, with the coherent state destroyed by the disorder, or is it governed by a tendency towards localization of the electrons. To address these issues we have performed a detailed investigation of $UPd_{2-x}Sn$, $0 \leq x \leq 0.15$. Here, we present the results of our study on the structural and physical properties of $UPd_{2-x}Sn$ by means of macro– and microscopic experimental techniques. We will discuss the relationship between disorder, magnetic ground state properties and electronic transport in this material class.

4.2 Metallurgy of $UPd_{2-x}Sn$

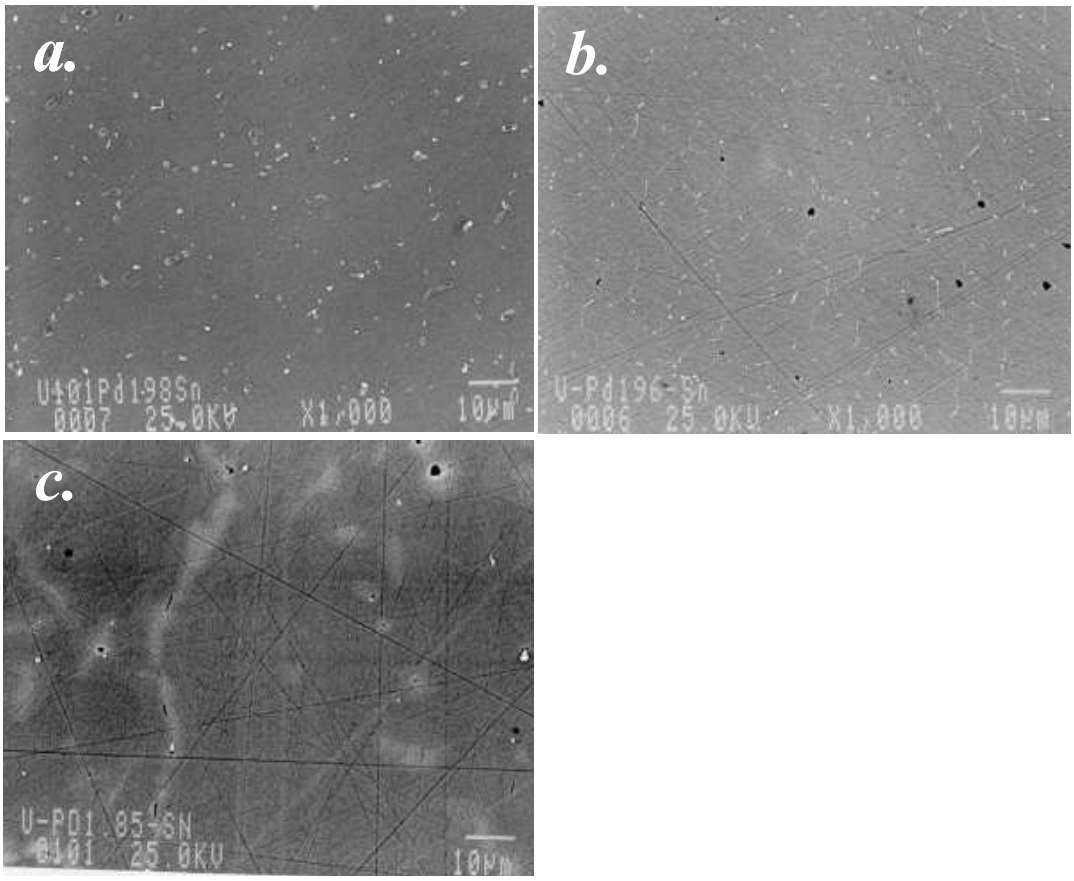

Figure 4.1: Electron backscattering photos of $UPd_{2-x}Sn$: x=0 (a), x=0.04 (b) and x=0.15 (c). The white areas indicate a secondary phase.

The samples $UPd_{2-x}Sn$, $0 \leq x \leq 0.15$, have been prepared at the Kamerlingh Onnes Laboratory, Leiden University, by R.W.A. Hendrikx. They have been produced by arc melting polycrystalline buttons (U: 3N; Pd: 4N; Sn: 5N) under

Ar-atmosphere in a water-cooled copper crucible. Annealing of cubic $UPd_{2-x}Sn$ at T=1073K led to samples containing a mixture of the orthorhombic and cubic phases. This observation suggests, that the structural transition temperature from $Fm\bar{3}m$ to orthorhombic $Pnma$ structure in off-stoichiometric $UPd_{2-x}Sn$ lies above room temperature. In consequence, after a study of the physical properties of $UPd_{2-x}Sn$, $0 \leq x \leq 0.15$, in as-cast (referred to as (ac)) form only orthorhombic samples were heat treated at T=1073K for 1 week (ann). Electron probe micro analysis (EPMA) detected the presence of a secondary phase in the material, but only with a small volume amount, *i.e.*, less then 2% for $UPd_{1.96}Sn$ and less than 1% for the other samples. The spatial dimensions of the secondary phase inclusions (see Fig. 4.1) are too small (diameter$\sim 1\mu$m) to allow a quantitative determination of their composition. Samples with starting composition $x > 0.15$ could not be produced in single phase form, as a secondary phase of composition 1:1:1 segregated (Fig. 4.1).

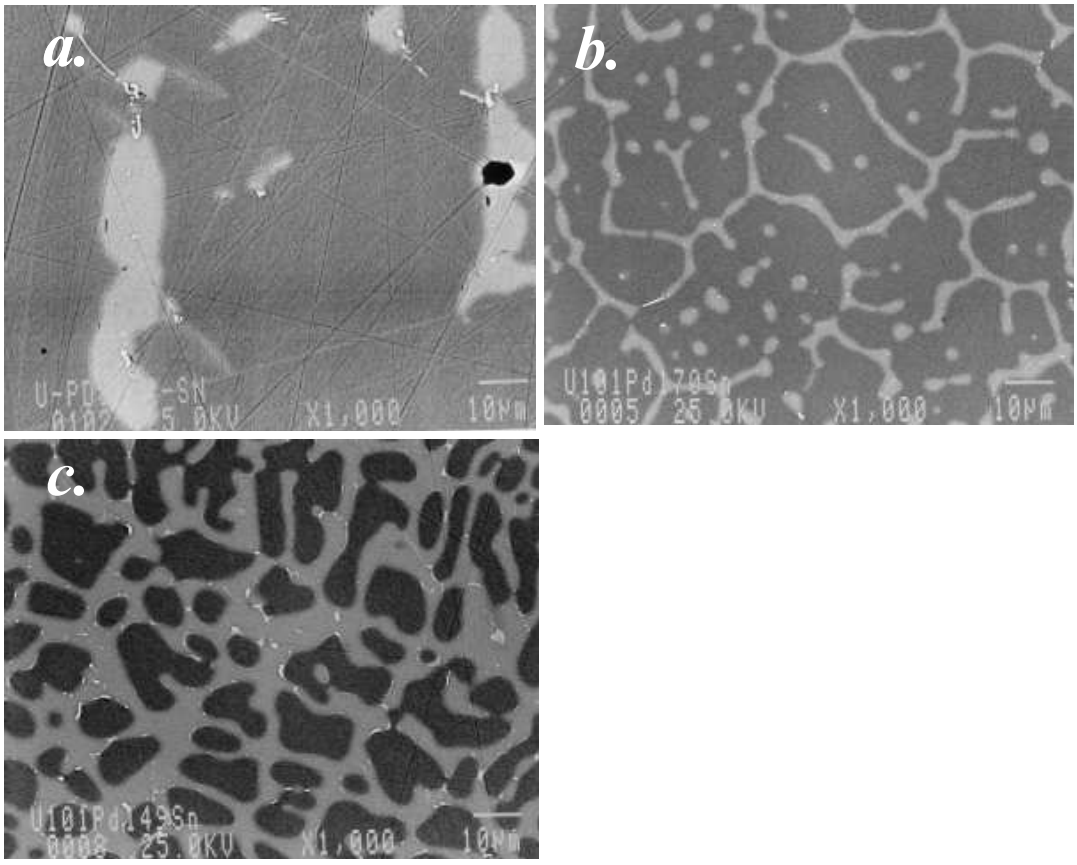

Figure 4.2: Electron backscattering photos of $UPd_{2-x}Sn$: x=0.18 (a), x=0.3 (b), x=0.51 (c). The photos reveal the separation into two phases for large *Pd*-deficiency. The secondary phases can be recognized as a light grey pattern.

Nominal composition	Matrix composition (EPMA)
UPd_2Sn (ac)	1:2.01(6):1.00(3)
$UPd_{1.96}Sn$	1:1.91(6):0.99(3)
$UPd_{1.95}Sn$	1:1.90(6):0.98(3)
$UPd_{1.85}Sn$	1:1.89(6):0.99(3)

Table 4.1: The nominal and actual compositions of $UPd_{2-x}Sn$.

Further, EPMA revealed a difference between nominal and actual compositions of the samples. This is indicated in Table 4.1, where we summarize the measured matrix compositions of the different samples. The nominal matrix compositions of the samples with $x > 0$ differ from the actual measured ones. According to this study, the three samples x=0.04, 0.05 and 0.15, within the experimental resolution of EPMA (2%), all have the same actual matrix composition $U : Pd : Sn$ of 1:1.9:1, indicating a metallurgical stability of this stoichiometry. In spite of these metallurgical anomalies, in the following we will refer to all samples by their nominal composition.

Irrespective of the actual composition, there is a sharp structural transition as function of the composition parameter x: while the orthorhombic $Pnma$ space group symmetry is detected for UPd_2Sn and $UPd_{1.96}Sn$ [10], the cubic Heusler structure $Fm\bar{3}m$ is found for $UPd_{1.95}Sn$ and $UPd_{1.85}Sn$. This is established by an investigation of the crystallographic structure of the samples $UPd_{2-x}Sn$ by means of X-Ray diffraction. In Fig. 4.3(a) we plot the X-Ray diffraction spectrum for the sample x=0 (ac), including here the result of a Rietveld refinement of the data. In Table 4.2 we summarize the refinement results, which are in good agreement with those reported in Ref. [10]. Further, in the table we list the parameters obtained from the refinement of x=0 (ann). It indicates that aside from minor lattice parameter changes the annealing does not have a profound effect on the structural properties of UPd_2Sn, as measured in X-Ray diffraction.

The unit cell volume of the samples as function of nominal and actual composition is presented in Fig. 4.4. The difference in volume of the unit cell for x=0, (ac) and (ann), ΔV ∼0.1%, for typical intermetallic bulk modulus ($B_0 \sim$ 100GPa^{-1}) corresponds to a chemical pressure effect of only ∼0.1GPa.

In contrast, for both $UPd_{2-x}Sn$, x=0.05 and 0.15, in the X-Ray diffraction spectra the peak positions correspond to the cubic Heusler lattice of $Fm\bar{3}m$ symmetry (Fig. 4.3(b)). However, a Rietveld refinement of the spectra did not yield reasonably low values R_{Bragg} (Table 4.2). Therefore, we performed additional structural investigations of cubic $UPd_{2-x}Sn$, x=0.15 at the Berlin Neutron Scattering Center, HMI, Berlin, in collaboration with R. Feyerherm. A typical neutron scattering spectrum for temperatures above the magnetic transition ($T_N = 25.7$K) of $UPd_{1.85}Sn$ is displayed in Fig. 4.5. Note that the intensity of the main peak at 62° exceeds the scale by a factor 4. A full Rietveld refinement of the diffraction

	$Pnma$ X–ray (ac) 293 K	$Pnma$ X–ray (ann) 293 K	$Fm\bar{3}m$ X–ray 293 K	$Fm\bar{3}m$ Neutron 32 K
a (Å)	9.9415(4)	9.9580(6)	6.7697(1)	6.742(4)
b (Å)	6.8633(3)	6.8808(4)	-	-
c (Å)	4.6050(2)	4.5810(3)	-	-
V (Å^3)	314.2	313.9	310.3	306.5
R_{Bragg} (%)	7.3	8.5	19	7.8
Pnma	x	y	z	
U (ac)	0.3953(4)	$\frac{1}{4}$	0.2928(5)	
(ann)	0.3960(5)	$\frac{1}{4}$	0.2988(7)	
Pd (ac)	0.1265(10)	$\frac{1}{4}$	0.5223(10)	
(ann)	0.1239(13)	$\frac{1}{4}$	0.5191(12)	
Pd (ac)	0.1721(7)	$\frac{1}{4}$	0.0445(10)	
(ann)	0.1751(9)	$\frac{1}{4}$	0.0458(13)	
Sn (ac)	0.3683(7)	$\frac{1}{4}$	0.7737(12)	
(ann)	0.3685(9)	$\frac{1}{4}$	0.7767(13)	

Table 4.2: The results of the Rietveld refinement of UPd_2Sn ($Pnma$) and $UPd_{1.85}Sn$ ($Fm\bar{3}m$) from X-ray and Neutron scattering investigations. We include positional parameters x, y, z of the $Pnma$ lattice of UPd_2Sn, (ac) and (ann), assuming Model I from Ref. [10].

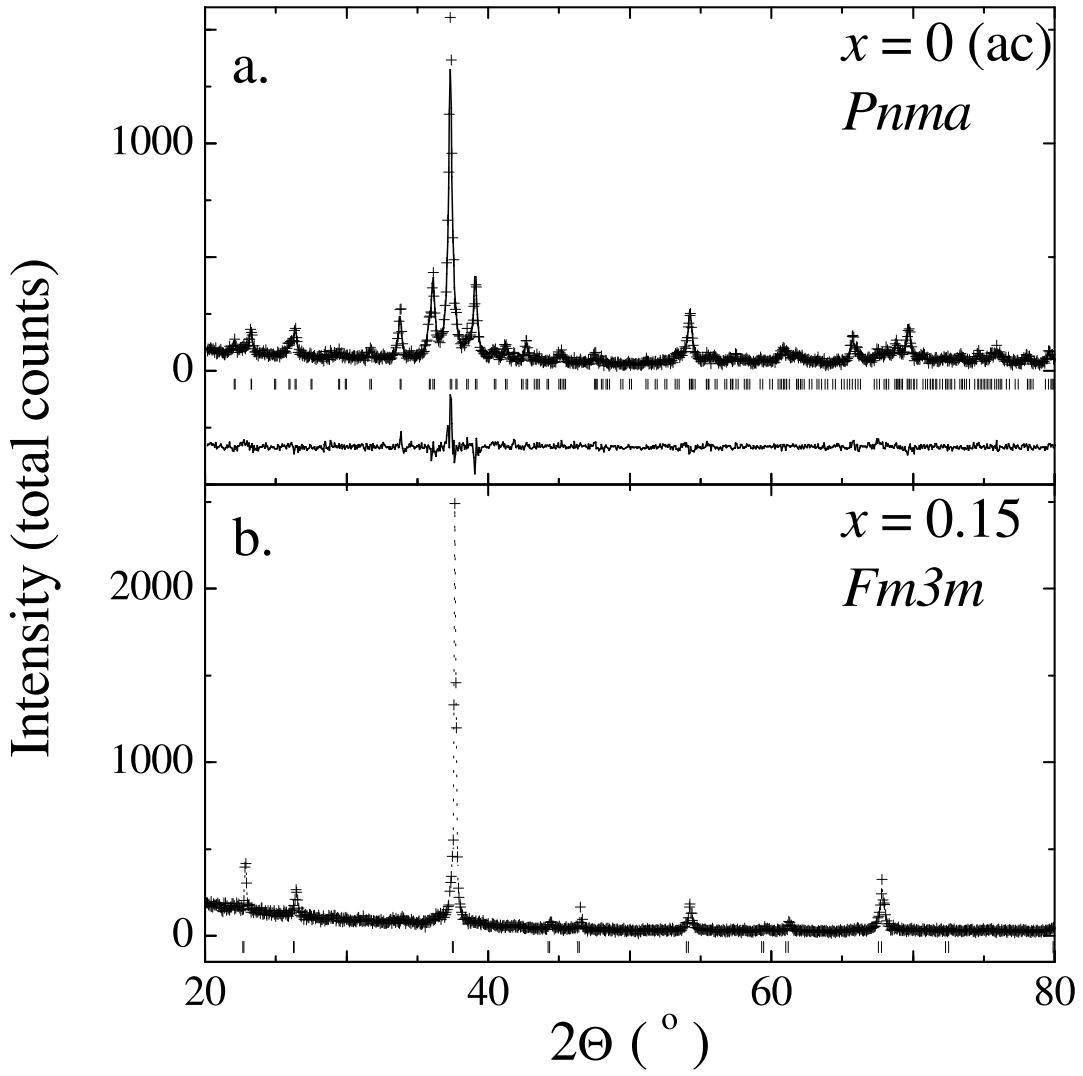

Figure 4.3: The room temperature X-Ray diffraction spectra of $UPd_{2-x}Sn$ in the orthorhombic *Pnma* (x=0 (ac)) (*a.*) and cubic $Fm\bar{3}m$ (x=0.15) (*b.*) phase. (+) represent experimental data, tics indicate Bragg positions, the result of refinement and the difference between refinement and fit are plotted as solid line.

spectrum is obtained by assuming a fully ordered cubic Heusler structure $Fm\bar{3}m$, yielding a Bragg value $R_{Bragg} = 7.8\,\%$. The lattice parameter $a = 6.742(4)$ Å is in good agreement with the value estimated by means of X-ray diffraction. From the comparison of the refinement with the data we find four peaks from a minority phase. The peak positions correspond to those of the orthorhombic *Pnma* lattice. Therefore we attribute the peaks to regions in the matrix crystallizing in this superstructure of the Heusler lattice (about 5 % volume amount). The fact that we could not appropriately refine the X-Ray spectra we attribute to preferential

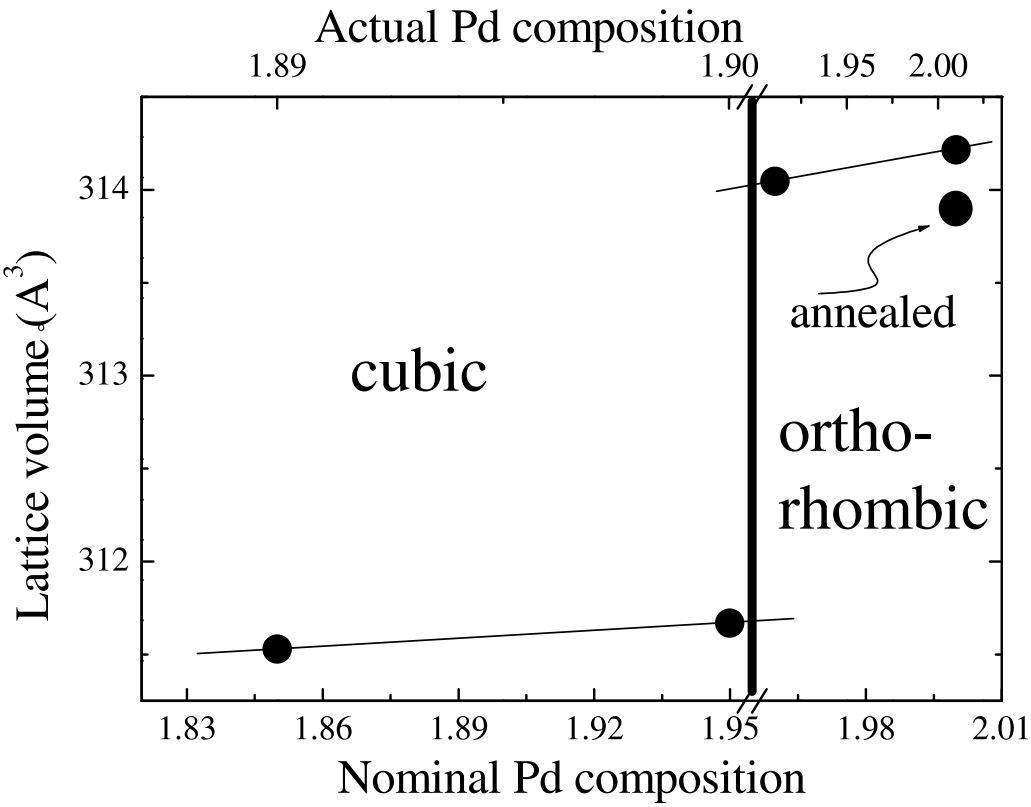

Figure 4.4: Unit cell volume V as function of nominal and actual composition.

orientation of the powder grains.

As was discussed in [10], the site occupation of the inequivalent positions in the $Pnma$ structure cannot unambiguously be determined in the X-ray experiments. For the refinement in Fig. 4.3(a) we employed model I from Ref. [10], but model IIA yields equally low R_{Bragg} values. The models II, IIB, III and IV from Ref. [10] yield significantly larger R_{Bragg} values, hence we discard them as structural models for orthorhombic $UPd_{2-x}Sn$. Analogously, for cubic $Fm\bar{3}m$ $UPd_{2-x}Sn$ we cannot unambiguously establish the site occupation.

Finally, we note that the structural transition from the orthorhombic $Pnma$ to cubic $Fm\bar{3}m$ lattice is accompanied by a decrease of the volume of the unit cell of V_{orth}-$V_{cub}$$\sim$1% (Table 4.2, Fig. 4.4). Disregarding band structure or band filling effects, the transition into cubic symmetry thus corresponds to the exertion of the chemical pressure of the order of 1GPa.

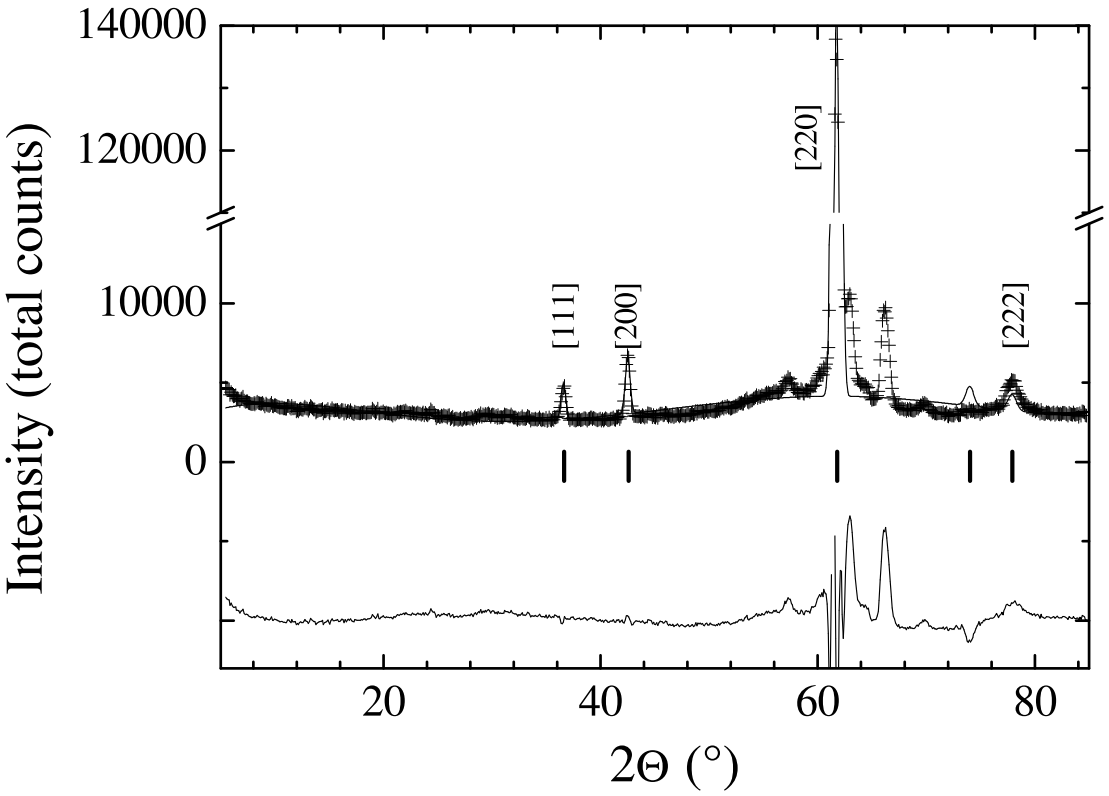

Figure 4.5: The neutron diffraction spectra of $UPd_{2-x}Sn$, x=0.15, at T=32K.(+) represent experimental data, tics indicate Bragg positions, the result of the refinement and the difference between refinement and fit are plotted as solid line.

4.3 Magnetic properties of $UPd_{2-x}Sn$

4.3.1 Magnetization and specific heat

In order to clarify the nature of the magnetic ground state properties of $UPd_{2-x}Sn$ we measured the susceptibility χ_{dc}. We plot in Fig. 4.6 the susceptibility and in Fig. 4.7 inverse susceptibility of the samples $UPd_{2-x}Sn$, $x = 0$ (ac), 0 (ann), 0.04, 0.05 and 0.15. The dc susceptibility χ exhibits Curie–Weiss behavior at high temperatures for all samples. In Table 4.3 we summarize the results of Curie–Weiss fits to the data above 100 K, revealing that for all samples the effective moment μ_{eff} is close to that of either U^{3+} and U^{4+}. Moreover, we observe negative intercepts of χ^{-1} with the T axis, with $\Theta_{CW} \sim$–80 K, implying antiferromagnetic coupling between the U ions.

At low temperatures an antiferromagnetic anomaly is observed at $T_N = 25.7$ K for $UPd_{2-x}Sn$, $x = 0.15$ and $T_N = 24.6$ K for $x = 0.05$ (Fig. 4.8), determined from the maximum of $d(\chi T)/dT$. In addition, irreversibility occurs between suscepti-

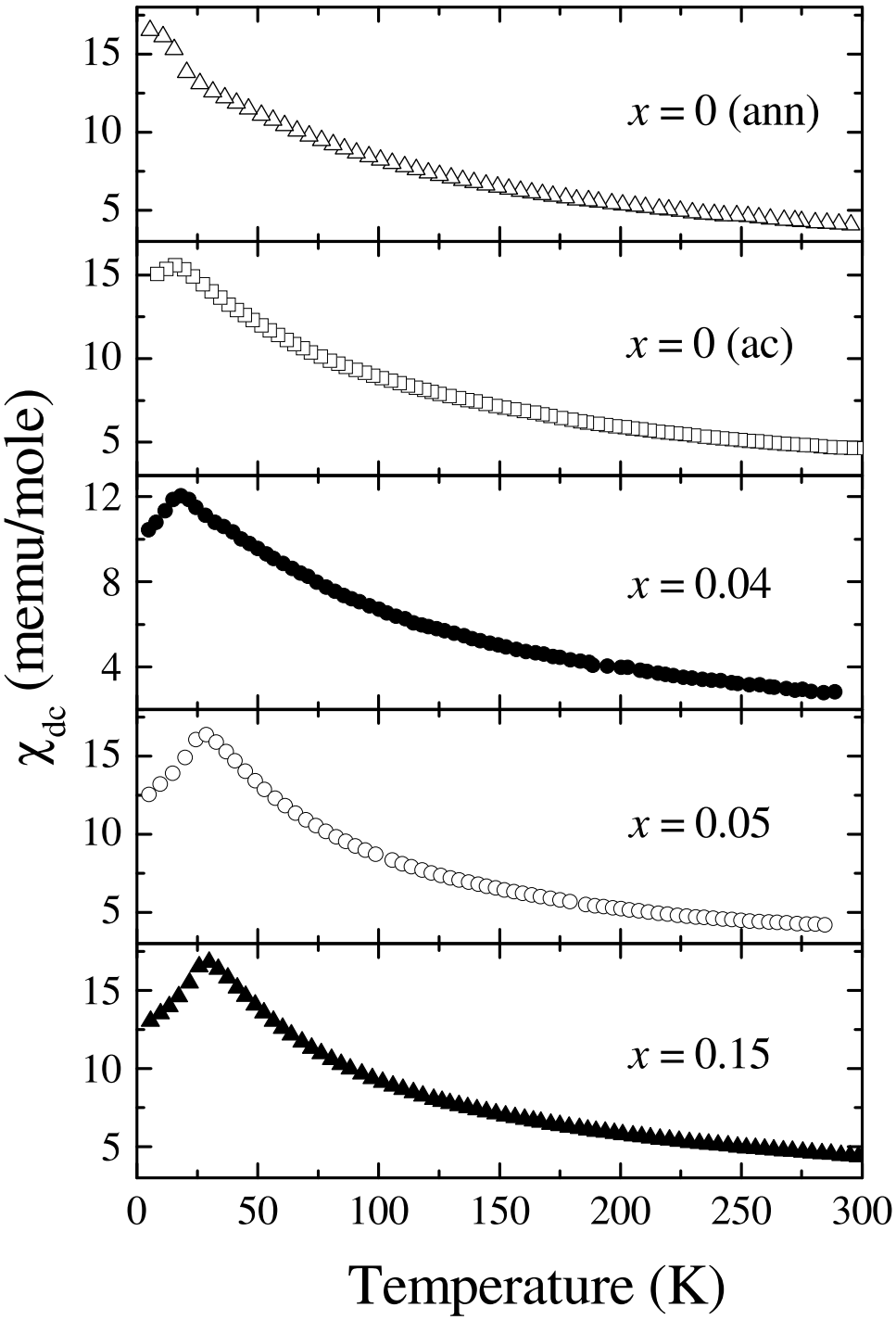

Figure 4.6: Dc-susceptibility of $UPd_{2-x}Sn$, $x = 0$ (ac), 0 (ann), 0.04, 0.05 and 0.15.

bility measurements determined in field cooled (FC) and zero field cooled (FC) mode below a blocking temperature $T_B > T_N$ (Table 4.3). The observation of mag-

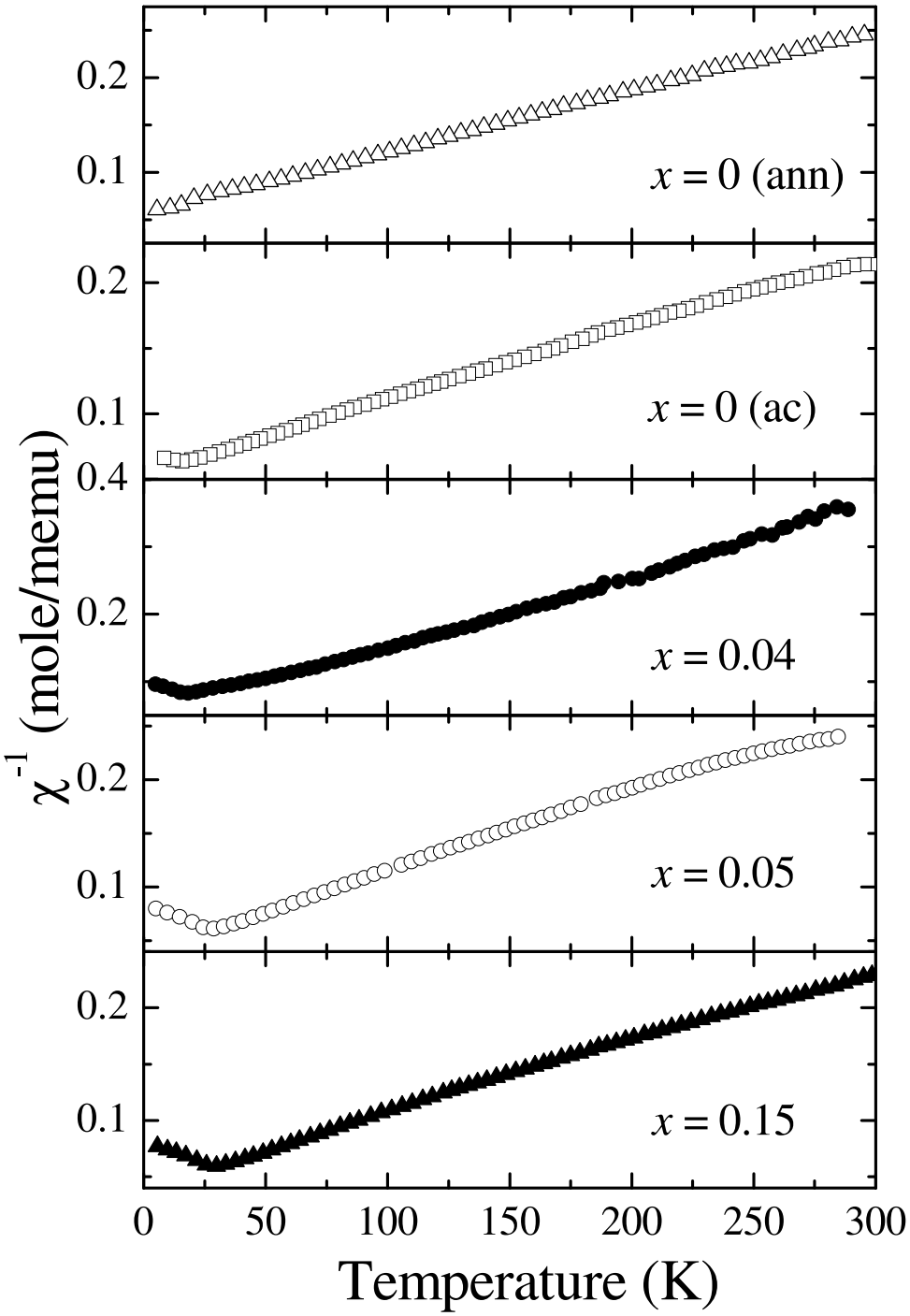

Figure 4.7: Inverse susceptibility of $UPd_{2-x}Sn$, $x = 0$ (ac), 0 (ann), 0.04, 0.05 and 0.15.

netic irreversibility indicates that crystallographic disorder affects the magnetic properties. The irreversibility does not indicate spin glass behavior, as there is

x	0 (ac)	0 (ann)	0.04	0.05	0.15
μ_{eff} (μ_B)	3.8	3.5	3.5	3.3	3.6
Θ_{CW} (K)	-100	-88	-88	-75	-87
T_N (K)	-	-	-	24.6	25.7
T_B (K)	27	19	27	31	31

Table 4.3: The results of Curie–Weiss fits to the susceptibility, antiferromagnetic transition (T_N) and blocking temperatures (T_B) of $UPd_{2-x}Sn$.

no frequency dependence of the ac susceptibility cusp [2].

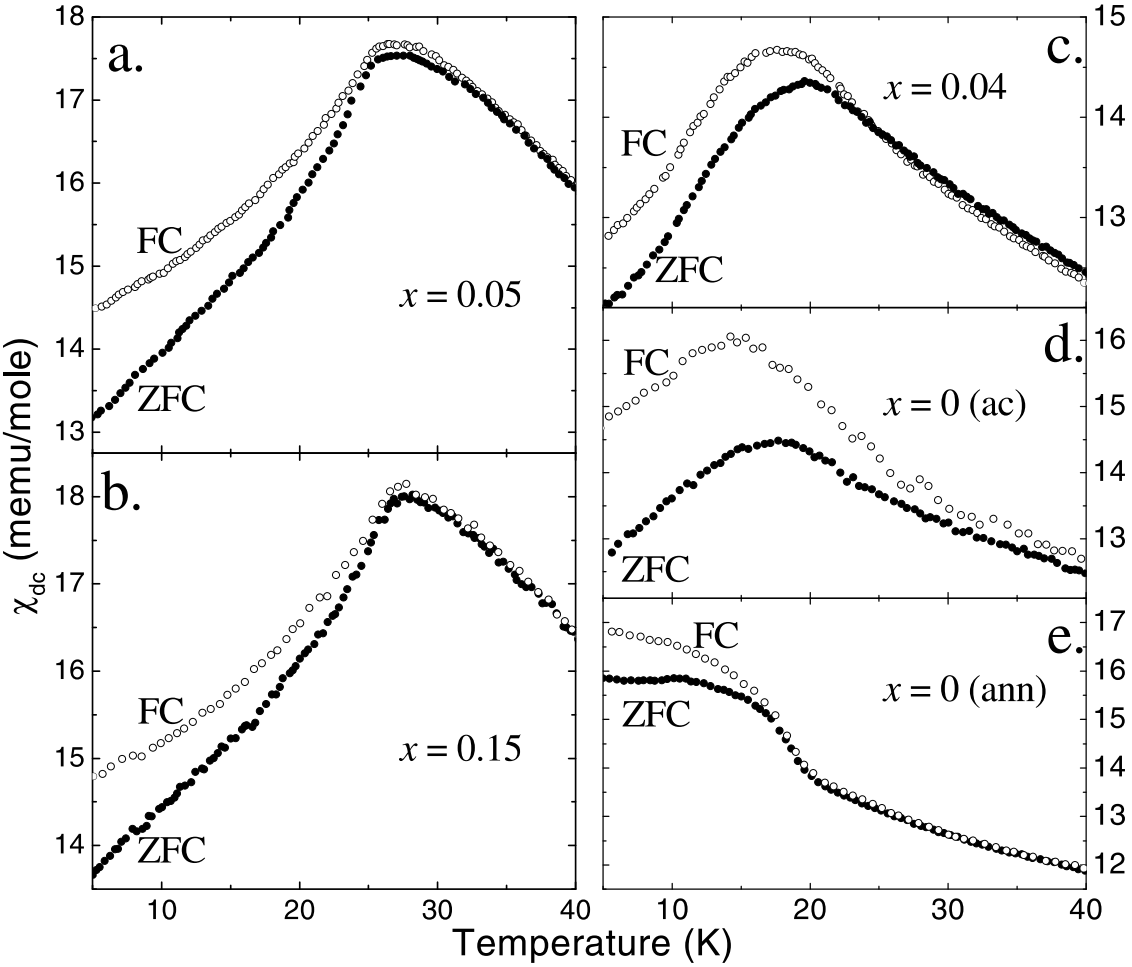

Figure 4.8: Low temperature susceptibility of $UPd_{2-x}Sn$, $x = 0.05$ (a.), 0.15 (b.), 0.04 (c.), 0 (ac) (d.) and 0 (ann) (e.) measured in field cooled (FC) and zero field cooled (ZFC) mode.

Surprisingly, for as–cast material $UPd_{2-x}Sn$, $x = 0$ and 0.04, similarly an antiferromagnetic–like anomaly is observed at about 17 K (Fig. 4.8(c,d)). As well,

irreversibility occurs between FC and ZFC experiment, denoting a freezing transition of clusters of U spins below a blocking temperature T_B (see Table 4.3). Annealing $UPd_{2-x}Sn$, $x=0$ (ann), modifies the temperature dependence of the susceptibility at low temperatures. The susceptibility measured in FC mode now resembles that reported in Ref. [9]. There is no maximum in χ, but rather a Kondo–like saturation for $T \to 0$. However, we still observe irreversibility between FC and ZFC measurement below T_B, albeit less than in the as–cast case (Fig. 4.8(e)). The strong sample dependence and the absence of a signature of an AFM transition in the specific heat and the resistivity (see below) indicate that the antiferromagnetic–like features in $UPd_{2-x}Sn$, $x=0$ and 0.04, are not arising from a bulk transition. Rather, it appears that clusters of U ions diluted in a non–magnetic matrix undergo a blocking transition with accompanying irreversibility below T_B. It implies that in as–cast $UPd_{2-x}Sn$, $x=0$ and 0.04, crystallographic disorder is present, which in previous investigations has been overlooked. The disorder can be reduced by an annealing procedure, although it is not completely removed.

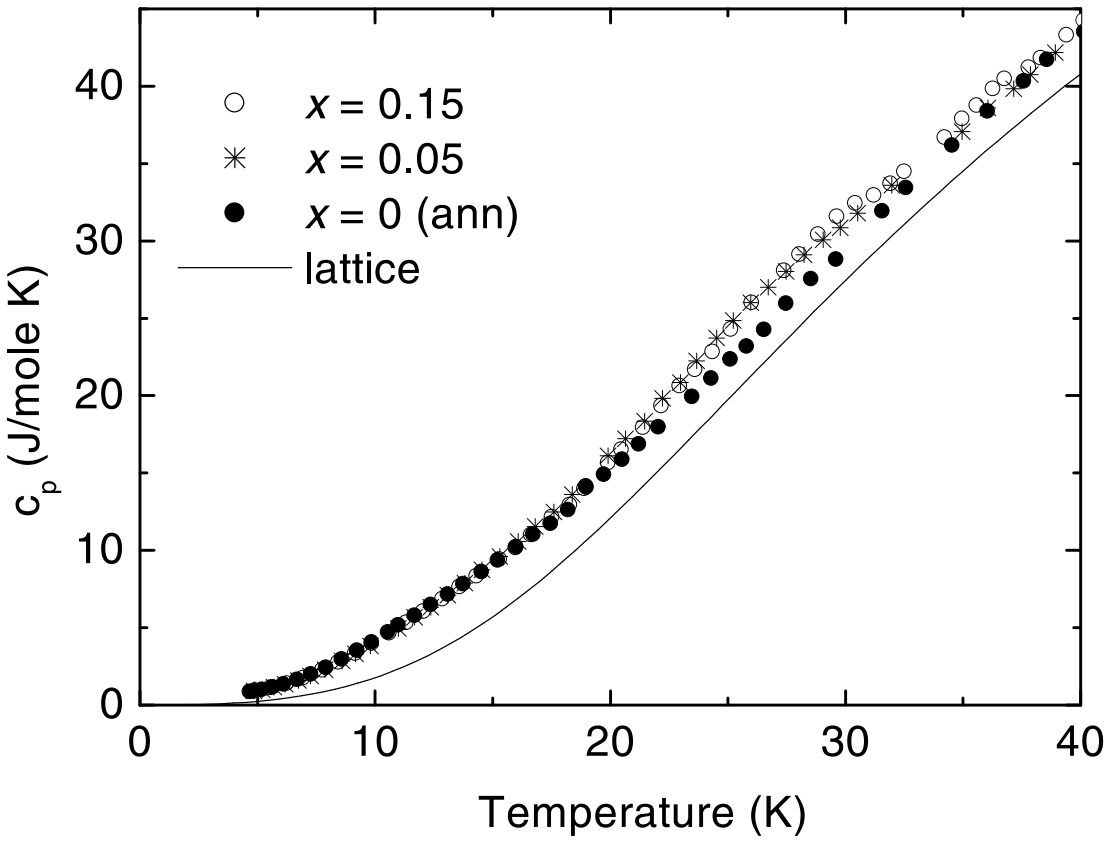

Figure 4.9: The temperature dependence of the specific heat c_p of $UPd_{2-x}Sn$, $x=0$ (ann) (•), 0.05 (+) and 0.15 (○). The solid line represents the lattice contribution $c_{p,lat}$.

To establish if the antiferromagnetic features in $UPd_{2-x}Sn$ are of bulk nature we performed specific heat measurements. In Fig. 4.9 we plot the total specific heat c_p of $UPd_{2-x}Sn$, $x = 0$, 0.05 and 0.15. From the total specific heat we subtract the lattice contribution, reported in Ref. [9] for $ThPd_2Sn$. This lattice specific heat $c_{p,lat}$ can be parameterized by using two Debye temperatures $\Theta_D(\mathrm{U}) = 138\,\mathrm{K}$, $\Theta_D(Pd,Sn) = 159\,\mathrm{K}$ and an Einstein mode $\Theta_E(Pd,Sn) = 319\,\mathrm{K}$ (solid line in Fig. 4.9). We obtain the magnetic specific heat $c_{p,mag} = c_p$ - $c_{p,lat}$ in Fig. 4.10(a).

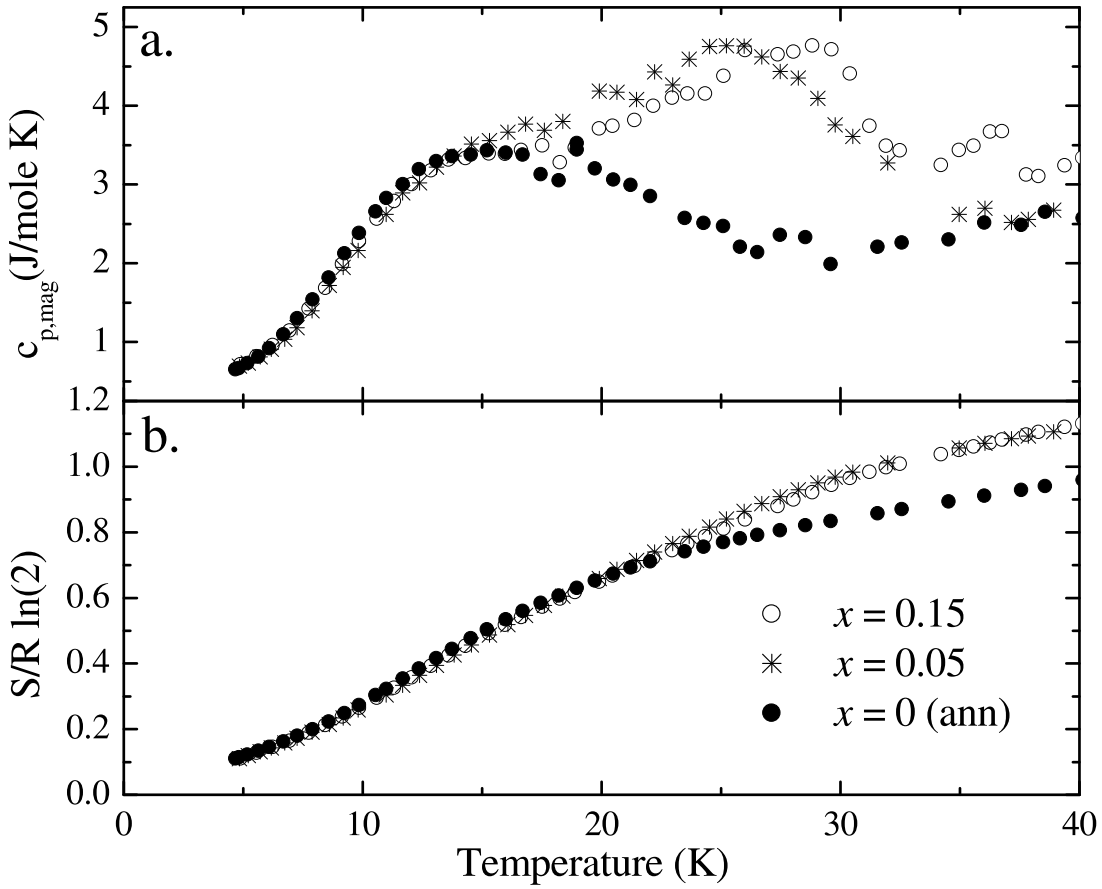

Figure 4.10: a.) The magnetic specific heat $c_{p,mag} = c_p$ - $c_{p,lat}$ of $UPd_{2-x}Sn$, $x = 0$ (ann) (•), 0.05 (+) and 0.15 (○). b.) The entropy S, calculated from the magnetic specific heat $c_{p,mag}$ in Fig. 4.10(a).

For $UPd_{2-x}Sn$, $x = 0$ (ann), we qualitatively and semi–quantitatively reproduce the findings from Ref. [9], *i.e.* an archetypical Kondo lattice specific heat with a maximum in $c_{p,mag}$ at about 15 K, and Fermi–Liquid behavior $c_{p,mag} = \gamma T + \beta T^3$ for $T \to 0$. A γ value of 130 mJ/mole K^2 indicates moderate mass enhancement. However, it is noteworthy that in Ref. [9] the maximum in $c_{p,mag}$ occurs at a somewhat lower temperature of $\sim 10\,\mathrm{K}$. In view of the results of

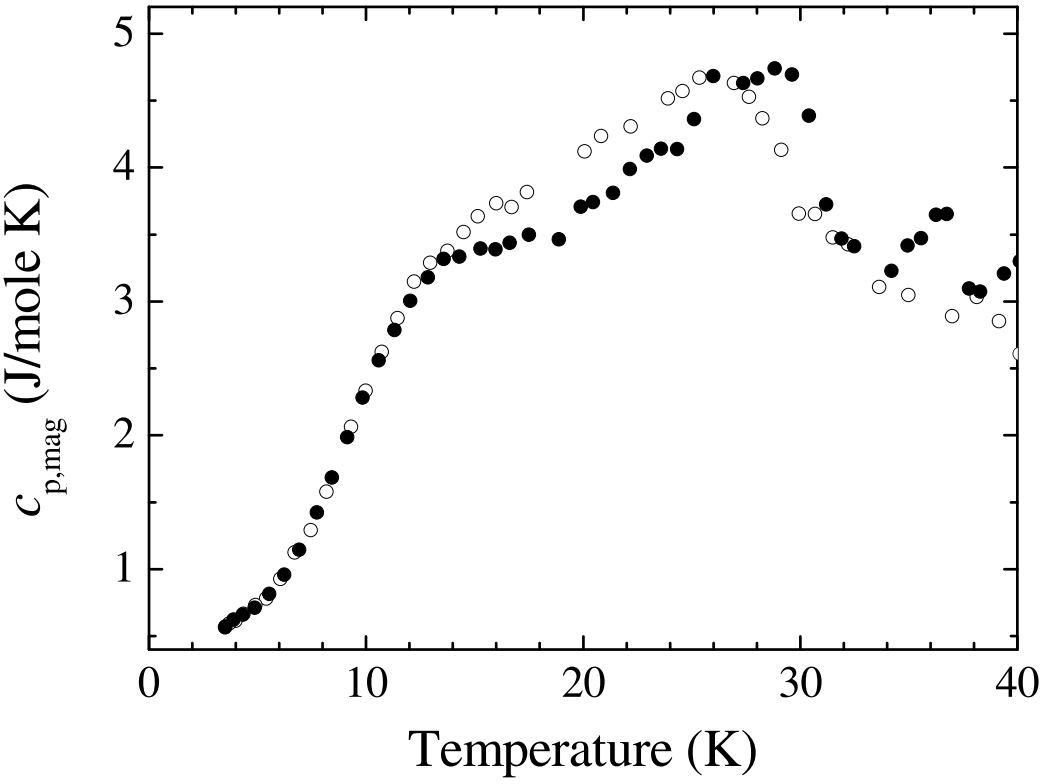

Figure 4.11: The magnetic specific heat $c_{p,mag} = c_p$ - $c_{p,lat}$ of $UPd_{2-x}Sn$, $x = 0.15$ in the field B=0T (filled symbols) and 3T (open symbols).

the susceptibility study it might indicate that $c_{p,mag}$ in part arises from magnetic clusters.

At low temperatures the specific heat of $UPd_{2-x}Sn$, $x = 0.05$ and 0.15, also is well reproduced by $c_{p,mag} = \gamma T + \beta T^3$, with $\gamma = 130\,\mathrm{mJ/mole\,K^2}$. Dissimilarly, at higher temperatures additional magnetic specific heat contributions are observed. Peak like maxima occur at 29 K for $x = 0.15$ (26 K for $x = 0.05$), with the contributions from magnetic fluctuations ranging up to 40 K. Application of magnetic fields hardly affects the specific heat, with the peak like maximum (and hence T_N) lowered by about 2K in fields of 3T for the sample x=0.15 (Fig. 4.11).

Based on the data for $c_{p,mag}$, the entropy can be derived from $S = \int (c_{p,mag}/T) dT$. In Fig. 4.10(b) we plot the entropies as function of T. The magnetic entropy for the samples $UPd_{2-x}Sn$, $x = 0.05$ and 0.15, at 40 K is evaluated to $S = 1.13\,R\ln(2)$. The difference to the value of $UPd_{2-x}Sn$, $x = 0$ (ann), $S = 0.94\,R\ln(2)$, represents the contribution from magnetic ordering below T_N and cluster formation around T_B.

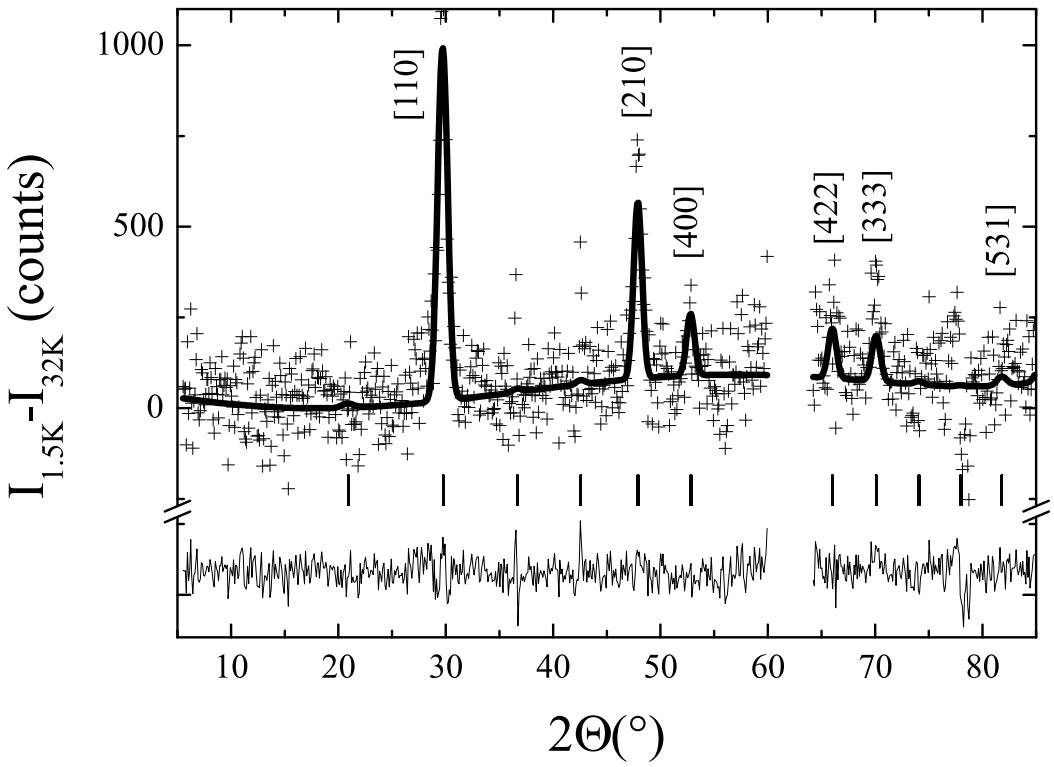

Figure 4.12: The magnetic Bragg intensity $I_{1.5\mathrm{K}}$ - $I_{32\mathrm{K}}$ of $UPd_{1.85}Sn$. The data (+) is refined (solid line) assuming the structure from Fig. 4.13. Bragg peak positions are indicated by tics, the solid line in the lower panel represents the difference between fit and data. The area of the main structural Bragg peak at 62^o is omitted.

4.3.2 Magnetic structure

In the context of disorder, it is important to establish the magnetic structure of cubic $UPd_{2-x}Sn$ on a microscopic scale. Neutron diffraction spectra taken in the antiferromagnetic state reveal the presence of additional magnetic Bragg peaks. By subtracting the spectra measured at $T = 32\,\mathrm{K}$ from the 1.5 K spectrum we obtain the magnetic difference spectrum $I_{1.5\mathrm{K}}$ - $I_{32\mathrm{K}}$ plotted in Fig. 4.12.

We can fit the magnetic spectrum assuming a simple antiferromagnetic arrangement of the spins as depicted in Fig. 4.13. In the refinement we obtain a comparatively large value $R_{Bragg} = 22\,\%$, which, however, mostly is due to the large scattering of the background. The marks "+" and "−" indicate spin up/down alignment relative to the nearest neighbor. From our powder data we cannot determine the direction of the moment with respect to the unit cell axes. The structure corresponds to an antiferromagnetic ordering vector $\vec{k} = [0\ 0\ 0]$, *i.e.*, structural and magnetic unit cells are identical.

From the temperature dependence of the scattering intensity of the mag-

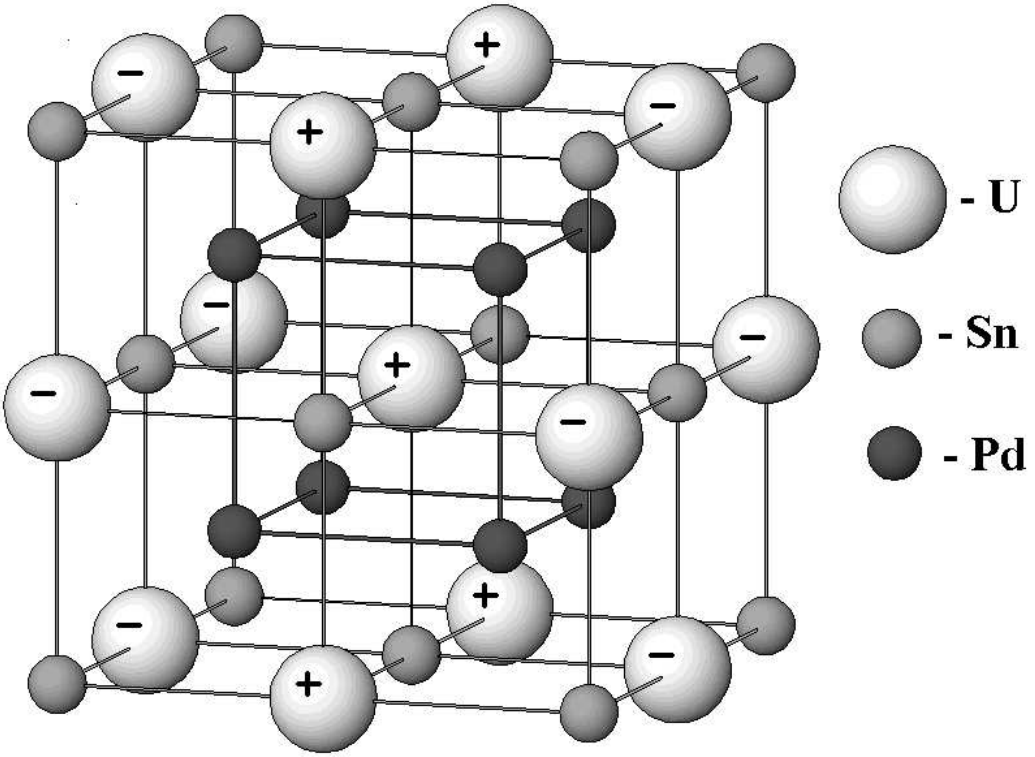

Figure 4.13: The cubic Heusler $Fm\bar{3}m$ structure of $UPd_{1.85}Sn$, indicating the antiferromagnetic spin arrangement by "+" and "-" in the magnetically ordered state.

netic Bragg peaks we obtain the T dependence of the ordered magnetic moment (Fig. 4.14). A fit to the data with $\mu_{ord}(T) = \mu_{ord,0}\,(T_N - T)^{2\beta}$ yields a value $\mu_{ord,0} = 1.03(9)$ and $\beta = 0.31(8)$. The moment is typical in size for moderate heavy fermion compounds, with partial reduction from Kondo screening (for comparison: U_2Pd_2Sn: $\mu_{ord} = 2\,\mu_B$ [12]; $U_2Rh_3Si_5$: $\mu_{ord} = 2.4\,\mu_B$ [13]; UPdSn: $\mu_{ord} = 1.3\,\mu_B$ [14]).

The influence of the crystallographic disorder is directly observed in the magnetic Bragg spectrum. In Fig. 4.15 we plot the magnetic [1 1 0] and [2 1 0] peaks as function of angle 2Θ. A comparison to the experimental resolution of the E6 spectrometer at the Berlin Neutron Scattering Center (bars indicate resolution limit) demonstrates that both peaks (as all others observed) are not resolution limited. It implies that the correlation length ξ in the antiferromagnetic state is comparatively small. From the width of the Bragg peaks we calculate $\xi \simeq 100$ Å. This behavior is analogous to the findings in materials with atomic site disorder like U_2PtGa_3 and U_2PdGa_3 [15].

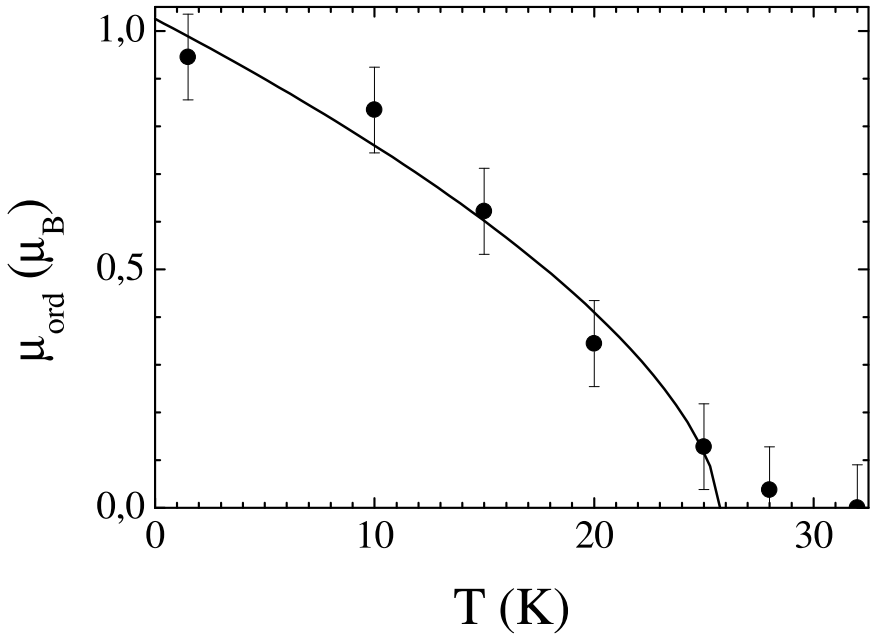

Figure 4.14: The temperature dependence of the magnetic Bragg peak intensity of $UPd_{2-x}Sn$, $x = 0.15$. The solid line represents a fit to the data employing $\mu_{ord}(T) = \mu_{ord,0}\,(T_N - T)^{2\beta}$; for details see text.

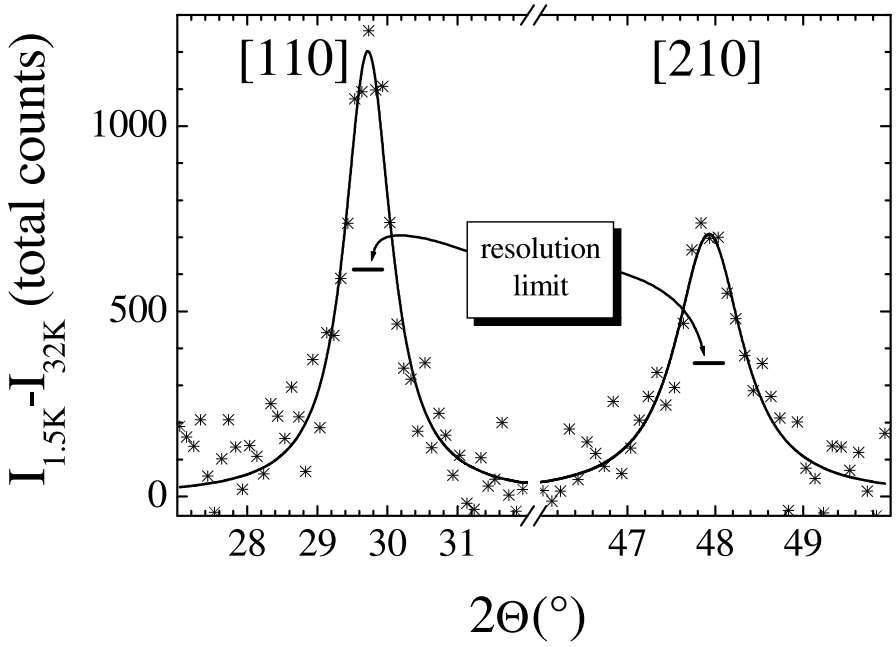

Figure 4.15: The angular dependence of the magnetic [1 1 0] and [2 1 0] peaks of $UPd_{2-x}Sn$, $x = 0.15$, at 1.5 K. The solid bars indicate the experimental resolution.

4.4 Transport properties of $UPd_{2-x}Sn$

4.4.1 Electrical resistivity

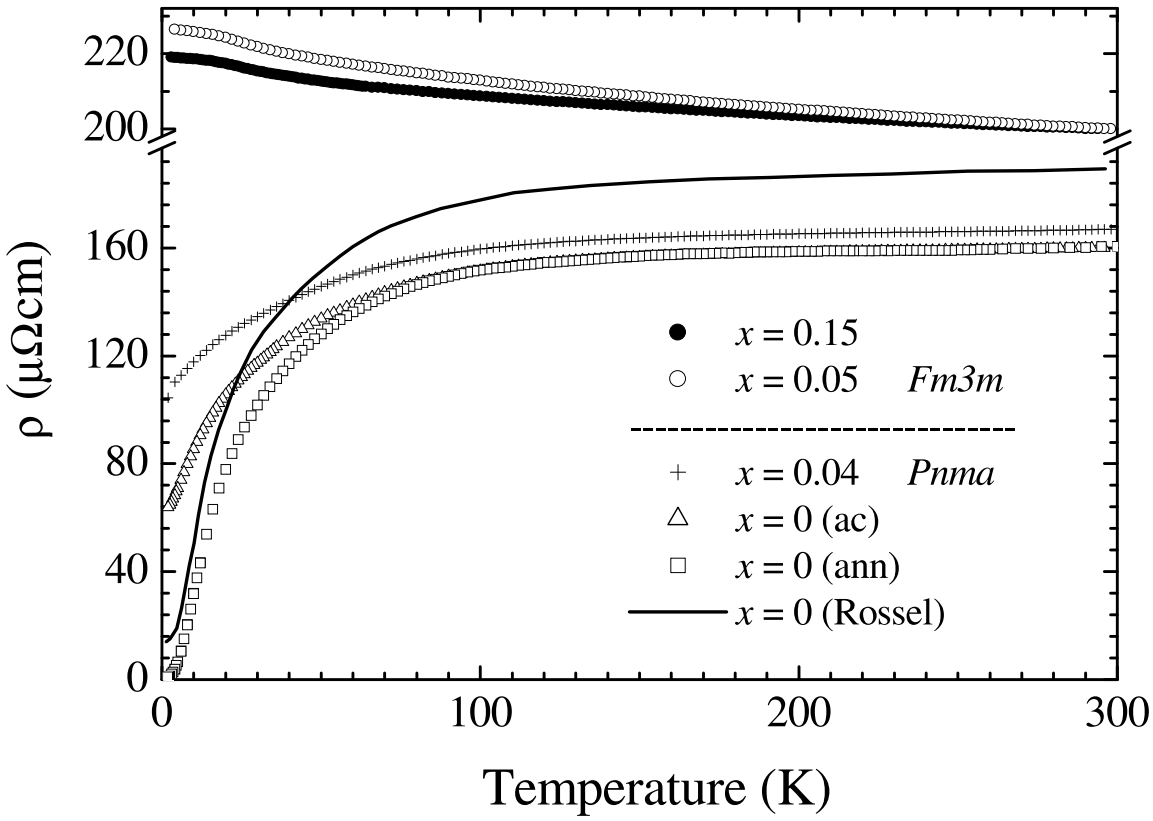

Figure 4.16: The resistivity of $UPd_{2-x}Sn$ as function of temperature for the cubic $Fm\bar{3}m$ samples $x = 0.05$, 0.15 and the orthorhombic $Pnma$ x=0.04, 0 (ac), (ann) and from Ref. [9].

The structural transition from the orthorhombic $Pnma$ lattice to the cubic $Fm\bar{3}m$ structure in $UPd_{2-x}Sn$ is accompanied by a qualitative change of the electronic transport characteristics [11]. This is illustrated in (Fig. 4.16), where we plot the resistivity of $UPd_{2-x}Sn$, $0 \leq x \leq 0.15$, as function of temperature. For the orthorhombic samples archetypical metallic heavy fermion behavior is observed: at high temperatures ρ is comparatively large and almost temperature independent, but at low temperatures, as coherence sets in, the resistivity drops and exhibits a Fermi-Liquid behavior $\rho = \rho_0 + AT^2$ for $T \rightarrow 0$. There is no indication for antiferromagnetic ordering at or below T_B. The residual resistivity is strongly dependent on the heat treatment and the stoichiometry, ranging from 98$\mu\Omega$cm for $UPd_{2-x}Sn$, x=0.04 to 1$\mu\Omega$cm for the x=0 (ann) sample. In contrast, for the cubic material the overall resistivity is much larger and with a

negative $d\rho/dT$ "semiconducting–like" at all temperatures. The overall temperature dependence of the cubic samples is weak, resembling the behavior of strongly disordered metals [16, 17]. Only in a limited temperature range 30 – 80 K can the resistivity be described by a Kondo–like dependence $\rho - \rho_0 \propto \ln(T)$. However, associating the resistivity here to Kondo scattering appears very awkward with the weak T dependence, as the resistivity merely changes by 7 $\mu\Omega$ cm from 30 to 80 K, that is by 3 %.

In spite of the unusual resistivity of the cubic samples a signature of the antiferromagnetic transition is seen at T_N (Fig. 4.17(a)). The behavior is reminiscent of the opening of a spin density wave gap, but less distinct than in cases like URu_2Si_2 [18, 19, 20]. To qualitatively extract the temperature dependence of the AFM resistive contribution we assume that the resistivity can be decomposed into two components: $\rho(T) = \rho_{metal} + \rho_{AFM}$. Here, ρ_{metal} represents the disordered metal–like resistivity, which we approximate as $\propto T$ (solid lines in Fig. 4.17(a)). We obtain $\rho_{AFM} = \rho(T) - \rho_{metal}$ in Fig. 4.17(b). While ρ_{AFM} is only a fraction (~ 0.3 %) of ρ_{metal}, the resemblance to the opening of a spin density wave gap is still apparent: ρ_{AFM} suddenly increases close to T_N, traverses a maximum at 18 K and approaches 0 for $T \to 0$.

From the plot a value $T_N \approx 30$ K is extracted. Probably, the deviation from the values obtained in the susceptibility or neutron scattering is a consequence of the simple parametrization of ρ_{metal}. A more accurate value for T_N in $UPd_{2-x}Sn$ is obtained from the temperature derivative of $d\rho/dT$, plotted in Fig. 4.17(c). Here, a minimum occurs in $d\rho/dT$ at T_N.

The magnetoresistivity also reveals a clear distinction of the electronic transport modi of cubic and orthorhombic $UPd_{2-x}Sn$ (Fig. 4.18). In the coherent regime orthorhombic $UPd_{2-x}Sn$, represented by the samples x=0 (ac) and 0.04, exhibits an archetypical Kondo lattice magnetoresistivity, *i.e.*, $\Delta\rho/\rho$=$\rho(B)$-$\rho(B$=0)/$\rho(B$=0)<0, a weak initial curvature and almost linear field dependence at higher fields [21]. A value $|\ \Delta\rho/\rho\ |$∼2-3% for x=0 (ac) and 0.2-0.6% for x=0.04 in 5T reflects the suppression of Kondo and spin disorder scattering, which are the dominant low temperature resistive terms beyond the residual resistivity ρ_0=62 and 98$\mu\Omega$cm. $\rho(B$=0)-$\rho(B)$ traverses a maximum at about T^* ∼5-10K, which is generally taken as a measure for the lattice Kondo temperature. For $T \gg T^*$ (300K) the magnetoresistivity is negative and very small (6×10^{-5}).

The magnetoresistivity of cubic $UPd_{2-x}Sn$, represented by x=0.05 and 0.15, exhibits a much more complex behavior. For instance, for the sample x=0.05 at all temperatures the size of $\Delta\rho/\rho$ is of the order of a few 10^{-4}. At 300K the magnetoresistivity is positive, and larger than for the orthorhombic samples. Upon lowering temperature it becomes negative, with an almost quadratic dependence (50K), until at lowest temperature both negative and positive magnetoresistive contributions superimpose, giving rise to a change of sign $\Delta\rho/\rho$ at about 3-4T for T below ∼10K. The resistive contributions responding to an external magnetic field represent only a very small fraction of the total resistivity (∼0.1$\mu\Omega$cm), con-

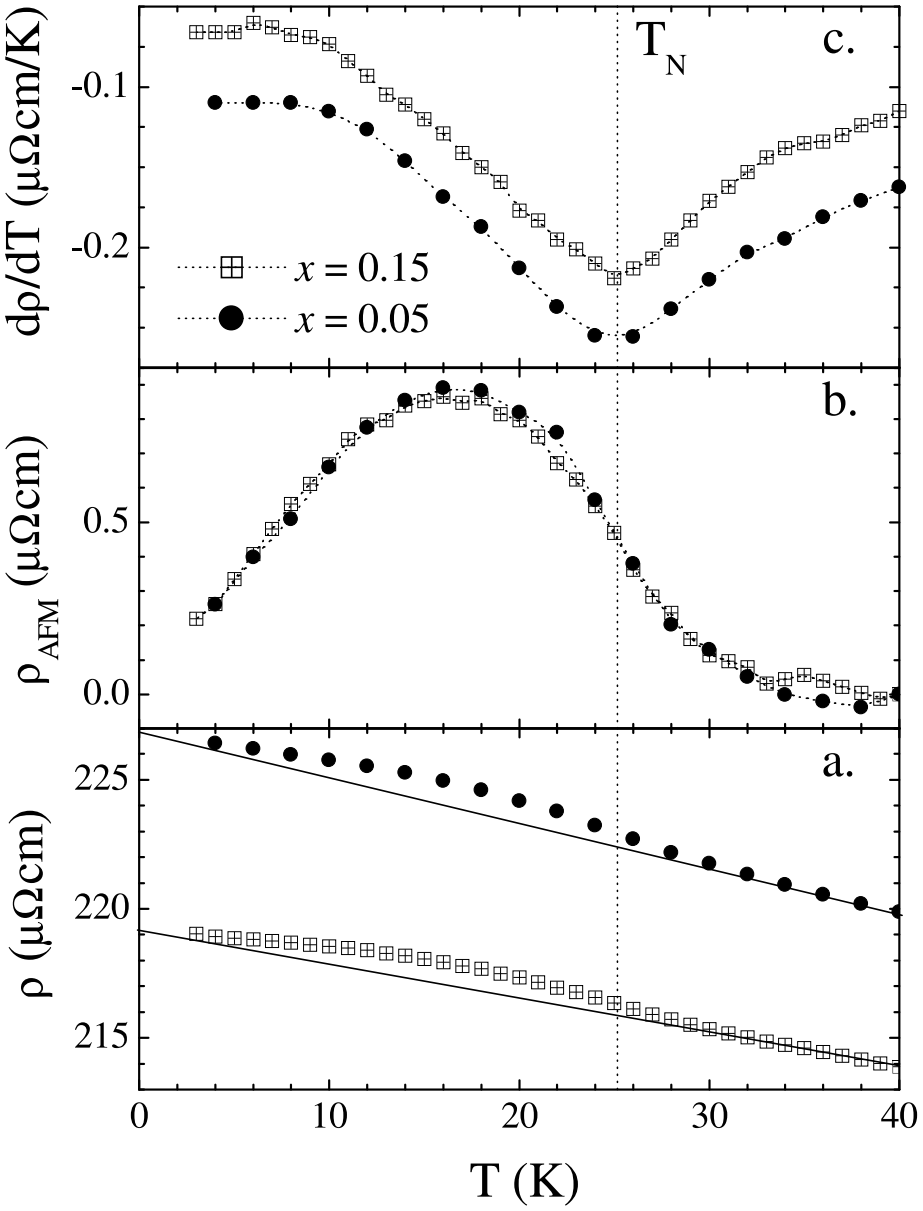

Figure 4.17: (a) The low temperature resistivity of $UPd_{2-x}Sn$, x=0.05 and 0.15. (b) The antiferromagnetic resistive component ρ_{AFM}=ρ_T-ρ_{metal}. (c) The temperature derivative $d\rho/dT$ of $UPd_{2-x}Sn$; for details see text.

sistent with the small magnetic resistive contribution ρ_{AFM}. This magnetoresistive behavior is unlike that of other antiferromagnetically ordered heavy fermion compounds [22, 23, 24].

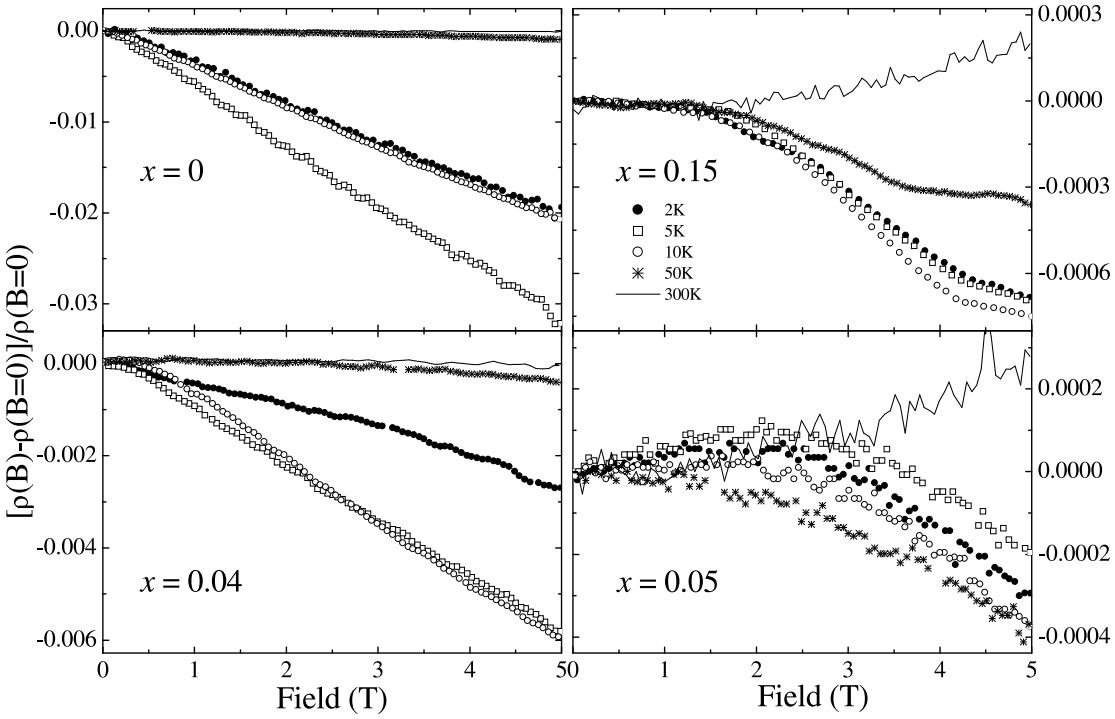

Figure 4.18: The magnetoresistivity of $UPd_{2-x}Sn$, x=0 (ac), 0.04, 0.05 and 0.15, at various temperatures.

4.4.2 Hall effect

To determine if the carrier density controls the transport characteristics of $UPd_{2-x}Sn$ we have carried out measurements of the Hall effect on a cubic and orthorhombic representative. In Fig. 4.19 we plot the Hall constant R_H as function of temperature for $UPd_{2-x}Sn$, $x = 0$ (ac) and 0.15. $UPd_{2-x}Sn$, $x = 0$ (ac) exhibits a smooth temperature dependence, with a broad maximum at 70 K, resembling the behavior of archetypical heavy fermion compounds like UPt_3 [25]. In contrast, for $x = 0.15$ a sharp maximum is seen at T_N.

Commonly, to analyze such data in heavy fermion materials it is decomposed into ordinary and skew scattering contribution [26]:

$$R_H = R_0 + \chi\rho_{mag}R_{S,Kondo}. \tag{4.1}$$

R_0 represents the ordinary Hall constant and measures the carrier density. The second term $\chi\rho_{mag}R_{S,Kondo}$ arises from anomalous Skew scattering in heavy fermions (ρ_{mag} magnetic resistive contribution).

For $UPd_{2-x}Sn$, x=0 (ac), following the argument of Ref. [26] of $\rho_{mag} \gg \rho_{lat}$, we take ρ rather than ρ_{mag} to describe the temperature evolution of R_H. In Fig. 4.19 we include the product of the experimental quantities resistivity and susceptibility, $\rho\chi$. A common heavy fermion behavior is observed, with $\rho\chi$ matching R_H

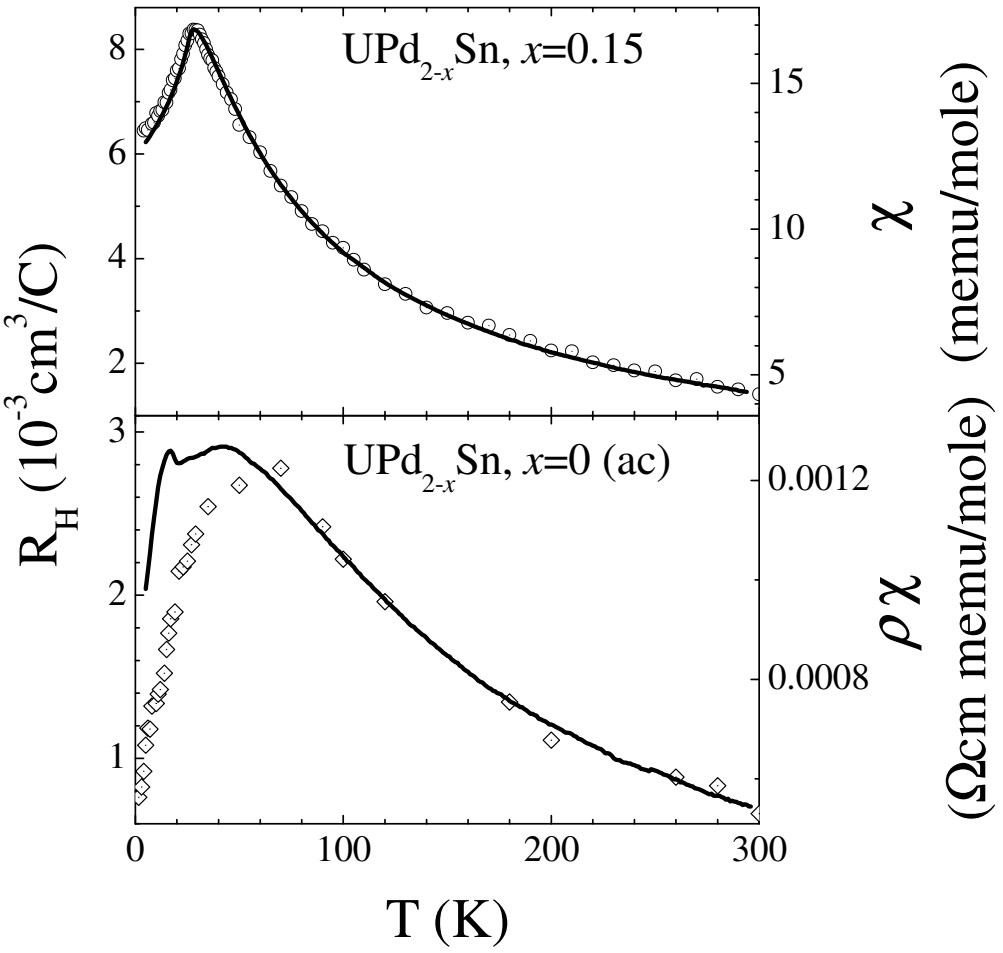

Figure 4.19: The Hall constant R_H of $UPd_{2-x}Sn$, x=0 (ac) and 0.15. For x=0 (ac) we include the product of the experimental quantities susceptibility and resistivity, $\rho\chi$, while for x=0.15 only the susceptibility is plotted (solid lines; right axes).

down to its maximum, which denotes the transition into the coherent state at about T_{coh} ∼70K. As usual for heavy fermions, the matching fails at $T < T_{coh}$.

As pointed out, for cubic $UPd_{2-x}Sn$, x=0.15, if we assume that the resistivity can be decomposed according to ρ=ρ_0+$\rho_{mag}(T)$ (again assuming the lattice contribution ρ_{lat} to be negligible), it requires a large value $\rho_0 \simeq 190\mu\Omega$cm to account for the experimental observation. Than, $\rho_{mag}(T)$ would represent a contribution changing by a factor ∼3 between room temperature and 2K. In consequence,

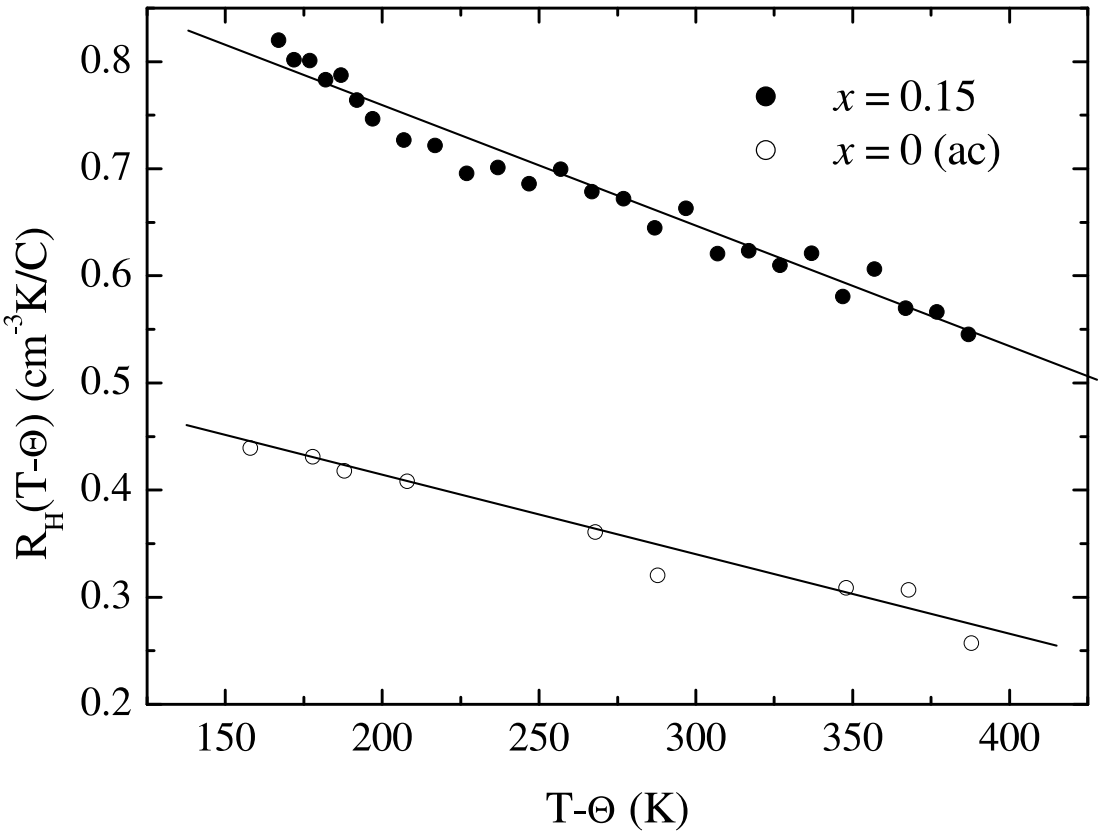

Figure 4.20: The decomposition of the Hall constant of $UPd_{2-x}Sn$, x=0 (ac) and 0.15 into the normal and anomalous parts for T>100K.

Eq. 4.1 does not account for the Hall constant of $UPd_{2-x}Sn$, x=0.15. This is demonstrated by the fact that the relationship

$$R_H = R_0 + \chi R_{S,mag}. \tag{4.2}$$

with a constant $R_{S,mag}$ yields full scaling over the complete temperature range. This is illustrated in Fig. 4.19.

In correspondence with Eqs. 4.1 and 4.2 and the fact that the susceptibility of $UPd_{2-x}Sn$ can be fitted by a Curie-Weiss law χ=$C/(T$-Θ) at high temperatures, in Fig. 4.20 we plot the dependence of $R_H(T$-Θ) as function of (T-Θ). This procedure allows the determination of the Hall effect parameters R_0, $R_{S,Kondo}$ and $R_{S,mag}$. The intersection of the straight line with the ordinate axis yields a value of 0.980(cm^{3}K/C) for $UPd_{2-x}Sn$, x=0.15 and 0.556(cm^{3}K/C) for x=0 as measure for R_0 [26]. Thus, we extract values R_0=-1.1*10^{-3}(cm^3/C) and $R_{S,mag}$=-4.6*10^2(cm^3/C) for $UPd_{2-x}Sn$, x=0.15, and R_0=-7.4*10^{-4}(cm^3/C); $R_{S,mag}$=-2.7*10^2(cm^3/C) for $UPd_{2-x}Sn$, x=0 (ac), respectively. The negative sign of R_0 implies that electronic transport dominates over holes in the current. In a one-band model for a spherical Fermi surface the value R_0 corresponds to carrier den-

sities of n=5.9*10$^{21}e^-$/cm^3 (1.8e^-/unit cell) and n=8.4*10$^{21}e^-$/cm^3 (2.6e^-/unit cell) for x=0.15 and 0 (ac), respectively. Thus, while there is a reduction of the carrier density accompanying the structural transition, both samples x=0.15 and 0 (ac) are metallic. A (pseudo)gap from (Kondo)insulating behavior can be discarded [27, 28, 29]. In consequence, the difference in the carrier density does not account for the qualitatively different behavior of the electronic transport.

4.5 Crystallographic disorder

It has been established that in Heusler compounds crystallographic disorder can be present in form of random displacements of ions from their high symmetry sites in the $Fm\bar{3}m$ lattice [8]. The disorder can be sufficient to affect and control the ground state properties.

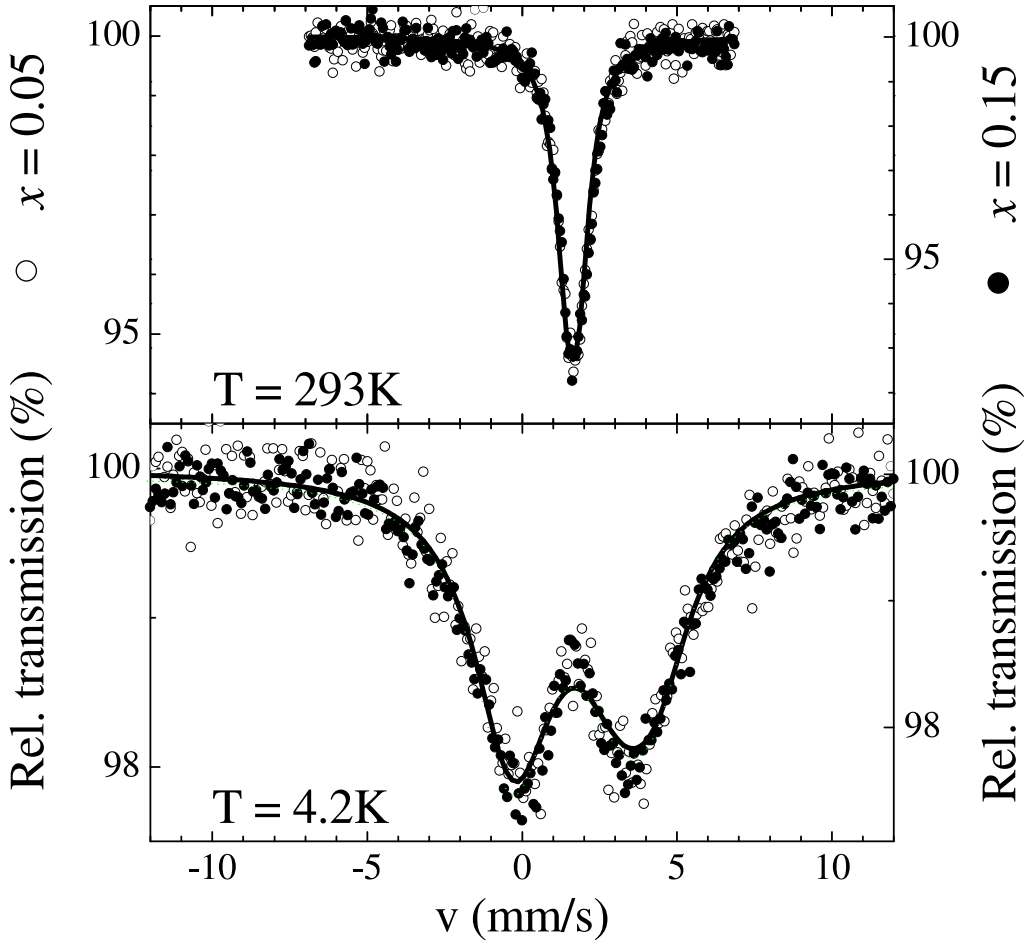

Figure 4.21: The Mössbauer spectra of $UPd_{2-x}Sn$, x=0.05 and x=0.15, at temperature T=293K and 4.2K. The result of a fit to the data is plotted as solid line.

Since the elements U, Pd and Sn have similar neutron scattering cross sections (U: 8.42×10^{-15}m; Pd: 5.91×10^{-15}m; Sn: 6.225×10^{-15}m), and their atomic weights are not differing by orders of magnitude, it is very difficult to extract information about atomic site exchange from diffraction experiments. In consequence, the site occupation of the inequivalent positions in the $Pnma$ and $Fm\bar{3}m$ lattice cannot unambiguously be determined. Moreover, the structural Bragg peaks are not anomalously broadened. Therefore, based on our diffraction experiments we cannot judge on the degree of order or disorder in $UPd_{2-x}Sn$. On the other hand, crystallographic disorder might give rise to different local environments resolvable with a local probe technique like for instance Mössbauer spectroscopy.

Previously, Mössbauer experiments have been performed on $UPd_{2-x}Sn$, x=0 [30]. In this study no anomalous line broadening from structural disorder has been reported. The data have been fitted assuming quadrupolar split Lorentzians with isomer-shifts IS, quadrupole splittings QS and line widths Γ (FWHM) of $IS = 1.73(1)\,\mathrm{mm/s}$, $QS \sim 0.4\,\mathrm{mm/s}$ and $\Gamma = 1.04(2)\,\mathrm{mm/s}$. In order to test if in cubic $UPd_{2-x}Sn$ hitherto unobserved types of crystallographic disorder are present, we have carried out ^{119}Sn Mössbauer–spectroscopy on $UPd_{2-x}Sn$, $x = 0.05$ and 0.15, using a $Ca^{119m}SnO_3$ source in conventional transmission–geometry. In Fig. 4.21 we plot the resulting spectra taken at 295 and 4.2 K.

At room temperature, for both samples single absorption lines are observed, which can be scaled onto each other. Further, the Mössbauer–spectra measured in the antiferromagnetic state at 4.2 K reveal a splitting of the absorption lines each into two lines by the hyperfine internal field. Again, the spectra from both compounds can be scaled onto each other, reflecting their close similarity in terms of magnetic and structural properties. Remarkably, the AFM line splitting is not symmetric, implying that both a Zeeman hyperfine field and a quadrupolar splitting need to be taken into account to describe the data. Since we have not observed a significant modification of the structural properties of cubic $UPd_{2-x}Sn$ between room and cryogenic temperatures, the quadrupolar splitting is also present at 295 K.

At room temperature the absorption lines are well described by a quadrupole split Lorentzian. From fits to the spectra we obtain values of $IS = 1.69(1)\,\mathrm{mm/s}$ $(1.72(1)\,\mathrm{mm/s})$, $QS = 0.41(3)\,\mathrm{mm/s}$ $(0.36(4)\,\mathrm{mm/s})$ and $\Gamma = 0.89(3)\,\mathrm{mm/s}$ $(0.94(5)\,\mathrm{mm/s})$ for $x = 0.05$ (0.15) (natural ^{119}Sn Mössbauer line width $\Gamma = 0.62\,\mathrm{mm/s}$).

In the fully ordered Heusler lattice no electric field gradient exists, and thus no quadrupolar splitting occurs (see for instance Dunlap and Jones [31]). Therefore, the presence of an electric field gradient in cubic $UPd_{2-x}Sn$ indicates a deviation from the fully ordered Heusler lattice. It might either arise from Sn ions not positioned on the high symmetric sites of the Heusler lattice, or from a non–cubic Sn environment. The latter possibility could be realized in a situation, in which the next nearest neighbors of Sn are removed from the $L2_1$ high symmetry positions, or via atomic site exchange on these lattice points breaking the cubic

symmetry. From our data we cannot decide which scenario is realized in cubic $UPd_{2-x}Sn$.

It is instructive to compare these findings to those of the closely related Heusler system UNi_2Sn, which undergoes a transition from an orthorhombic $Pnma$ to a cubic $Fm\bar{3}m$ lattice as T rises from 150 to 330 K [7]. Here, in Sn Mössbauer spectroscopy experiments a similar line width $\Gamma \sim 1$ mm/s is observed both in the $Pnma$ and $Fm\bar{3}m$ structure [32]. This similarity suggests two things: First, as in cubic $UPd_{2-x}Sn$ an electric field gradient might be present at the Sn site in UNi_2Sn. In consequence, the assertion in Ref. [32] that no quadrupolar splitting occurs UNi_2Sn might not necessarily be valid. Hence, the interpretation of the data on the structural transition in UNi_2Sn ought to be reevaluated. Secondly, since the line width in UNi_2Sn is the same above and below the structural transition, and the values QS are equivalent for cubic and orthorhombic $UPd_{2-x}Sn$ [30], it indicates that the source for the field gradient is the same in both crystallographic structures, *i.e.*, likely a local distortion from cubic symmetry, which is not seen by integrating scattering techniques.

In context of disorder, the line widths of cubic $UPd_{2-x}Sn$ ought to be compared to isostructural compounds like disordered Co_2NbSn ($\Gamma = 1.77$ mm/s and 1.22 mm/s) [8], or Co_2ScSn ($\Gamma = 0.96 - 1.13$ mm/s) [33]. It suggests that the disorder level in cubic $UPd_{2-x}Sn$, as measured by Mössbauer spectroscopy, is comparable to annealed Co_2ScSn. For this material, it has been established that a relationship exists between the heat treatment procedure and the line widths. For as–cast Co_2ScSn the largest value $\Gamma = 1.13$ mm/s is found, which through an annealing treatment is reduced to $\Gamma = 0.96$ mm/s. This reduction of Γ has been correlated with corresponding changes of the physical properties, indicating that in this compound annealing reduces disorder. Further, the comparison of the line widths Γ for orthorhombic and cubic $UPd_{2-x}Sn$ indicates similar disorder levels in both systems [30].

Investigating now the spectra taken in the AFM phase, from fits to the data we obtain values for the hyperfine field $B_{HF} = 3.58(5)$ T (3.57(6) T), the isomer shift $IS = 1.67(5)$ mm/s (1.77(4) mm/s) and line width $\Gamma = 2.89(9)$ mm/s (3.0(1) mm/s) for $UPd_{2-x}Sn$, $x = 0.05$ (0.15). In these fits we fixed the quadrupolar splitting to the room temperature value $QS = 0.4$, because otherwise the fits became unstable. This assumption is motivated by the fact, that structurally no modifications occur upon lowering T from room temperature to 4.2 K. The very large line widths Γ observed in the AFM phase are consistent with the disordered magnetic state observed in neutron scattering, specific heat and susceptibility.

4.6 Discussion

From our study of $UPd_{2-x}Sn$ by means of bulk and microscopic techniques we have established the main physical properties of this series of materials. We have

found that cubic $UPd_{2-x}Sn$ has an antiferromagnetic heavy fermion ground state, while orthorhombic samples are non–ordering mass enhanced Fermi liquids. The orthorhombic lattice can be viewed as a slightly distorted derivative of the cubic Heusler lattice [9, 32]. Hence, the question arises if the magnetic/non–magnetic transition accompanying the structural transformation can be understood as being primarily a band structure effect, possibly involving f electrons of varying degrees of localization [34], or as a band filling effect, which controls the hybridization in a Doniach model like picture [35].

Recently, it has been suggested by Zwicknagl et al. [34] that the heavy fermion behavior in UPt_3 and UPd_2Al_3 is caused by the differing degrees of localization of $5f$ electrons in the various orbitals of the U ions. Concomitant band structure calculations for UPt_3 nicely reproduced the experimental Fermi surface data. Additional work indicates that the nature of the ground state of these materials sensitively depends on the degree of intermediate valency of the delocalized f electron [36]. In consequence, the presence or absence of magnetic order is primarily controlled by the $5f$ level occupation and delocalization, which depends upon the volume available to the U ion as well as the crystalline electric field (CEF) scheme.

Alternatively, the Doniach model is commonly used to account for the variation of the ground state properties of Ce and U heavy fermion materials [35, 37, 38]. As described in the introduction, in this model the evolution of different ground states is ascribed to the competition of the Kondo effect with the RKKY interaction between the f ions. Both interactions are dependent on the parameter $J\,N(E_F)$ (J hybridization strength; $N(E_F)$ Fermi level density of states).

Both, the model of partial $5f$ delocalization as the Doniach model, predict a sensitivity of the ground state properties of the materials under consideration to the application of external pressure, either by tuning the intersite hopping or via control of the product $J\,N(E_F)$. We noted that the structural transition into the cubic lattice corresponds to the exertion of chemical pressure. This fact alone would imply that cubic material should be more intermediate valent like than the orthorhombic samples, in conflict with the experimental observations. However, via Hall effect we have established that the carrier density of cubic $UPd_{2-x}Sn$ is smaller than that of the orthorhombic samples. With respect to the U $5f$ levels it could give rise to a more localized $5f$ character, and thus to antiferromagnetic ordering [36]. Conversely, within the Doniach model it might imply a lower band filling, and correspondingly, with a reduced product $J\,N(E_F)$, put cubic $UPd_{2-x}Sn$ closer to antiferromagnetism in a Doniach style phase diagram than orthorhombic material.

In consequence, judging from the bulk properties, cubic and orthorhombic $UPd_{2-x}Sn$ are situated close to a magnetic instability separating an antiferro– from a paramagnetic phase. Hence, we expect that with moderate pressure cubic, antiferromagnetic $UPd_{2-x}Sn$ can be tuned through the magnetic instability into a paramagnetic ground state. Conversely, if the lattice of orthorhombic $UPd_{2-x}Sn$

could be expanded (for instance by chemical pressure), the system should become antiferromagnetic.

Finally, to distinguish if the structurally induced magnetic/nonmagnetic transition arises from partial f electron delocalization or hybridization effects band structure calculations following those carried out for UPt_3 [34] would be very useful. Here, the goal would be to establish the relevance of the U f level scheme and delocalization in different lattice symmetries for the magnetic properties of $UPd_{2-x}Sn$, in order to prove or disprove the applicability of partial $5f$ delocalization to account for the ground state properties of $UPd_{2-x}Sn$.

Up to this point, we have neglected disorder in the discussion, although experimentally we have established its relevance in the magnetic, thermodynamic and transport properties. There are two aspects.

(i) Disorder in paramagnetic orthorhombic $UPd_{2-x}Sn$: This case contains the stoichiometric, nominally ordered compounds $UPd_{2-x}Sn$, $x = 0$, (ac) and (ann), as vacancy disordered $x = 0.04$. For all samples we have observed magnetic irreversibility in the susceptibility and a strong dependence of the residual resistivity ρ_0 on the annealing procedure and stoichiometry, while in the specific heat and the resistivity no signature of a magnetic transition is detected. We attribute this behavior to a minor fraction of U ions carrying magnetic moments not fully screened by the Kondo effect. With a finite magnetic coupling strength between these ions they form clusters, which undergo a blocking transition at T_B. Our finding of a cluster glass transition explains the anomalous line broadening observed for UPd_2Sn in Mössbauer experiments at low temperatures [30].

The disorder required to produce dilute, randomly distributed, non–screened U moments in a stoichiometric compound ($x = 0$) might be represented (a) either by a random site occupation of U, Pd and Sn atoms on equivalent crystallographic sites, or (b) by random displacements of ions from their high symmetry positions in the $Fm\bar{3}m$ lattice. From our data we cannot establish which of the two scenarios applies. In line with (a) there is the ambiguity to derive the site occupation in the $Pnma$ lattice from diffraction experiments [9]. In favor of scenario (b) is the vicinity of $UPd_{2-x}Sn$ to a structural instability, very similar to the cases of UPd_2In, UNi_2Sn or Co_2NbSn [6, 7, 8]. As well, the electric field gradient in orthorhombic and cubic $UPd_{2-x}Sn$ possibly arises from a local displacement of ions from high symmetry positions.

The off–stoichiometry of the sample $x = 0.04$ does not qualitatively alter the physical properties of the material. Its behavior is very similar to that of $x = 0$ (ann), with a metallic resistivity and a blocking transition observable in the susceptibility. The quantitative differences in the residual resistivity ρ_0 are only in part due to potential scattering from vacancies, as ρ_0 of $x = 0$ (ac) (actual composition U:Pd:Sn - 1:2:1) is only 36 $\mu\Omega$cm lower than of $x = 0.04$ (1:1.9:1), while the difference is 97 $\mu\Omega$cm to $x = 0$ (ann) (1:2:1). As well, both $x = 0$ (ac) and $x = 0.04$ undergo blocking transitions at the same T_B, while T_B is substantially reduced by an annealing treatment. It reflects that for the orthorhombic samples vacancy

disorder is not the dominant type of disorder.

(*ii*) Disorder in antiferromagnetic cubic $UPd_{2-x}Sn$: For these materials crystallographic disorder affects all physical properties. We have observed a blocking transition plus anomalous strong irreversibility in the antiferromagnetic state in the susceptibility. The AFM state is characterized by a small magnetic correlation length of about ~ 100 Å, which explains the very broad magnetic transition observed in the specific heat. Finally, the resistivity exhibits a resistivity with a negative $d\rho/dT$, while the carrier density is still in the metallic regime.

Although these materials are inherently disordered because of their off–stoichiometry, the actually measured composition of the cubic samples correspond to that of the off–stoichiometric orthorhombic sample. Further, judging from the quality of the structural refinement of the diffraction data or the width of the room temperature Mössbauer lines the level of crystallographic disorder in the cubic samples is comparable to that of the orthorhombic ones. As pointed out, for the orthorhombic samples the dominant source of disorder is either random site exchange of U, Pd and Sn ions or random displacements of these ions from high symmetry sites in the lattice. Since the structural transition in cubic $UPd_{2-x}Sn$ can also be induced by an annealing procedure, it is very likely that these types of disorder also exist in the cubic samples. In consequence, we believe that in as–cast samples the type of disorder and its level is similar in cubic and orthorhombic $UPd_{2-x}Sn$. Comparing the results of our Mössbauer study to those on other Heusler compounds we roughly estimate the disorder level to the order of 10 %, *i.e.*, moderate disorder in metallurgical terms (for comparison see the cases of Co_2NbSn, Co_2ScSn and UCu_4Pd [8, 33, 39, 40]). For the orthorhombic samples the disorder level can be reduced via annealing, while for cubic samples the partial transition into the orthorhombic phase hinders a study of different disorder levels.

Given the similar disorder levels, the qualitatively different behavior of the electronic transport properties between cubic and orthorhombic $UPd_{2-x}Sn$ is the more striking. Tentatively, we attribute this variation of "disorder efficiency" to a band structure effect. For the cubic samples the band structure contains more degenerate Fermi surface (FS) regions than for the orthorhombic samples. These degenerate portions of the FS can act as a bottleneck and enhance the efficiency of disorder, if the disorder primarily affects the degenerate FS areas. Here, band structure calculations as in Ref. [34] would be very useful to establish or disprove our proposal.

As pointed out, a description of the resistivity, magnetoresistivity and Hall effect of cubic $UPd_{2-x}Sn$ in terms of conventional heavy fermion behavior does not consistently account for our observations. In consequence, we believe that the unusual temperature and field dependencies of these quantities reflect that electronic transport in cubic $UPd_{2-x}Sn$ is diffusive rather than ballistic. Within this model, the weak T dependence of ρ is analogous to that of strongly disordered metals like metallic glasses [17], mostly arising from disorder induced localization.

Magnetic scattering only represents a minor correction to this overall resistivity, as indicated by the very weak signature of antiferromagnetic ordering in ρ. Then, for a description of the magnetoresistivity it might be necessary to include localization corrections, which might explain the complicated field dependence of $\Delta\rho$.

Under these circumstances, we speculate that the Hall effect possibly is dominated by the side jump mechanism, which for disordered materials usually is the most relevant contribution [41, 42, 43]. In principle, to test if either skew scattering or side jump contributions are the dominant terms of the anomalous Hall coefficient, the relationship between the anomalous Hall constant R_S and the resistivity ρ should be investigated, since $R_S = a\,\rho + b\,\rho^2$. Unfortunately, because of the very small magnetoresistivity we have not been able to unambiguously establish if R_S depends on ρ linearly or in a quadratic fashion.

Bibliography

[1] C.L. Seaman et al., Phys. Rev. B **53** (1996) 2651.

[2] S. Süllow et al., Physica B **230-232** (1997) 43.

[3] A. Ślebarski et al., Phys. Rev.B **65** (2002) 144430.

[4] F.M. Mulder et al., Phys. Rev. Lett. **77** (1996) 3477.

[5] A. Drost et al., Solid State Commun. **88** (1993) 327

[6] T. Takabatake et al., J. Phys. Soc. Jpn. **58** (1989) L1918; T. Takabatake et al., J. Phys. Soc. Jpn. **59** (1990) L16.

[7] T. Endstra et al., J. Phys.: Condens. Matter **2** (1990) 2447.

[8] A.U.B. Wolter et al., Phys. Rev. B **66** (2002) 174428.

[9] C. Rossel et al., Solid State Commun. **60**, (1986) 563.

[10] M. Marezio et al., Solid State Commun. **67**, (1988) 831.

[11] I. Maksimov et al., Physica B **312-313**, (2002) 283.

[12] A. Purwanto et al., Phys. Rev. B **50** (1994) 6792

[13] R. Feyerherm et al., Phys. Rev. B **56** (1997) 13693

[14] H. Nakotte et al., Phys. Rev. B **58** (1998) 9269

[15] V. Tran, F. Steglich, and G. Andre, Phys. Rev. B **65**, (2001) 134401.

[16] N.F. Mott, *Metal-insulator transitions*, 2nd ed. (Taylor&Francis, London, 1990).

[17] J. Dugdale, *The Electrical Properties of Disordered Metals* (Cambridge University Press, Cambridge, 1995).

[18] T.T.M. Palstra et al., Phys. Rev. Lett. **55** (1985) 2727.

[19] M.B. Maple et al., Phys. Rev. Lett. **56** (1986) 185.

[20] T.T.M. Palstra et al., Phys. Rev. B **53** (1996) R6014.

[21] N. Grewe and F. Steglich, in *Handbook on the Physics and Chemistry of the Rare Earths*, *Vol. 13*, (Elsevier, New York, 1990), p. 341.

[22] V.K. Pecharsky et al., Phys. Rev. B **51** (1995) 954.

[23] J. McDonough and S.R. Julian, Phys. Rev. B **53** (1996) 14411.

[24] Z. Hossain et al., Phys. Rev. B **60** (1999) 10383.

[25] J. Schoenes and J.J. Franse, Phys. Rev. B **36** (1986) 5138.

[26] P. Levy and A. Fert, Phys. Rev. B **36** (1987) 1907.

[27] J. Cooley et al., Phys. Rev. Lett. **74** (1995) 1629.

[28] S. Paschen et al., Phys. Rev. B **56** (1997) 12916.

[29] J. DiTusa et al., Phys. Rev. B **58** (1998) 10288.

[30] B. Chevalier et al., Physica B **259-261** (1999) 252

[31] R.A. Dunlap and D.F. Jones, Phys. Rev. B **26** (1982) 6013.

[32] F.M. Mulder et al., Phys. Rev. Lett. **77** (1996) 3477.

[33] Z. W. Chen et al.,J. Apl. Phys. **73** (1993) 6974.

[34] G. Zwicknagl, A.N. Yaresko and P. Fulde, Phys. Rev. B **65** (2002) 081103(R).

[35] S. Doniach, Physica B **91**, (1977) 231.

[36] G. Zwicknagl and P. Fulde, J. Phys.: Condens. Matter, in print (2003).

[37] T. Endstra, G.J. Nieuwenhuys and J.A. Mydosh, Phys. Rev. B **48** (1993) 9595.

[38] S. Süllow et al., Phys. Rev. Lett. **82**, (1999) 2963.

[39] R. Chau, M.B. Maple and R.A. Robinson, Phys. Rev. B **58** (1998) 139.

[40] C.H. Booth et al., Phys. Rev. Lett. **81** (1998) 3960.

[41] F.E. Maranzana, Phys. Rev. **160** (1967) 421.

[42] L. Berger, Phys. Rev. B **2** (1970) 4559.

[43] *The Hall Effect in Metals and Alloys*, ed. by C. Hurd (Plenum, New York, 1972).

5 Magnetic ground state and electronic transport in disordered URh_2Ge_2

5.1 Introduction

Summarizing the findings so far, we have shown that for a number of materials, like Fe_2VAl and UPd_2Sn, crystallographic disorder is present and needs to be taken into account to understand the physical properties of these systems. While for Fe_2VAl the observation of disorder disproves claims of a strongly correlated insulator state, in UPd_2Sn we have demonstrated that disorder in a heavy fermion compound can cause a very anomalous behavior. In this chapter now, we will focus entirely on these anomalous properties due to crystallographic disorder in a heavy fermion, in order to gain more insight into the underlying physical mechanisms.

A not well-understood property of (correlated) metallic disordered compounds is the electronic transport. As long as the resistivity is small, as in relatively pure metals, the resistive scattering from phonons has a well-established temperature dependence. At high temperatures, above the Debye temperature, it is proportional to the mean-square amplitude of the lattice vibrations, *i.e.* to k_BT. In this case, typically a resistivity is found of the order of 10-20$\mu\Omega$cm at room temperature. According to Matthiessen's rule, a small level of disorder adds a residual resistivity ρ_0 from potential scattering. This type of a metallic resistivity, in compounds containing magnetic moments, is accompanied by temperature dependent magnetic scattering, ρ_{mag}, which vanishes for $T \rightarrow 0$. Hence, all in all, the resistivity of a common magnetic metal is described by $\rho = \rho_0 + \rho_{phonon}(T) + \rho_{mag}(T)$.

Now, if crystallographic disorder is strong, a qualitatively different behavior is observed. In particular, negative temperature coefficients of the resistivity, saturation effects and breakdown of Matthiessen's rule occur [1, 2]. Up to now, even for common metals, questions arise about this anomalous behavior [3]. The situation concerning the electronic transport is less clear for strongly correlated disordered materials.

In this section we present a detailed study on URh_2Ge_2, that is a heavy fermion

metal exhibiting an anomalous resistivity. In general, 1-2-2 compounds containing uranium crystallize in simple tetragonal lattices. Many of these system are magnetically ordered at low temperatures. Mostly, the ordered state is realized by simple antiferromagnetic stacking along the c-axis of spins ferromagnetically coupled in the a-b plane and pointing along the c-direction. Now, for one of the 1-2-2 compounds, URh_2Ge_2, spin glass behavior has been reported. The mere observation of a spin glass state in a heavy fermion compound poses a number of open questions:

1. Where does the crystallographic disorder necessary to generate spin glass behavior come from?
2. Is the spin glass state in a heavy fermion different compared to that in normal metals?
3. How does the electronic transport behave in such a disordered heavy fermion metal?

Concerning the first question, there are a few tentative answers. A peculiar property of 1-2-2 compounds is that they often contain an intrinsic level of disorder. Mostly, the 1-2-2 compounds crystallize in one of two tetragonal structures with $P4/nmm$ and $I4/mmm$ space group symmetry. The structures are closely related to each other, giving rise to structural instabilities [4, 5, 6]. In consequence, for some cases the transitions from the one to the other structure as function of temperature have been observed.

Accordingly, since in neutron scattering experiments [7, 8] on polycrystalline URh_2Ge_2 samples a unique crystal structure could not be unambiguously determined, it was proposed, that the structure is a mixture of the $I4/mmm$ and $P4/nmm$ lattices. However, recently XAFS experiments performed by C.H. Booth seem to cast doubt on this view, instead stating that the disorder is realized by Rh/Ge site exchange only.

With respect to the magnetic properties, single crystalline URh_2Ge_2 was found to be the first 3D random-bond Ising-like heavy-fermion spin glass [7, 9]. The Ising like symmetry is reflected in a pronounced magnetic anisotropy between c and a axes. In this situation, the spin glass properties can be studied for a strongly correlated electron system under very controlled circumstances for the first time. In particular, in URh_2Ge_2 the role of anisotropy in the spin glass freezing can be investigated in detail.

Concerning the electronic transport properties, it has been proposed that spin glass URh_2Ge_2 behaves analogously to metallic glasses [10]. Moreover, the transition from glassy to crystalline behavior has been looked at for URh_2Ge_2. It appears that the glassy behavior in this heavy fermion compound is present as long as the level of disorder exceeds a critical value. Thus, tuning the disorder in URh_2Ge_2 induces a transition from glassy metallic transport to crystalline

metallic behavior. This transition is accompanied by a transformation of the spin glass state into long-range antiferromagnetic ordering.

All in all, in this chapter we will address two issues. First, we will look in more detail into the spin glass properties of URh_2Ge_2, utilizing here the availability of single crystalline specimens. We will investigate the magnetic irreversibility in this compound, in particular with respect to its field dependence and anisotropy. We argue that the observed behavior in URh_2Ge_2 can be accounted for by the theory of Vieira et al. [11], who considered the role of single ion anisotropy for freezing in a m-vector spin glass.

Secondly, we will establish the electronic transport properties of URh_2Ge_2, again as function of field and anisotropy. This way, for the first time, the electronic transport properties of a moderately disordered heavy fermion compound have been thoroughly studied, hopefully forming the basis for future theoretical investigations. We will discuss the relationship between magnetic ground state properties and electronic transport, which appears to be disconnected for moderately disordered heavy fermions.

Finally, the Hall effect of URh_2Ge_2 closely resembles the behavior of cubic $UPd_{2-x}Sn$, indicating that the proportionality of the anomalous Hall effect only to the susceptibility χ is a more general feature of moderately disordered heavy fermion compounds.

5.2 Metallurgy

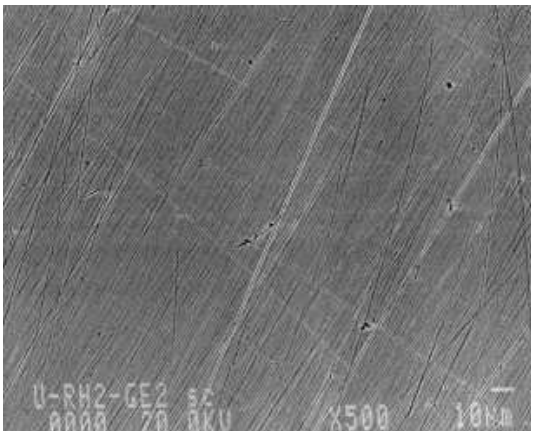

Figure 5.1: Electron backscattering photo of single crystalline URh_2Ge_2.

The ground state properties of URh_2Ge_2 sensitively depend on the material preparation procedure. This has been established in a metallurgy study at the Kamerlingh Onnes Laboratory (KOL), Leiden University, by D. Tomuta. While preparing several polycrystalline samples URh_2Ge_2, stoichiometric as off-stoichiometric, she observed that samples of the same starting composition and

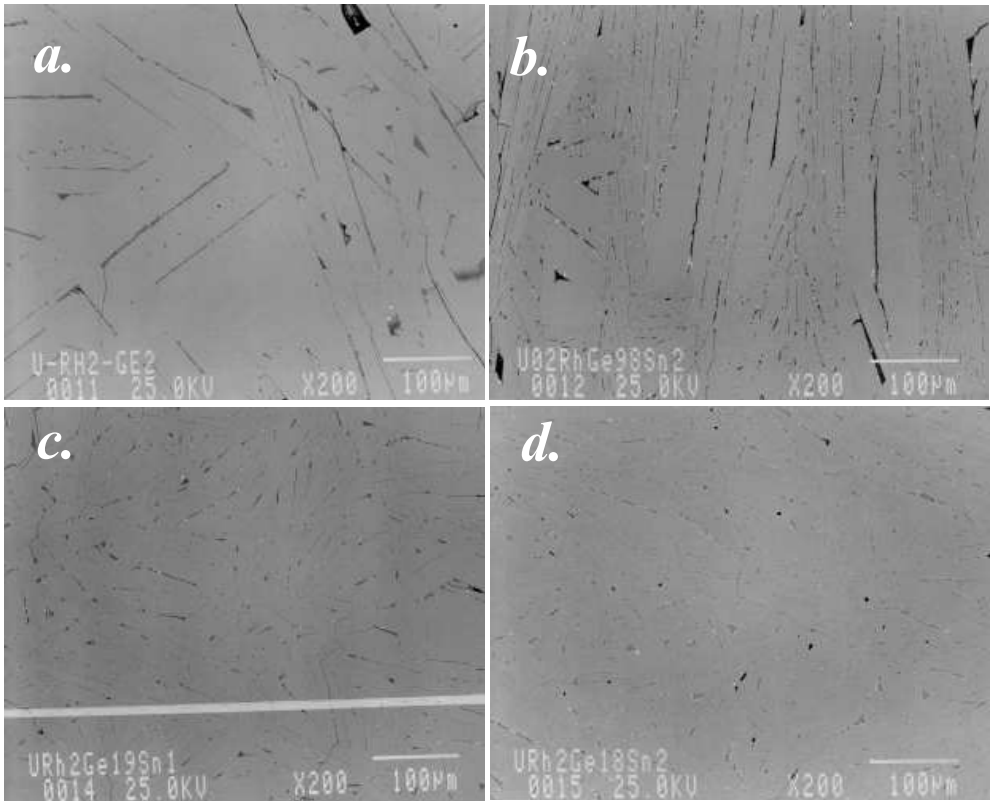

Figure 5.2: Electron backscattering photo of $URh_2Ge_{2-x}Sn_x$: a) x=0; b) x=0.02, c) x=0.1 and d) x=0.2. The black pattern indicates a secondary phase.

nominally produced following the same recipe, could exhibit either an antiferromagnetic ground state below T_N=13.5K, spin glass freezing below T_f ≈10K, or a mixture of both phases [12]. In consequence, it is very difficult to control the magnetic ground state properties during the sample production.

For the present work, various single crystalline samples URh_2Ge_2 have been investigated. These crystals have been prepared at the KOL within FOM-ALOMOS[1]. The single crystals URh_2Ge_2 were grown using the Czochralski technique in a tri-arc furnace. The stoichiometry of the samples was checked by EPMA and found to be the correct 1-2-2 composition within the experimental resolution limit of ±3%. Scanning electron microscopy proves the single phase nature of the URh_2Ge_2 crystals, (Fig. 5.1).

In addition, polycrystalline samples of isoelectronically alloyed $URh_2Ge_{2-x}Sn_x$ were produced by S. Süllow at the KOL by arc-melting the constituents in stoichiometric ratio under purified argon atmosphere on a water cooled copper crucible. No further heat treatment was applied to the specimens. The polycrystalline

[1]Fundamenteel Onderzoek der Materie-Amsterdam/Leiden Material Onderzoek Samenwerking

Nominal composition $URh_2Ge_{2-x}Sn_x$	Matrix composition (EPMA) $U : Rh : Ge : Sn$
x=0 (single crystal)	1:2.00(6):2.00(6)
x=0 (polycrystal)	1:1.95(6):1.95(6)
x=0.02	1:1.98(6):1.96(6):<0.01
x=0.04	1:1.97(6):1.94(6):0.01(1)
x=0.1	1:1.99(6):1.89(5):0.07(1)
x=0.2	1:2.01(6):1.91(5):0.06(1)

Table 5.1: The nominal and actual compositions of $URh_2Ge_{2-x}Sn_x$.

buttons contain mm-sized preferentially oriented single crystalline grains. Phase homogeneity was checked by means of EPMA, indicating that the samples consist of a majority phase plus a small volume fraction (less then 1% volume amount) of μm-sized inclusions of a Sn rich secondary phase (Fig. 5.2). The actually measured matrix composition for the samples is shown in Table 5.1. For all samples $U : Rh : Ge/Sn$ ratios of 1:2:2 are found within experimental resolution. However, the actual Sn content of the matrix is smaller than the nominal value x. For x=0.02 a weak Sn signal too low for a quantitative evaluation (<0.5%) was detected in the matrix. Still, in the following we refer to the samples by their nominal compositions.

On the single crystals investigated in this work X-ray absorption fine structure (XAFS) experiments have been performed at the Lawrence Berkeley National Laboratory by C.H. Booth in order to assess type and level of crystallographic disorder (Fig. 5.3). The basic structure of URh_2Ge_2 is the tetragonal $I4/mmm$ lattice. The disorder arises from regions in the sample with different symmetry. In the XAFS experiments, this local disorder is obvious in the data from all three measured absorption edges (UL_3, RhK and GeK). The GeK edge data with the incident photon polarization ϵ parallel to the a-axis indicate that the dominant phase cannot be $P4/nmm$, as was previously suggested [9]. The data are consistent with the $P4/mmm$ symmetry, with 13%±5% of the Ge on the nominally $Rh(4d)$ site. Only very subtle differences between the spin-glass and antiferromagnetic sample are measured [13].

5.3 Anisotropy of the irreversibility lines in URh_2Ge_2

For the study of the anisotropy of the spin glass behavior we investigated an as-grown single crystal URh_2Ge_2, whose spin glass ground state previously had been established. The dc-susceptibility was measured by D. Menzel employing a SQUID magnetometer at the Institut für Halbleiterphysik und Optik, TU Braunschweig. The experiments have been performed in the temperature range between 5 and 20K, thus in the range of the transition from the paramagnetic to spin glass

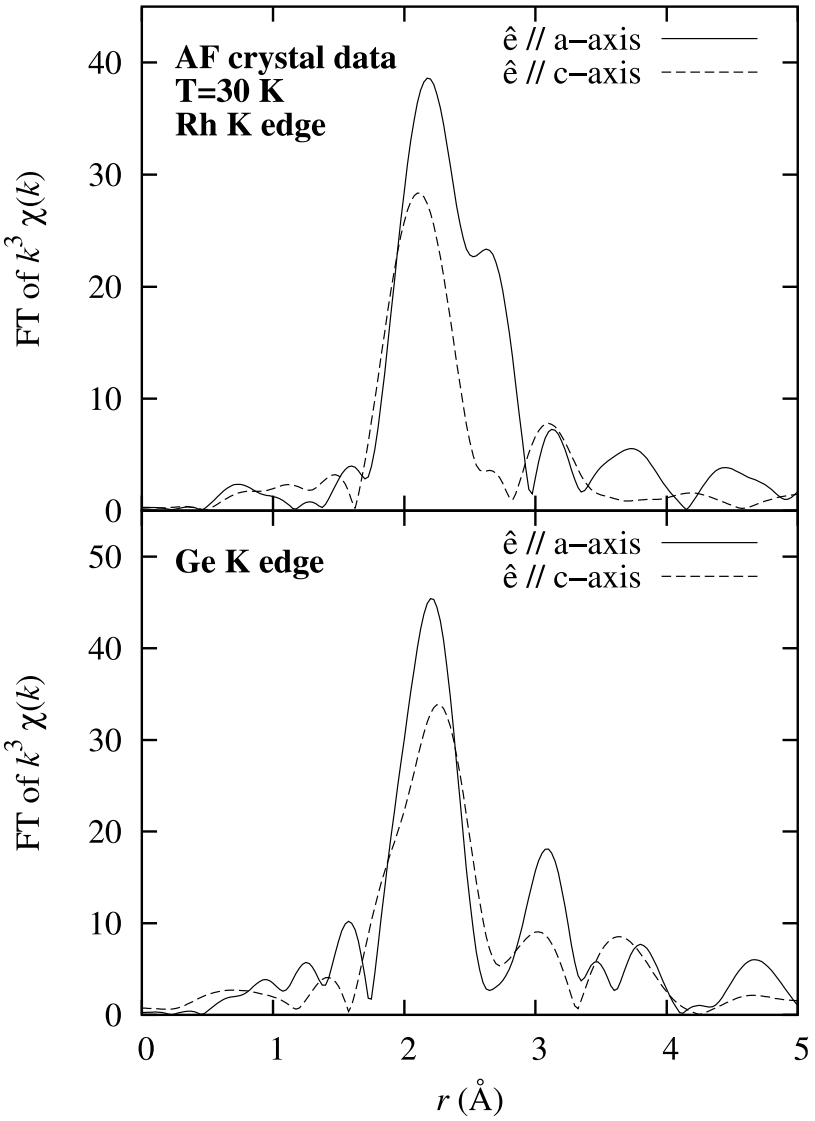

Figure 5.3: Fourier transform of the X-ray absorption fine structure spectrum of URh_2Ge_2 with the photon polarization along a and c axes.

phase. In the paramagnetic phase we observe single ion anisotropy along the crystallographic a and c axes by a factor of 5-6 (Fig. 5.5). Further, the temperature dependence of χ_{dc} measured at low fields in zero field cooled mode exhibits a sharp cusp, indicating the freezing transition at T_f into the spin glass state [10]. In contrast, in field cooled measurements we observed a temperature independent susceptibility χ_{dc} below the freezing temperature T_f, as is usual for spin glass systems.

Application of large external magnetic fields leads to a smearing of the cusp (Fig. 5.6), and separates the crossover temperatures of the occurrence of weak

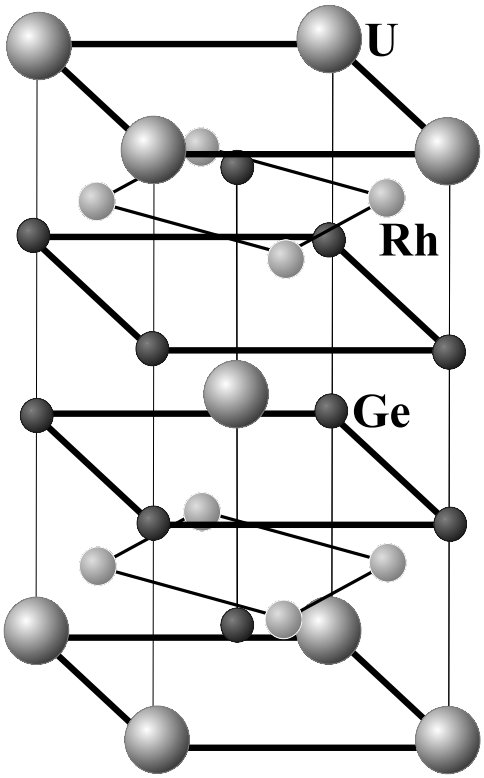

Figure 5.4: The $I4/mmm$ tetragonal lattice as basis for the structure of URh_2Ge_2.

and strong irreversibility in the magnetic behavior. Here, weak irreversibility occurs below the maximum in χ_{dc}, which is a measure for the spin glass freezing temperature. Strong irreversibility sets in below the temperature, at which FC and ZFC experiments deviate. Then, from our FC and ZFC experiments we determine these crossover temperatures: the upper one as the onset of spin freezing at T_f, the lower one, T_{irr}, defining the onset of strong irreversibility in the frozen-in state (Fig. 5.7).

From the field dependence of T_f and T_{irr} we establish a $B-T$ phase diagram (Fig. 5.8). In the zero field limit T_f is determined to 9.38K. For finite magnetic fields the phase diagram reveals anisotropy of both irreversibility temperatures T_f and T_{irr} for fields applied along a and c axes, respectively. The field dependence of T_{irr}, commonly associated with the Almeida-Thouless line (AT) [14], shows a behavior qualitatively similar to that of canonical spin glasses like $\underline{Cu}$**Mn** [15, 16, 17]. A fit to the data for $0.8 \leq T/T_f \leq 1$, employing $[1 - T/T_f^0] \propto (\mu_B g B/k_B T_f^0)^x$ [17, 18] yields x=0.56±0.03 for $B//a$-axis and 0.47±0.02 for $B//c$-axis. These values are significantly smaller than expected for the Ising case, x=2/3. Furthermore, T_f, which is associated with the Gabay-Toulouse crossover line (GT) [18], exhibits a highly unusual field dependence: instead of the typical

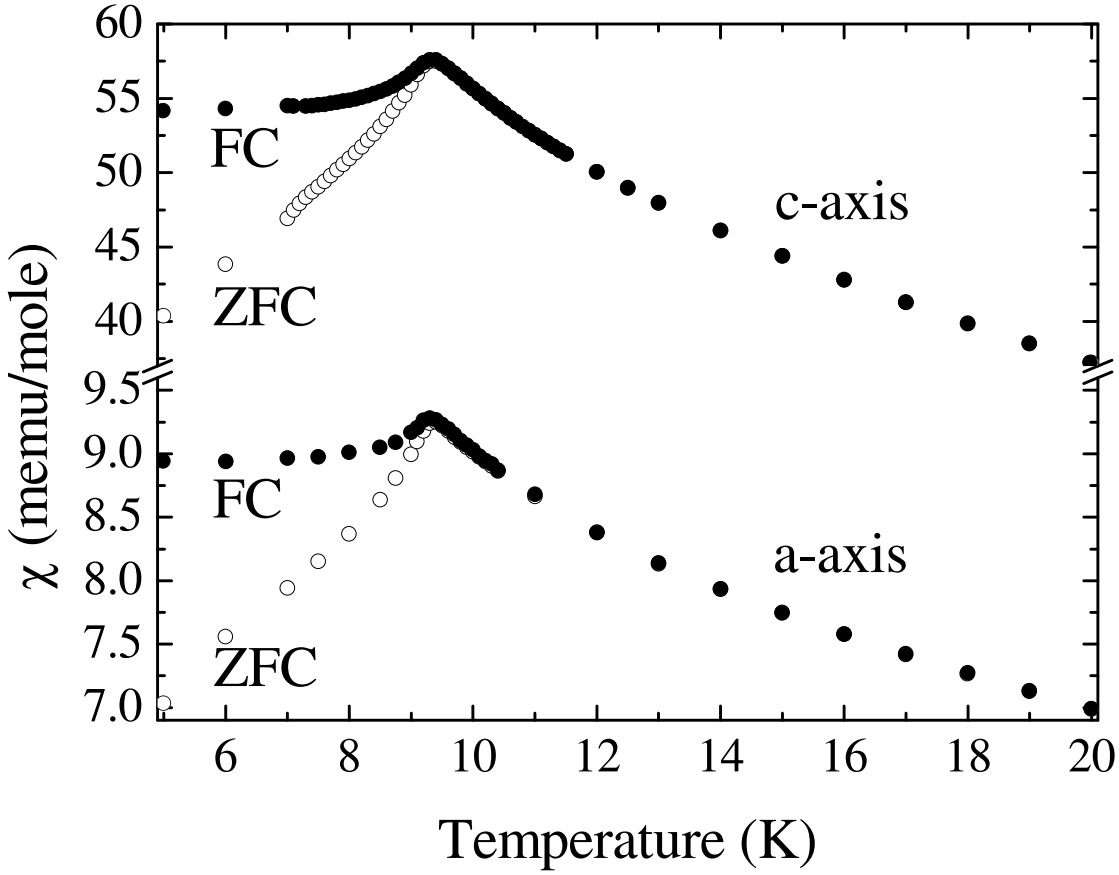

Figure 5.5: Magnetic susceptibility of single crystalline URh_2Ge_2 along the a and c-axes, measured in field cooled (FC, filled symbols) and zero field cooled (ZFC, open symbols) mode. The measurements have been performed at a field B=3×10^{-4}T.

observed decrease with field [19, 20], T_f is monotonically increasing for $B//a$-axis, and passing through a maximum at about 1T for $B//c$-axis. This behavior is qualitatively different from that predicted in Ref. [18].

The strong anisotropy between a and c axes in the susceptibility reflects the single ion anisotropy in URh_2Ge_2. Since the GT line can be associated with ordering of the transverse degrees of freedom in the presence of an external magnetic field, the existence of the single ion anisotropy needs to be taken into account in explaining the anomalous field dependence of the crossover temperatures. Recently, it has been proposed that the reentrant field dependence of the GT line might be the result of the freezing process in a m-vector spin glass in an external field: Vieira and co-workers [11, 21] calculated that for such a system the low field GT line for a Heisenberg spin glass should exhibit a reentrant behavior, with a maximum of $T_f(B)$ at a finite field as the result of a finite single ion anisotropy. Our data are in qualitative agreement with these predictions, suggesting that

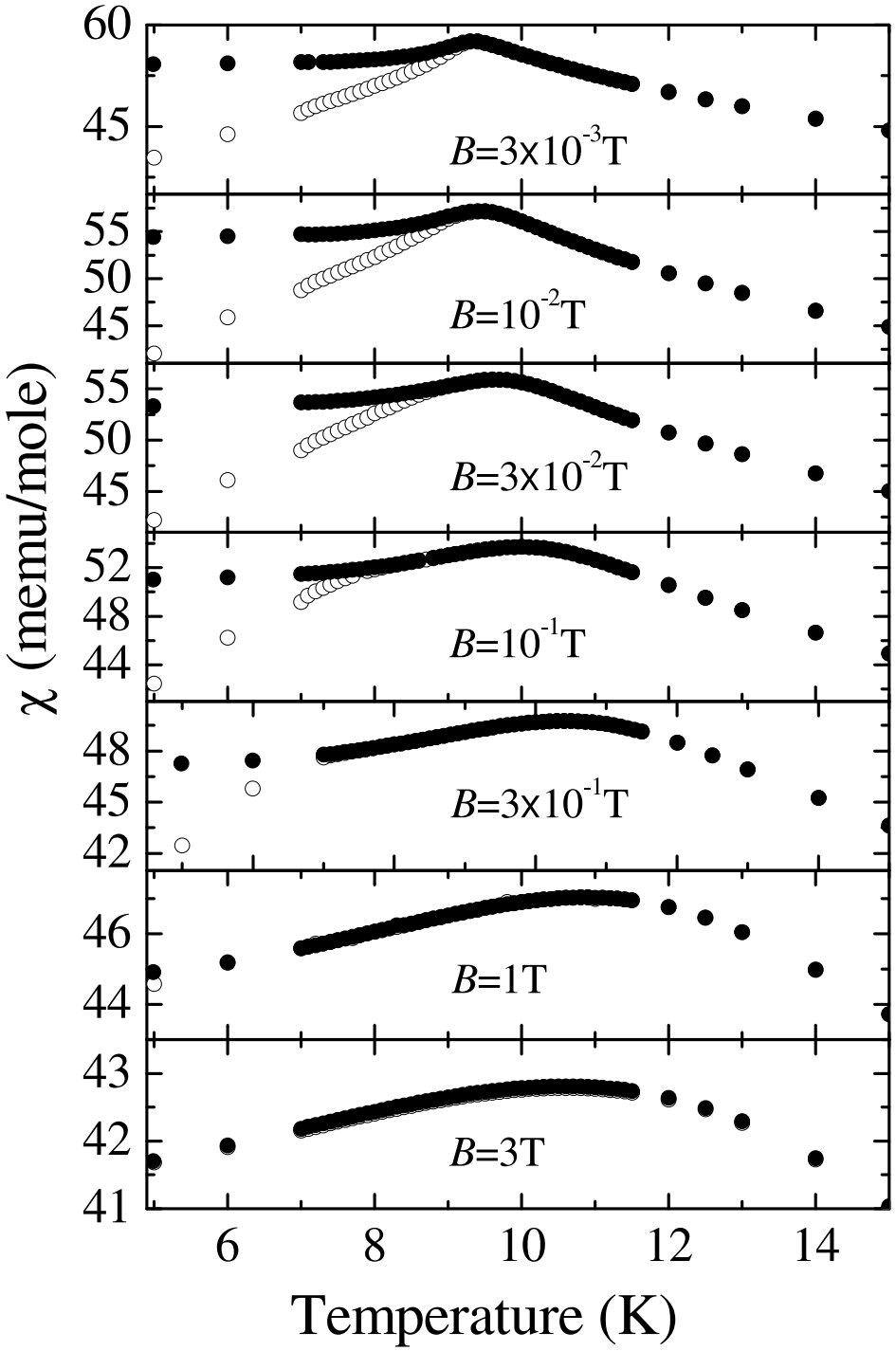

Figure 5.6: Magnetic susceptibility of single crystalline URh_2Ge_2 along the c-axis, measured in FC (filled symbols) and ZFC (open symbols) mode at different fields.

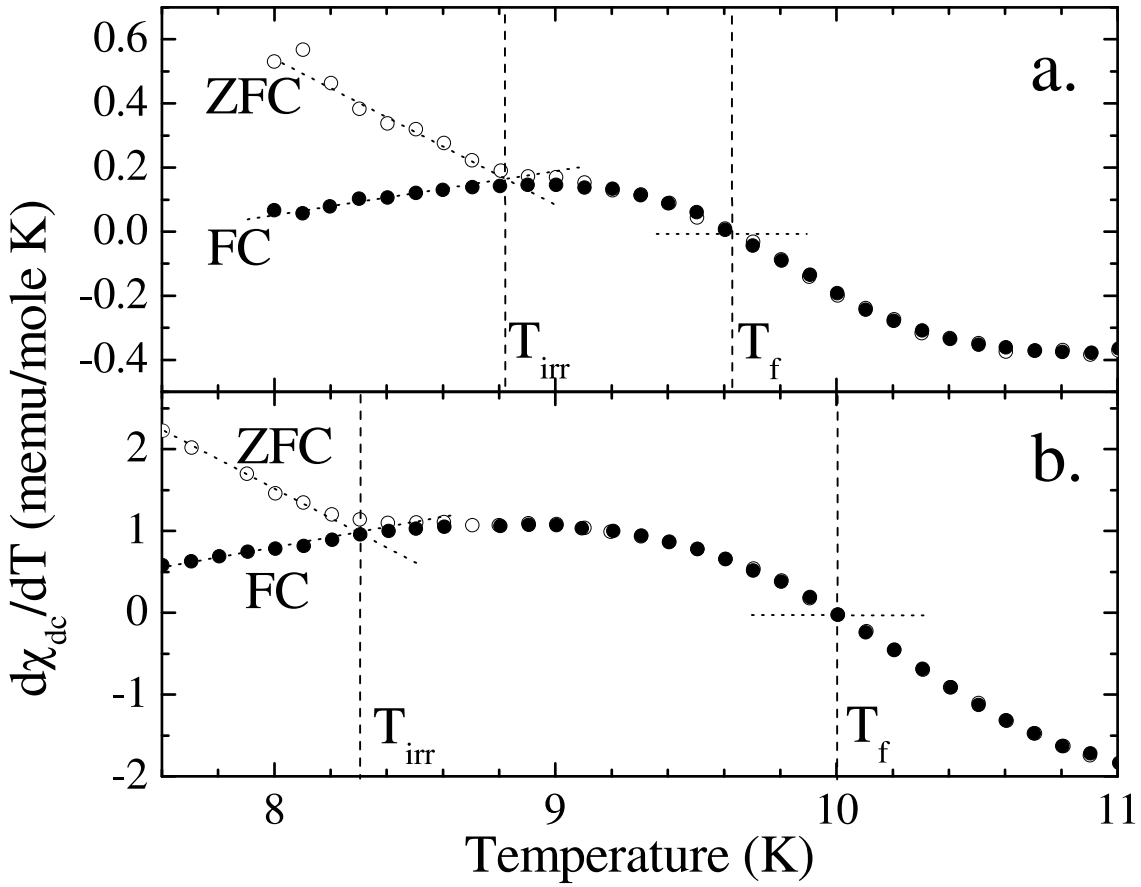

Figure 5.7: The susceptibility derivative $d\chi_{dc}/dT$ of URh_2Ge_2 as function of temperature in FC and ZFC modes in a magnetic field B=0.1T along the a-axis (a) and c-axis (b). The intersections of the dotted lines indicate weak and strong irreversibility defined in the text.

URh_2Ge_2 might be a model compound to test the predictions of Ref. [11] for the m-vector spin glass.

5.4 Magnetic and transport properties of $URh_2Ge_{2-x}Sn_x$

The magnetic properties of $URh_2Ge_{2-x}Sn_x$ have been studied by means of dc-susceptibility measurements. The experiments were carried out using a Foner magnetometer in the temperature range between 5 and 300K.

In Fig. 5.9 we plot the dc-susceptibility χ_{dc} of $URh_2Ge_{2-x}Sn_x$, x=0, 0.02, 0.04 and 0.1, measured in a field cooled and zero field cooled mode in B=0.05T. The absolute values χ_{dc} for the polycrystalline samples vary by a factor of 2, but

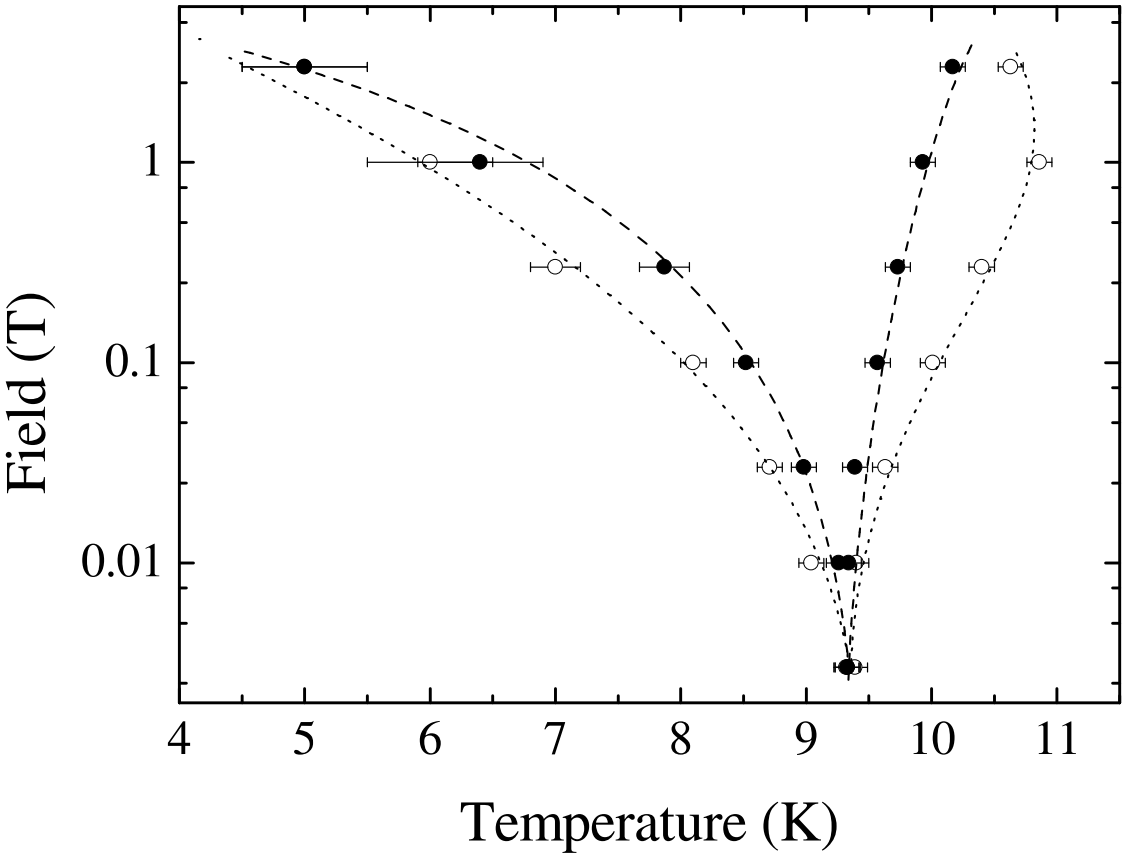

Figure 5.8: The $B - T_{irr}/T_f$ phase diagram of URh_2Ge_2 for fields applied along the crystallographic a-axis (filled symbols) and c-axis (open symbols).

within the limits of the single crystalline data (for comparison see Fig. 5.5). It reflects pronounced preferential orientation of the polycrystals.

As it was noted above, for stoichiometric material URh_2Ge_2 the magnetic ground state (spin glass or antiferromagnet) drastically depends on the sample preparation procedure. Here, under the same preparation conditions we obtain an antiferromagnetic sample for x=0 and 0.02, as indicated by an antiferromagnetic anomaly at T_N=13.3K, without irreversibility between FC and ZFC measurements [10]. Increasing the Sn content increases the disorder level and stabilizes the spin glass ground state. Thus, for x=0.04 we find coexistence of antiferromagnetic and spin glass phases, as corroborated by the antiferromagnetic anomaly at T_N and the onset of magnetic irreversibility below the freezing temperature T_f ∼10K between FC and ZFC experiments. This situation is analogous to that observed in the Ising system $Fe_{1-x}Mg_xCl_2$, where antiferromagnetic ordering is not destroyed by a spin glass transition [22]. Finally, for x=0.1 the susceptibility indicates pure spin glass behavior below T_f.

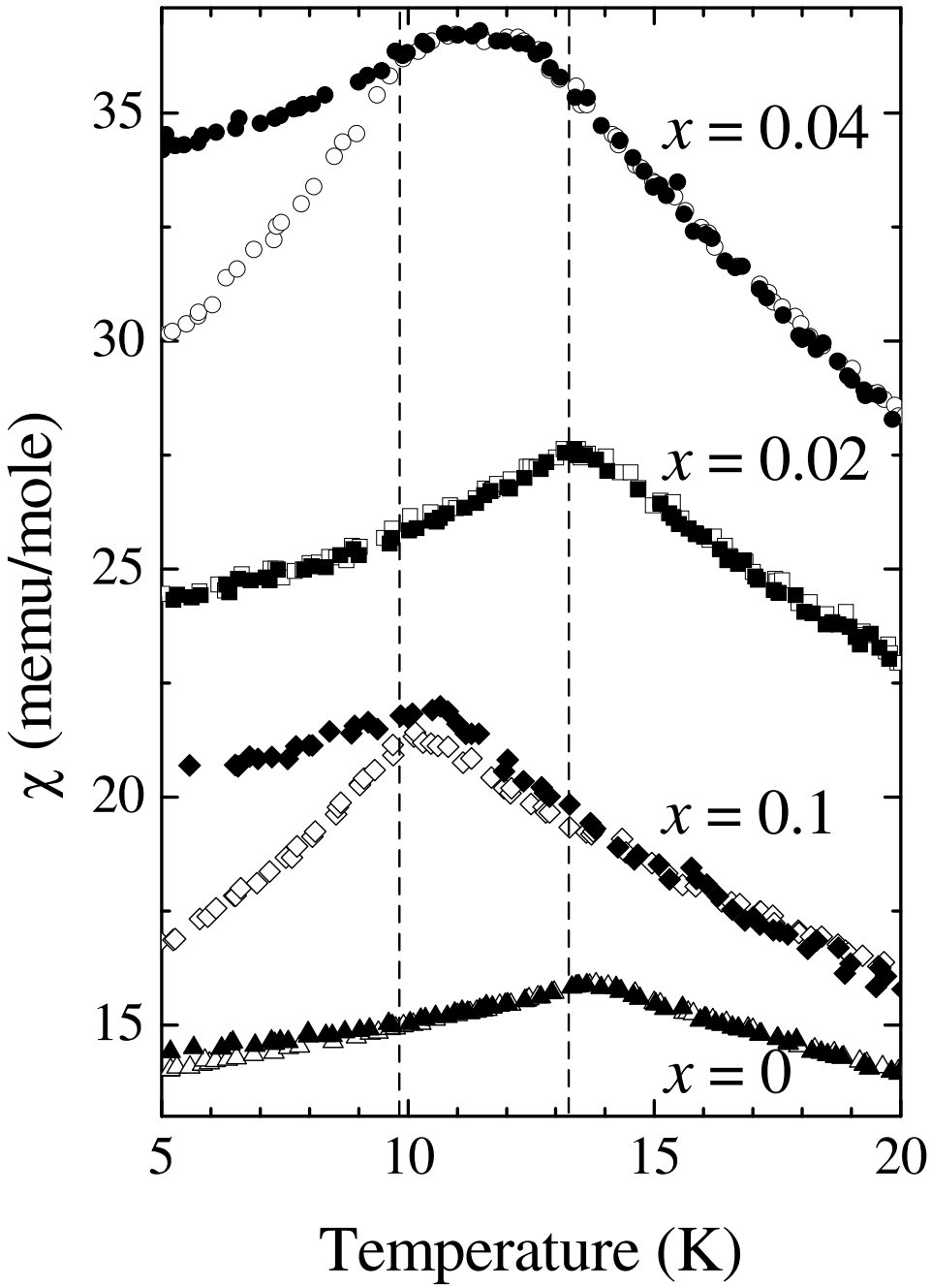

Figure 5.9: The dc-susceptibility of polycrystalline $URh_2Ge_{2-x}Sn_x$ x=0, 0.02, 0.04 and 0.1, measured in FC (filled symbols) and ZFC (open symbols) mode. The dash lines mark transition temperatures T_f=9.5K for spin glass and T_N=13.3K for antiferromagnetic states.

5.5 Electronic transport in URh_2Ge_2

We have seen that varying the disorder level in $URh_2Ge_{2-x}Sn_x$ changes the magnetic ground state of the compounds. Surprisingly, this modification of the

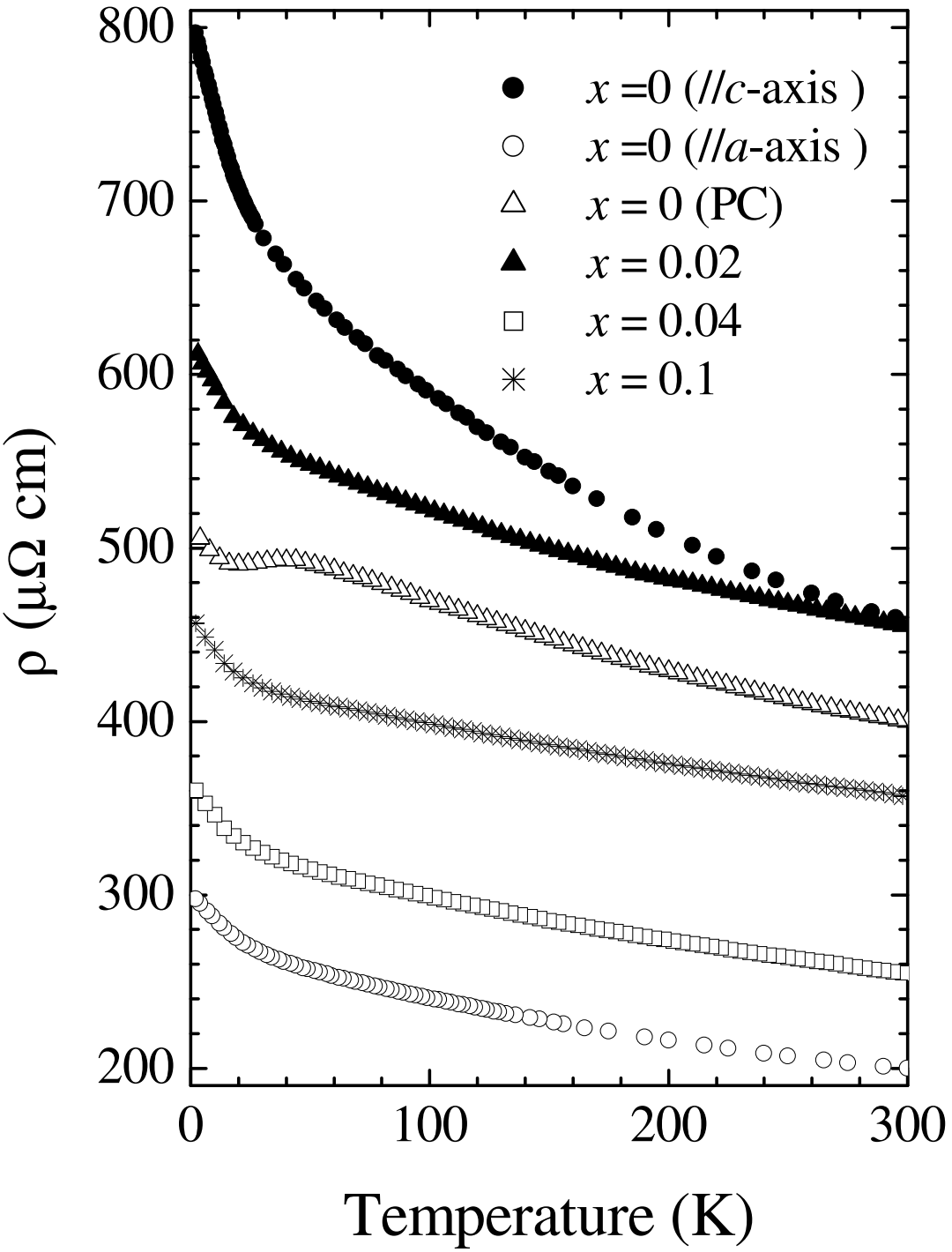

Figure 5.10: The resistivity of $URh_2Ge_{2-x}Sn_x$ x=0 (single crystal) and 0, 0.02 , 0.04, 0.1 (polycrystal).

magnetic ground state is not reflected in the electronic transport properties. In Figure 5.10 we present the resistivity of $URh_2Ge_{2-x}Sn_x$ x=0, 0.02, 0.04 and 0.1

as function of temperature. Similar to crystalline URh_2Ge_2, studied in Ref. [10], all samples exhibit unusually large resistivities and negative temperature coefficients. Only for the polycrystalline sample x=0 there is a temperature region with a pseudo-metallic resistivity. Tentatively, we attribute this behavior to the superposition of different resistive contributions from regions in the sample with a locally varying degree of disorder. Previously, it has been demonstrated that a transition from non-metallic ($d\rho/dT$ <0) to metallic ($d\rho/dT$ >0) resistivity can be attained by reducing the level of crystallographic disorder in URh_2Ge_2 [10]. In in a polycrystal locally the disorder level varies between the metallic and non-metallic limits, it would cause a superposition of corresponding resistive contributions, yielding a behavior similar to that observed here. As the resulting resistivity does not reflect the intrinsic behavior of a well-defined disordered metallurgical phase, we will not further consider these data here.

For none of the samples we observe resistive anomalies at the antiferromagnetic or spin glass freezing transitions. This implies that the magnetic ground state properties of $URh_2Ge_{2-x}Sn_x$ are decoupled from the electronic properties. Hence, the electronic transport probes a different aspect of the physics of URh_2Ge_2.

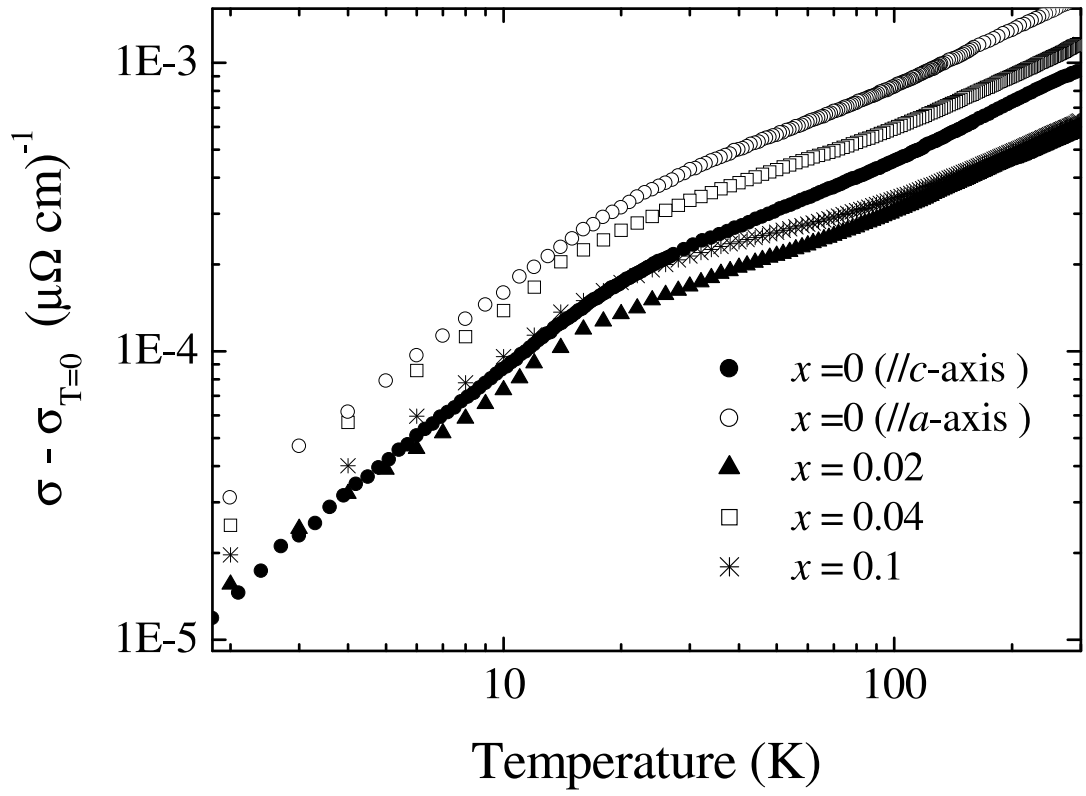

Figure 5.11: The reduced conductivity $\sigma-\sigma(T=0)$ of $URh_2Ge_{2-x}Sn_x$ x=0 (single crystal), 0.02 , 0.04 and 0.1.

Qualitatively, and in spite of the largely varying absolute values of ρ, the resis-

tivity of single and polycrystalline samples appear to be very similar. A quantitative analysis, however, indicates that the data from the different samples cannot be superimposed by adding a constant residual resistivity ρ_0. Hence, Matthiesen's rule appears to be not valid for these samples.

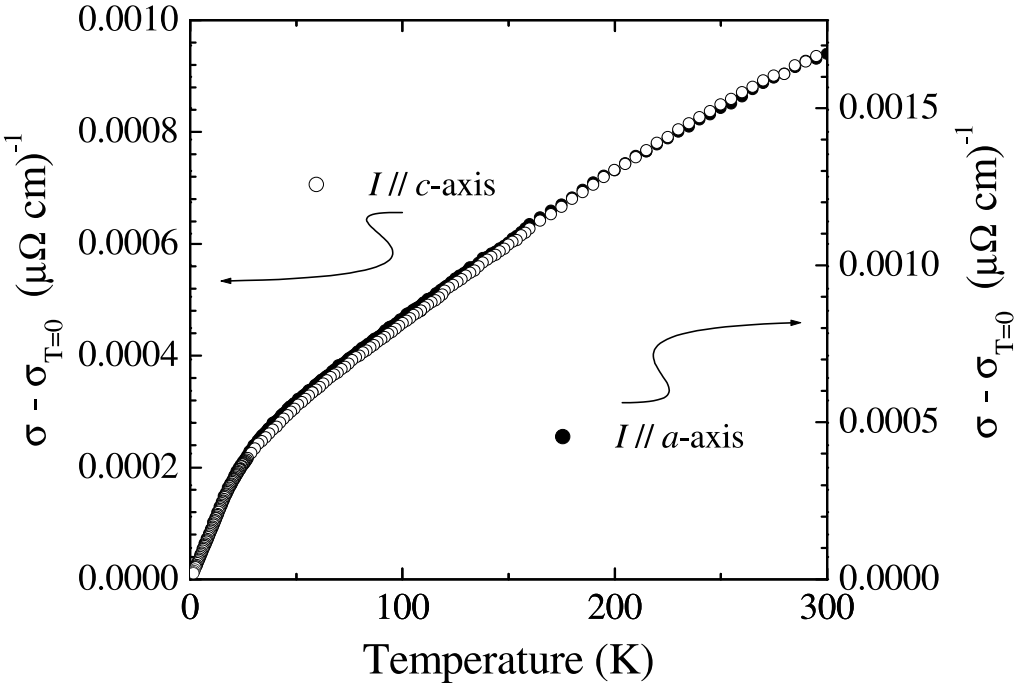

Figure 5.12: The reduced conductivity $\sigma - \sigma(T{=}0)$ of single crystalline URh_2Ge_2 along the crystallographic a and c axes.

Following Ref. [3], we plot the reduced conductivity $\sigma - \sigma(T{=}0)$ in Fig. 5.11 as function of T in a double-logarithmic representation. There are two qualitatively different temperature regimes, that are below and far above ∼20K. Theoretical models of localization (see Ref. [23]) predict a power law for the conductivity of a 3D material

$$\sigma = \sigma_0 + \frac{e^2}{\hbar\pi^3 a} T^{p/2} \tag{5.1}$$

with p as index depending on the scattering mechanism. Since there are two different regimes (T<10K and T>100K) the conductivity of URh_2Ge_2 is fitted separately for low and high temperature regions as $\Delta\sigma \propto T^x$ with x=1.0 and 0.6, respectively, for all samples.

To illustrate the close similarity of the temperature dependence of $\sigma - \sigma(T = 0)$, we plot the T dependencies of the conductivity for single crystalline URh_2Ge_2 for a and c axes in Fig. 5.12. As it is seen, the conductivity along a and c axes can be scaled onto each other by multiplication with a constant factor. In consequence, the conductivity reflects a generic behavior of electronic transport in this disordered strongly correlated material.

The two power law exponents in the temperature dependent conductivity imply that different scattering mechanisms dominate the behavior at low and high temperatures. It has been earlier proposed [10] that a behavior $\Delta\sigma \propto T$ can be attributed to inelastic electron-electron collisions [1], while a high temperature behavior $\sigma \propto \sqrt{T}$ stems from electron-phonon interaction, this in disordered media cutting short electronic localization processes.

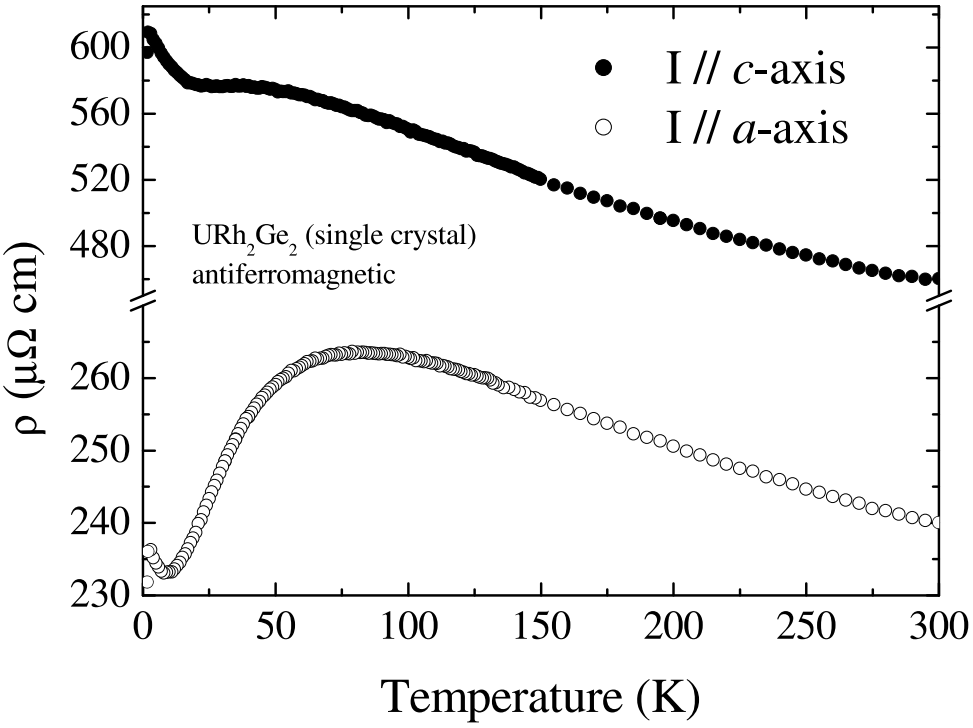

Figure 5.13: The resistivity of an antiferromagnetic single crystal URh_2Ge_2 along c and a axes.

For comparison and completeness, in Fig. 5.13 we plot the resistivity of an antiferromagnetic single crystal URh_2Ge_2. Down to 100K the resistivity of this sample behaves similar to that of the spin glass compounds, with a negative temperature coefficient $d\rho/dT$. At around 50K, however, the behavior varies from the spin glass crystals, with a metallic resistivity along the a-axis and additional curvature along the c-axis. At temperatures $T < 2$K there is a jump to lower resistivities for both axes. This jump we tentatively associate with a transition (magnetic or superconducting) of a second phase with a minute volume amount. A similar behavior had been previously observed in a study on polycrystalline material [24]. Fitting the conductivity by $\Delta\sigma \propto T^x$ above 150K is qualitatively in agreement with the spin glass samples, yielding x=0.6 for the a and c axes. It implies that the same high temperature mechanism accounts for the behavior of antiferromagnetic and spin glass URh_2Ge_2. As for polycrystalline URh_2Ge_2, we suggest a coexistence of metallic and pseudo-insulating phases in the antifer-

romagnetic single crystalline compound, because of a locally varying degree of disorder. Again, in the following we will not further consider these data.

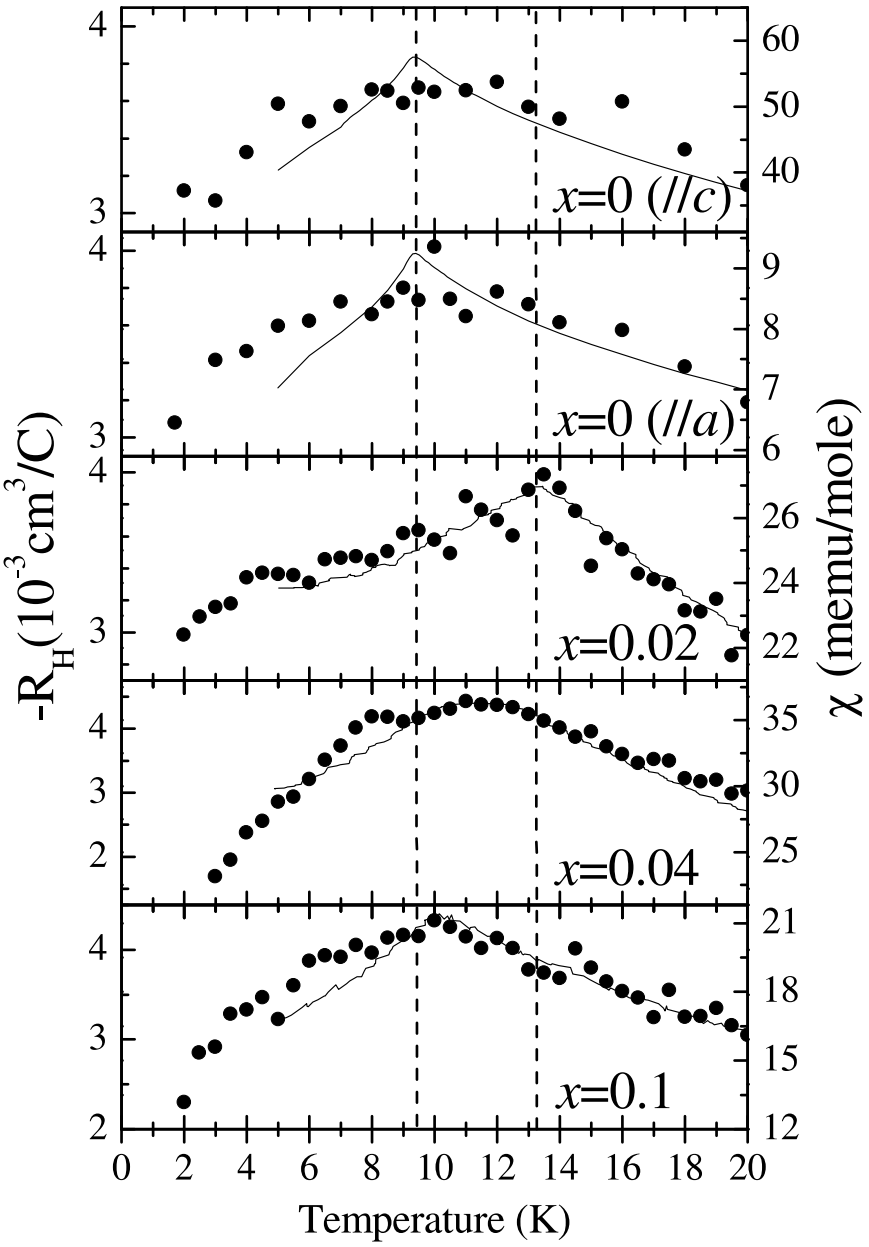

Figure 5.14: The Hall constant R_H of $URh_2Ge_{2-x}Sn_x$ x=0 (single crystal) along c and a axes, and polycrystalline samples x=0.02, 0.04 and 0.1. On the right axis we include the experimentally determined susceptibility (solid lines); for details see text.

To determine if the level of disorder and the change of the magnetic ground state is reflected in the carrier density, we performed Hall effect measurements

	R_0 $\times 10^{-3}$ (cm^3/C)	R_S $\times 10^{-5}$ (cm^3/C)	carrier density n (e^-/cm^3)	electrons/unit cell n_{cell}
x=0 (V_H//a-axis)	-0.5	-40	12×10^{21}	2.1
x=0 (V_H//c-axis)	-1.6	-4.2	3.9×10^{21}	0.7

Table 5.2: The ordinary Hall constant R_0, anomalous contribution R_S and carrier density n and n_{cell} of single crystalline URh_2Ge_2 (spin glass).

for all samples. The results of the measurements for $URh_2Ge_{2-x}Sn_x$ are plotted in Fig. 5.14. The Hall constant R_H exhibits a sample dependent maximum at low temperatures. Thus, single crystalline spin glass URh_2Ge_2 and polycrystalline spin glass $URh_2Ge_{2-x}Sn_x$, x=0.1, show a sharp cusp at the freezing temperature T_f=9.5K . On the other hand, antiferromagnetic $URh_2Ge_{2-x}Sn_x$, x=0.02, reveals an anomaly in R_H at T=13.4K, while the coexistence of antiferromagnetic and spin glass phase for x=0.04 can also be seen in the T-dependence of R_H

In the same way as in $UPd_{2-x}Sn$, we analyze the data by decomposing it into ordinary and anomalous contributions:

$$R_H = R_0 + \chi R_S \ , \tag{5.2}$$

with R_0 as ordinary Hall constant and χR_S as anomalous scattering. In Fig. 5.14 we include the susceptibility χ, illustrating that a matching R_H-R_0~χR_S exists over the full temperature scale, and in all details regarding the different magnetic ground states.

Moreover, we have measured the Hall effect for the single crystalline spin glass samples URh_2Ge_2 up to room temperature. The result is depicted in Fig. 5.15, together with the susceptibility χ for both axes. From the data, taking into account Eq. 5.2, we have determined the values of the ordinary Hall constant R_0, anomalous scattering contribution R_S and, in the limit of an one-band model for a spherical Fermi surface, the carrier density n for single crystalline URh_2Ge_2 along c and a axes (Tab. 5.2). The negative sign of R_0 implies a dominant electronic transport. Further, we observe a pronounced anisotropy of the carrier density, which along a and c axes differs by a factor of 3. Qualitatively, this is in agreement with the anisotropic electronic transport of this system. The values of the carrier density are typical for metallic heavy fermion compounds, thus excluding the possibility of a (pseudo) gap in the density of states accounting for the non-metallic resistivity. The close resemblance of the Hall effect of URh_2Ge_2 to cubic $UPd_{2-x}Sn$, with the scaling $R_H - R_0 \propto \chi$ suggests that this behavior is more common to disordered heavy fermion compounds. As noted for $UPd_{2-x}Sn$, a possible explanation might be a side jump mechanism [25, 26, 27].

Further, we performed a study of the transverse (TMR) and longitudinal (LMR) magnetoresistance of spin glass URh_2Ge_2, respectively. The TMR and LMR along the crystallographic a and c axes are plotted as function of magnetic field at different temperatures in Fig. 5.16. For both axes the longitudinal

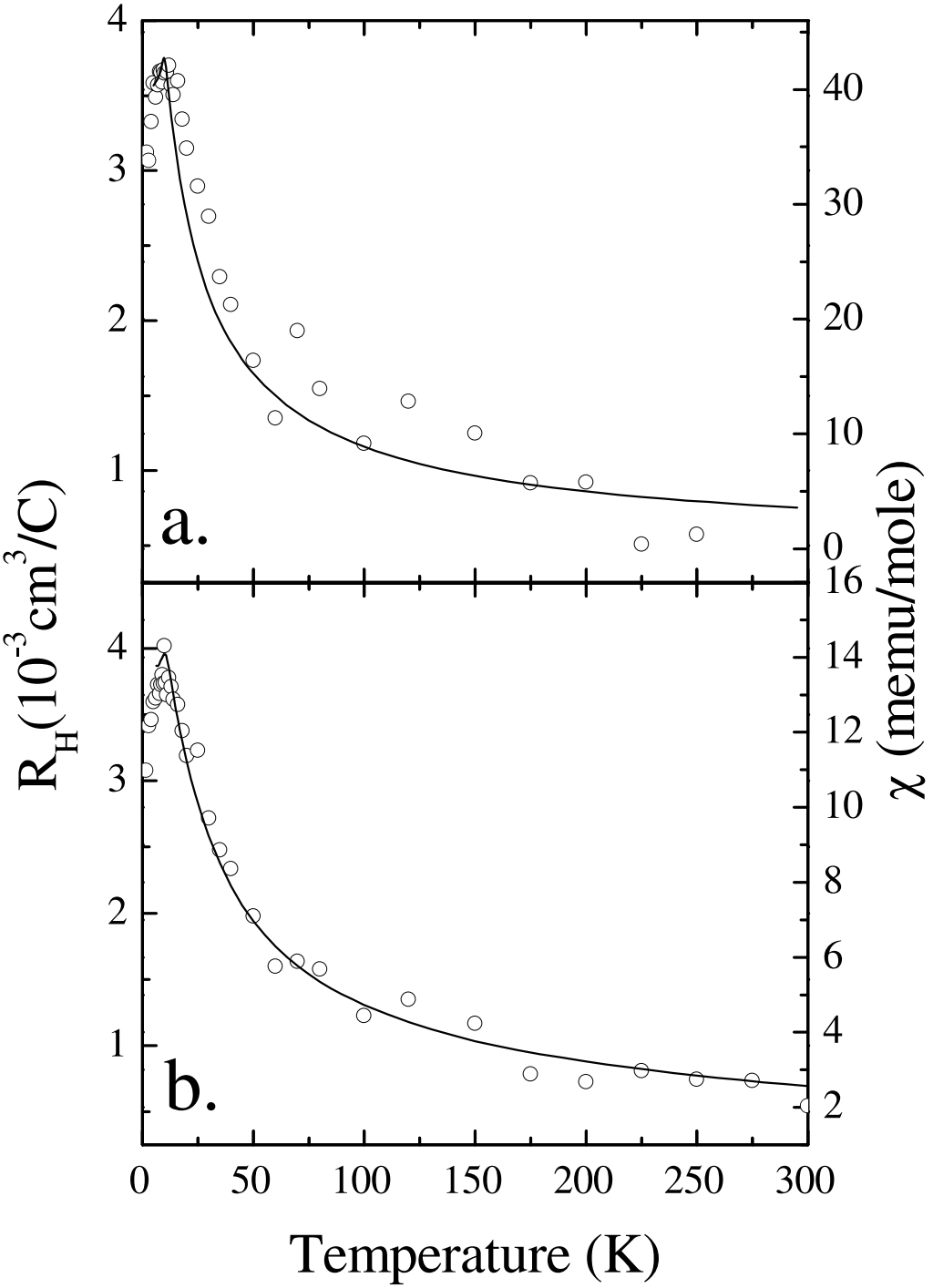

Figure 5.15: The Hall constant R_H of single crystalline spin glass URh_2Ge_2 measured along c-axis (a) and a-axis (b). On the right axis we include the experimentally determined susceptibility (solid lines).

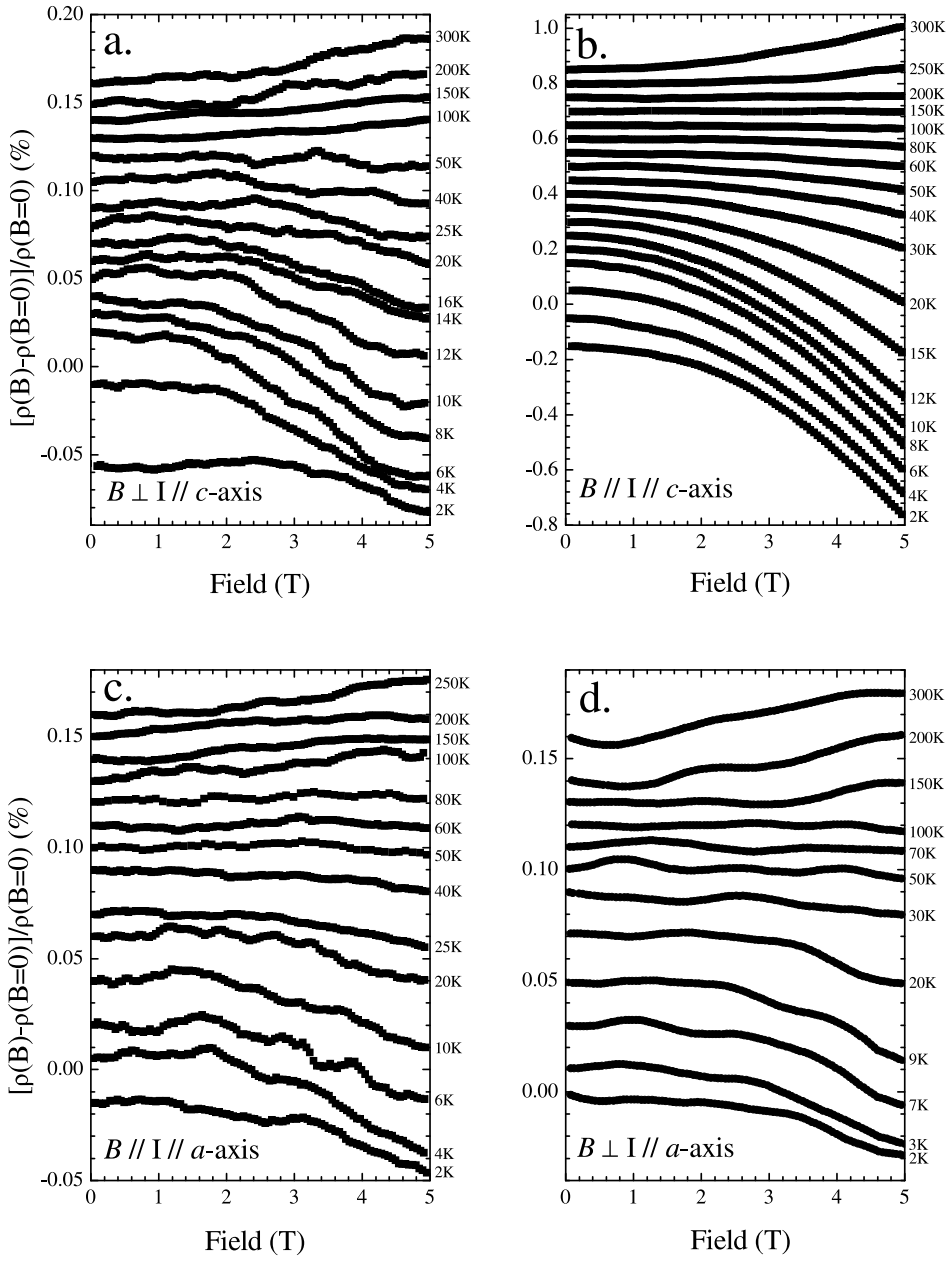

Figure 5.16: The magnetoresistance $(\rho_B - \rho_{B=0T})/\rho_{B=0T}$ of single crystalline URh_2Ge_2 (spin glass) with the current I along the c-axis and perpendicular to B (a), along the c-axis and parallel to B (b), along the a-axis and perpendicular to B (c) and along a-axis parallel to B (d). The temperatures at which the magnetoresistance was measured are indicated in the plot. The curves are shifted with respect to each other for clarity.

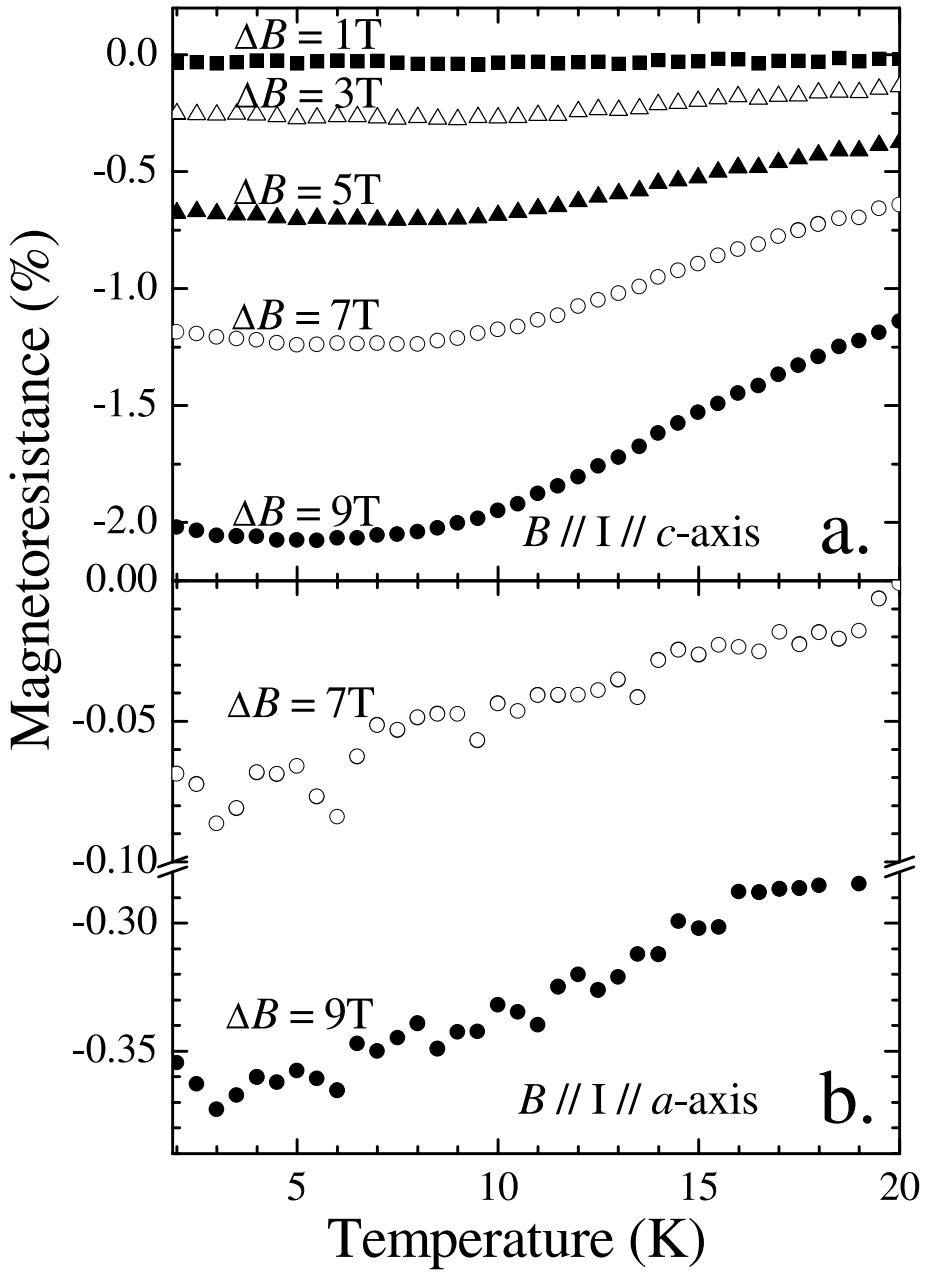

Figure 5.17: The magnetoresistance $(\rho_B - \rho_{B=0T})/\rho_{B=0T}$ of the single crystal URh_2Ge_2 (spin glass) with current I along c-axis (a) and a-axis (b). In both cases the field was parallel to the current.

and transverse magnetoresistance is negative up to ∼80-100K, but than changes its sign. Similar to the resistivity, the magnetoresistance exhibits a pronounced anisotropy along crystallographic a and c axes in the LMR mode. In contrast, the anisotropy of the TMR data is an order of magnitude smaller. Overall, the

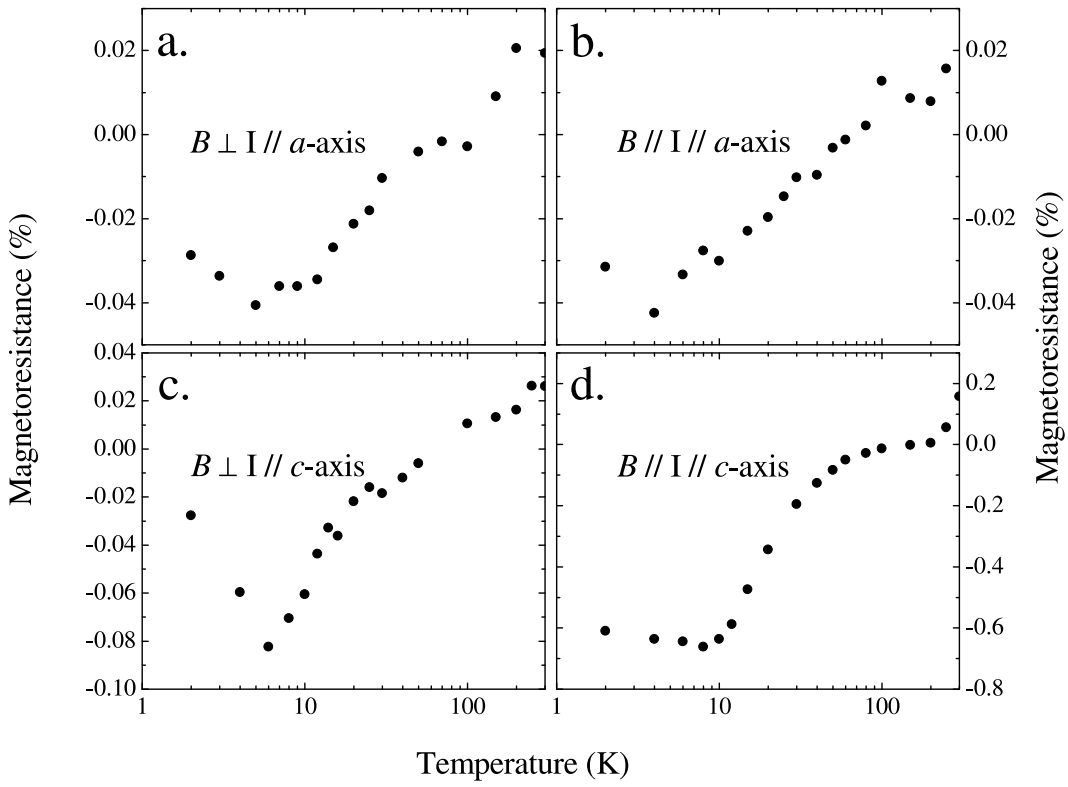

Figure 5.18: The magnetoresistance $(\rho_{B=5T} - \rho_{B=0T})/\rho_{B=0T}$ of the single crystal URh_2Ge_2 (spin glass) with current I along a-axis perpendicular to B (a), along a-axis parallel to B (b), along c-axis perpendicular to B (c) and along c-axis parallel to B (d).

magnetoresistance is small and aside from $B \parallel I \parallel c$, of the order of 0.1%, which explains the scatter of the data.

Moreover, temperature dependencies of the magnetoresistance, measured directly as $\Delta\rho/\rho_0$ and estimated from the field dependent measurements, are shown in Fig. 5.17 and Fig. 5.18 respectively. For all data sets there is a minimum in $\Delta\rho/\rho$ in the range 5-7K. Thus, unlikely other cases disordered U heavy fermion systems like U_2PdGa_3 [28], this minimum does not coincide with T_f, and does not indicate a spin ordering transition. The negative magnetoresistance can be caused by two reasons. Application of magnetic fields suppresses electronic localization [23], and as consequence, the conductivity is increased. A second possibility is suppression of spin disorder scattering [29, 30].

As we have demonstrated, for spin glass URh_2Ge_2 it is more appropriate to consider the conductivity rather than the resistivity, as Matthiesen's rule does not apply. Hence, in Fig. 5.19 we plot the reduced conductivity $\sigma - \sigma(B = 0)$, but now as function of the square of the magnetic field, B^2. At all temperatures the data lie on straight lines, implying that $\sigma - \sigma_0 \propto B^2$. We note that the

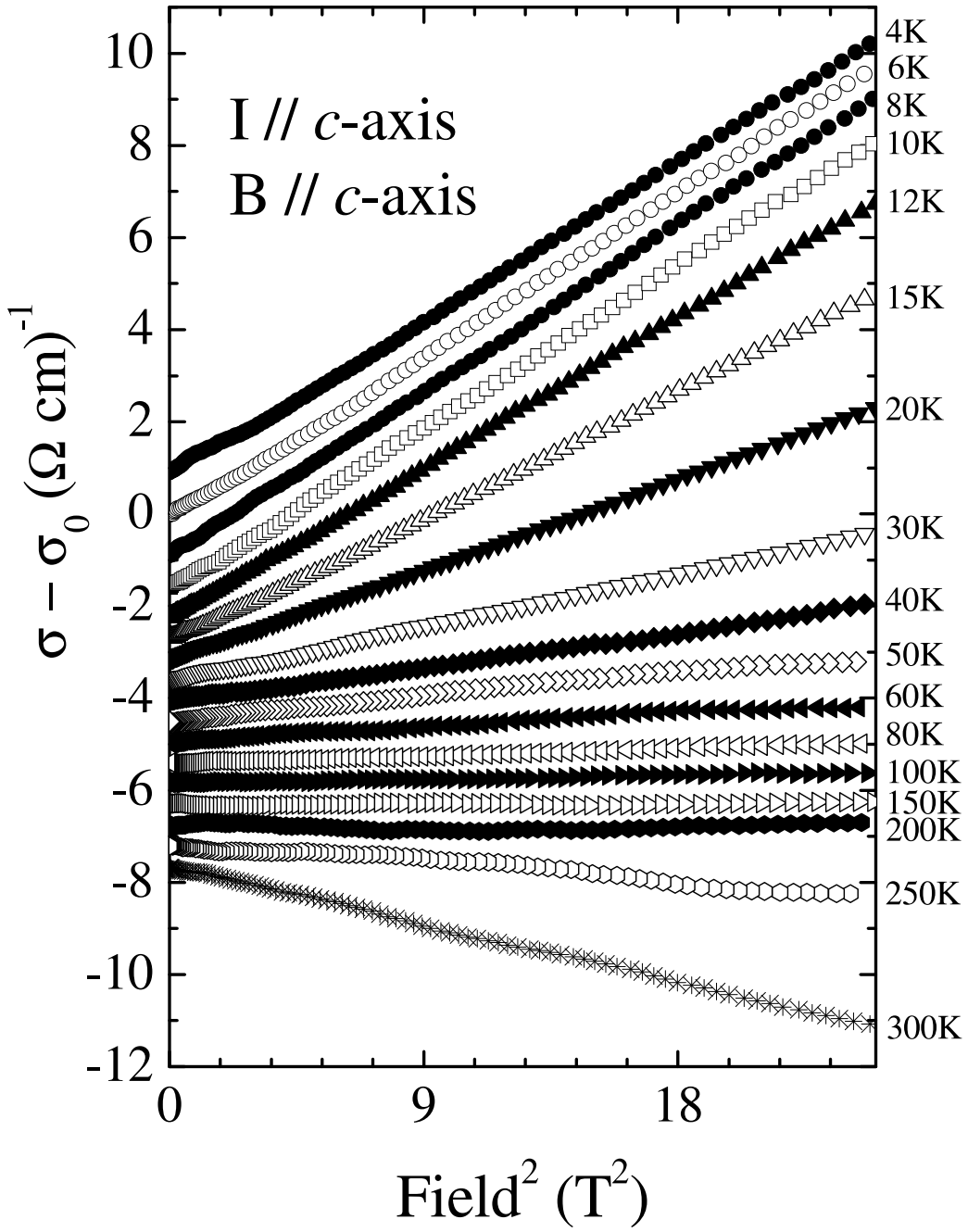

Figure 5.19: The reduced conductivity $\sigma - \sigma(B = 0)$ of single crystalline, spin glass URh_2Ge_2 with $B \parallel I \parallel c$-axis. The curves are shifted with respect to each other for clarity.

proportionality $\sigma - \sigma_0 \propto B^2$, within experimental resolution, also seems to apply for the magnetoconductance experiments with $B \parallel a$, $\parallel$ and $\perp I$, and $B \perp I \parallel c$-axis.

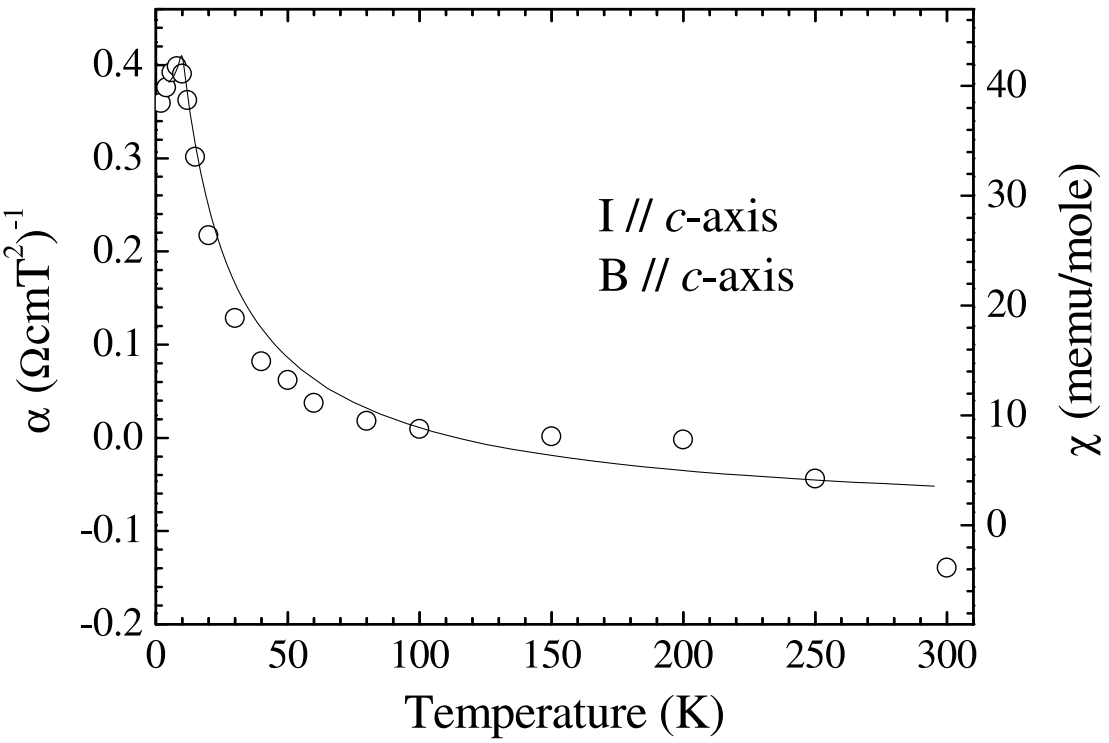

Figure 5.20: The fitting parameter α vs. temperature of spin glass URh_2Ge_2 along the c-axis (open symbols): for details see text. For comparison, the dc-susceptibility along the c-axis is included as solid line (right axis).

A positive magnetoconductance in spin glass systems and metallic magnetic alloys at low temperatures is well known and ascribed to the suppression of spin disorder scattering [28, 30, 31]. Surprisingly, we observe the same B^2 dependence even at high temperatures, where the magnetoconductance changes its sign. This is inconsistent with a suppression of spin disorder scattering. Therefore, to explain the temperature and field dependence of the magnetoconductance, another ingredient needs to be taken into account.

We can quantify the magnetoconductance by fitting the data to $\sigma = \sigma_0 + \alpha B^2$. In Fig. 5.20 we summarize the T-dependence of the parameter α. Its temperature dependence resembles the susceptibility χ, if a constant offset is taken into account. Only, the maximum of α is at a slightly lower temperature ($T \sim 8$K) than that of χ ($T \sim 10$K). This observation might indicate that α contains two contributions. The suppression of spin disorder scattering yields a B^2-dependence of $\sigma - \sigma_0$, whose T-dependence α_{SF} is primarily controlled by the susceptibility. In addition, the field dependence of electronic localization causes a constant offset α_{Loc}, with $\alpha = \alpha_{SF} + \alpha_{Loc}$.

At low temperatures, at least, a negative magnetoconductivity with a B^2 de-

pendence has been observed previously for amorphous metals like YNi, and has been attributed to weak localization effects [32]. Here, weak localization in the spin orbit dominated regime has been considered. In view of these results, we speculate that at high temperatures our negative magnetoconductance reflects a similar behavior.

Bibliography

[1] N. Mott, $Metal-InsulatorTransition$, 2nd ed. (Taylor&Francis, London, 1990).

[2] J. Dugdale, *The Electrical Properties of Disordered Metals* (Cambridge University Press, Cambridge, 1995).

[3] S. Süllow et al., J. Magn. Magn. Mat. **226-230** (2001) 35.

[4] M. Kuznietz et al., Phys. Rev. B **40** (1989) 7328.

[5] T. Endstra et al., J. Appl. Phys. **69** (1991) 4816.

[6] A. Drost, Ph.D. Thesis, Leiden University (1995), unpublished.

[7] S. Süllow, Ph.D. Thesis, Leiden University (1995), unpublished.

[8] H. Ptasiewicz-Bak et al., J. Phys. F **11** (1981) 1225; Solid State Commun. **55** (1985) 601.

[9] S. Süllow et al., Phys. Rev. Lett. **78** (1997) 354.

[10] S. Süllow et al., Phys. Rev. B **61** (2000) 8878.

[11] S.R. Vieira, F.D. Nobre and F.A. da Costa, Phys. Lett. A **250** (1998) 288.

[12] D. Tomuta, private communications.

[13] C.H. Booth, private communications.

[14] J.R.L. Almeida and D.J. Thouless, J. Phys. A **11** (1978) 983.

[15] J.A. Mydosh, *Spin Glasses: An Experimental Introduction* (Taylor&Francis, London, 1993).

[16] D. Chu, G.G. Kenning and R. Orbach, Phys. Rev. Lett. **72** (1994) 3270.

[17] R.V. Chamberlin et al., Phys. Rev. B **25** (1982) 6720.

[18] M. Gabay and G. Toulouse, Phys. Rev. Lett. **47** (1981) 201.

[19] M.A. Girtu et al., Phys. Rev. B **57** (1998) 11058.

[20] D.H. Ryan et al., Phys. Rev. B **63** (2001) 140405(R).

[21] S.R. Vieira, F.D. Nobre and C.S.O. Yokoi, Phys. Rev. E **61** (2001) 4760.

[22] Po-zen Wong et al., Phys. Rev. Lett. **19** (1985) 2043; J. Appl. Phys. **57** (1985) 3462.

[23] P.A. Lee and T.V. Ramakrishnan, Rev. Mod. Phys. **57** (1985) 325.

[24] B. Lloret et al., J. Magn. Magn. Mat. **67** (1987) 232.

[25] F.E. Maranzana, Phys. Rev. **160** (1967) 421.

[26] L. Berger, Phys. Rev. B **2** (1970) 4559.

[27] *The Hall Effect in Metals and Alloys*, ed. by C. Hurd (Plenum, New York, 1972).

[28] V.H. Tran et al., Phys. Rev. B **66** (2002) 54421; Phys. Rev. B **65** (2002) 134401.

[29] M.T. B*é*al-Monod and R.A. Weiner, Phys. Rev. **170** (1968) 552.

[30] A.K. Nigam and A.K. Majumdar, Phys. Rev. B **27** (1983) 495.

[31] N. van der Post et at., Phys. Rev. B **22** (1996) 15106.

[32] B. Barbara et al., J. Appl. Phys. **70** (1991) 5813.

6 Summary

The purpose of this work was to investigate the role of disorder in strongly correlated electron systems. From our study of Fe_2VAl and the two heavy fermion compounds $UPd_{2-x}Sn$ and $URh_2Ge_{2-x}Sn_x$ we conclude that in these materials the disorder can control the physical properties.

For Fe_2VAl, we have disproved a Kondo-insulating behavior as was previously proposed. Instead, the properties of the material are driven by disorder. Level and type of disorder dominating in this system have been estimated. In particular, the Kondo-insulating behavior does not play a role in the anomalous resistivity of Fe_2VAl, instead the "semiconducting-like" behavior is due to the ability of *Al*-vacancies to localize the electrons.

For the heavy fermion compounds $UPd_{2-x}Sn$ we have observed that disorder drives the anomalous physical behavior. Surprisingly, the levels of disorder for cubic and orthorhombic $UPd_{2-x}Sn$ are similar, but the "efficiency" of disorder appears to be higher in the first case.

A description of the resistivity, magnetoresistivity and Hall effect of cubic $UPd_{2-x}Sn$ in terms of conventional heavy fermion behavior does not consistently account for our observations. Alternatively, we attributed it to disorder induced diffusive electronic transport. Further, for cubic $UPd_{2-x}Sn$ we have determined the magnetic structure and ground state, which is characterized by small antiferromagnetic domains with correlation lengths of about 100Å.

Finally, we have studied in detail the influence of crystallographic disorder on the class of compounds $URh_2Ge_{2-x}Sn_x$. In the parent compound URh_2Ge_2 the level of disorder can be modified by different means - by varying the cooling speed during sample production, heat treatment or isoelectronic substitution. Correspondingly, we observe a very strong dependence of the magnetic properties from the particular treatment of the material, with antiferromagnetic, spin glass and mixed phase ground states appearing.

Regarding the electronic transport properties, we find for all samples/ground states a non-metallic behavior. By means of Hall effect measurements we disprove a (pseudo)gap scenario of the anomalous electronic transport. Therefore, we conclude that the "semiconducting-like" resistivity arises from disorder induced localization. Spin dependent scattering appears to be only of minor relevance for the electronic transport, although it contributes to the magnetoresistivity. Finally, we observe a close resemblance of the Hall-constants of $UPd_{1.85}Sn$ and

$URh_2Ge_{2-x}Sn_x$, $R_H - R_0 \propto \chi$, which probably indicates that this phenomenon is of more general relevance.

Zusammenfassung

Ziel der vorliegenden Arbeit war die Kläarung des Einflusses von Unordnung auf die Eigenschaften stark korrelierter Elektronensysteme. Anhand der Untersuchungen an Fe_2VAl sowie den Schwer-Fermion-Verbindungen $UPd_{2-x}Sn$ und $URh_2Ge_{2-x}Sn_x$ ist zu folgern, dass in solchen Materialien Unordnungseffekte deren Eigenschaften stark beeinflußen bzw. komplett kontrollieren können.

Für Fe_2VAl wurde gezeigt, dass dieses Material nicht - wie behauptet - als Kondo-Isolator zu betrachten ist. Stattdessen können die Materialeigenschaften von Fe_2VAl auf Unordnungseinflüsse zurückgeführt werden. Hierbei wurden Art und Grad der Unordnung bestimmt. In jenen Proben, welche Kondo-Isolator-artiges Verhalten zeigen, beruht dieses auf einigen Prozent Al-Fehlstellen, welche zu elektronischer Lokalisierung in einer Verbindung mit einer Pseudolücke an der Fermi-Kante führen.

Weiterhin wurde für das Schwer-Fermion-System $UPd_{2-x}Sn$ nachgewiesen, dass das hier beobachtete anomale physikalische Verhalten durch kristallographische Unordnung getriggert wird. Überraschenderweise finden wir für kubisches und orthorhombisches Material $UPd_{2-x}Sn$ ein ähnliches Unordnungs-Level, aber sehr unterschiedliche "Unordnungseffizienzen" - diese ist für kubische Proben sehr viel größer als für orthorhombische.

Entsprechend wird das Verhalten von kubischen $UPd_{2-x}Sn$ komplett durch die kristallographische Unordnung kontrolliert. So zeigt sich, dass eine Beschreibung des Widerstandes, Magnetowiderstandes sowie Hall-Effektes nicht im Rahmen konventioneller Schwer-Fermionen-Terminologie möglich ist. Alternativ führen wir daher das beobachtete Verhalten auf unordnungsinduzierten diffusen elektronischen Transport zurück. Weiterhin haben wir den magnetischen Grundzustand bestimmt, welcher antiferromagnetisch ist, allerdings mit einer aufgrund der kristallographischen Unordnung kleinen Kohärenzlänge von 100Å.

Schliesslich haben wir den Einfluss kristallographischer Unordnung detailliert an der Verbindungsklasse $URh_2Ge_{2-x}Sn_x$ untersucht. In der Ausgangsverbindung URh_2Ge_2 kann der Grad der Unordnung auf verschiedene Weisen variiert werden - durch unterschiedliche Abkühlgeschwindigkeiten während der Probenherstellung, Wärmebehandlung oder isoelektronische Substitution. Korrespondierend beobachten wir eine sehr starke der Abhängigkeit der magnetischen Eigenschaften von der Materialbehandlung, wobei antiferromagnetische, Spin-Glas-artige sowie gemischtphasige Grundzustände auftreten.

Hinsichtlich der elektronischen Transporteigenschaften finden wir für alle Proben/Grundzustände ein nicht-metallisches Verhalten. Aufgrund von Hall-Effektmessungen kann eine (Pseudo)Energielücke als Quelle dieses Verhaltens ausgeschlossen werden. Daher folgern wir, dass dieses Verhalten aus unordnungsinduzierter elektronischer Lokalisierung entspringt. Spinabhängige Streuung scheint von sekundärer Bedeutung für den elektronischen Transport zu sein,

trägt allerdings zum Magnetowiderstand bei. Schliesslich beobachten wir ein sehr ähnliches Verhalten der Hall-Konstanten für $UPd_{1.85}Sn$ und $URh_2Ge_{2-x}Sn_x$, $R_H - R_0 \propto \chi$, was möglicherweise ein Hinweis auf ein allgemeineres Phänomen darstellen könnte.

Lebenslauf

Maksimov Igor Sergeevich

Geburt:	08. Juni 1975 in Ust-Kamenogorsk, Kazachstan	
Eltern:	Sergey Maksimov Liliya Maksimova	
Schulbildung:	1982-1988	Grundschule in Ust-Kamenogorsk
	1988-1990	Orientierungsstufe in Donetsk, Ukraine
	1990-1992	Oberstufe (Abitur) in Donetsk, Ukraine
Studium:	1992-1997	Physik an der Donetsk State University
	Juli 1997	Diplom-Hauptprüfung
	1997-2002	Physik-Promotion
Beschäftigungen:	1997-1999	Doktorand an dem Physikalisch-Technischen Institut der NASU, Donetsk, Ukraine
	1999-2000	Doktorand am Fachbereich für Experimentalphysik, Umeå, Schweden
	seit 2000	Wiss. Mitarbeiter am Institut für Metallphysik und Nukleare Festkörperphysik der TU Braunschweig

for completeness...

Throughout my three years as a member of the AG Litterst, IMNF, I have received amount of support and inspiration from many people. Let me start by thanking Stefan Süllow. I am extremely grateful for his hospitality and expert supervision for his millions of ideas and remarks. I thank him also for his direction and support, without which I could not have come to Germany and received necessary experience for Ph.D. degree.

I would like to thank Professor Litterst for helpful comments for this thesis and assistance in the official questions. I also should like to thank all the staff members of the AG Litterst for their help during my research and for tolerating my language-consuming activities. In particular, to Anna, Anika, Anja, Ulf, HHK, Jan, Chrstofer, Oliver (AG Hesse) and Dirks. I can not forget the period I spent in Donetsk group and Umeå (Sundqvist). I do not hesitate to deliver my special thanks to Medvedev and Nikolaenko.

Next, there are all my friends I have made. The list is too long to mention but their friendship, parties and trips out of town helped to make my stay in Braunschweig a really happy one. I deeply appreciate the economic chats with Alexandr Alexandrov. And finally, my special thanks to Irishka for some great times.